ISSN 1881-7831 Online ISSN 1881-784X

DD&T

Drug Discoveries & Therapeutics

Volume 19, Number 3
June 2025

IRCA BSSA
IACMHR

www.ddtjournal.com

DD&T
Drug Discoveries & Therapeutics

ISSN: 1881-7831
Online ISSN: 1881-784X
CODEN: DDTRBX
Issues/Year: 6
Language: English
Publisher: IACMHR Co., Ltd.

Drug Discoveries & Therapeutics is one of a series of peer-reviewed journals of the International Research and Cooperation Association for Bio & Socio-Sciences Advancement (IRCA-BSSA) Group. It is published bimonthly by the International Advancement Center for Medicine & Health Research Co., Ltd. (IACMHR Co., Ltd.) and supported by the IRCA-BSSA.

Drug Discoveries & Therapeutics publishes contributions in all fields of pharmaceutical and therapeutic research such as medicinal chemistry, pharmacology, pharmaceutical analysis, pharmaceutics, pharmaceutical administration, and experimental and clinical studies of effects, mechanisms, or uses of various treatments. Studies in drug-related fields such as biology, biochemistry, physiology, microbiology, and immunology are also within the scope of this journal.

Drug Discoveries & Therapeutics publishes Original Articles, Brief Reports, Reviews, Policy Forum articles, Case Reports, Communications, Editorials, News, and Letters on all aspects of the field of pharmaceutical research. All contributions should seek to promote international collaboration in pharmaceutical science.

Editorial Board

Editorial and Head Office:

Pearl City Koishikawa 603,
2-4-5 Kasuga, Bunkyo-ku,
Tokyo 112-0003, Japan
E-mail: office@ddtjournal.com

Drug Discoveries & Therapeutics

Editorial and Head Office

Pearl City Koishikawa 603, 2-4-5 Kasuga, Bunkyo-ku,
Tokyo 112-0003, Japan

E-mail: office@ddtjournal.com
URL: www.ddtjournal.com

CONTENTS

Volume 19, Number 3, 2025

Review

Original Article

Correspondence

Letter to the Editor

Review

DOI: 10.5582/ddt.2025.01039

Kampo medicine in the management of menopausal symptoms: A narrative review of therapeutic potential

Yuanzheng Liu[1], Susumu Kobayashi[2], Ling Wang[3], Yanming Ren[1,*], Peipei Song[2,*]

[1] Department of Tranditional Chinese Medicine, Medical College, Qinghai University, Xining, China;
[2] Center for Clinical Sciences, Japan Institute for Health Security, Tokyo, Japan;
[3] Department of Obstetrics and Reproductive Immunology, Shanghai East Hospital, Tongji University School of Medicine, Shanghai, China.

SUMMARY: Menopausal symptoms primarily result from ovarian dysfunction and declining estrogen levels, leading to multisystem disorders. Although hormone therapy remains the most effective treatment, its long-term use is associated with significant risks, prompting interest in alternative options. Kampo medicine, a traditional Japanese system derived from Chinese herbal medicine, has gained renewed attention as a complementary and personalized therapeutic approach to menopausal health. This review aims to systematically summarize the current application and clinical evidence of Kampo medicine in the management of menopausal symptoms across multiple domains, including vasomotor, neuropsychiatric, musculoskeletal, skeletal, and genitourinary systems. Furthermore, the review seeks to further validate its efficacy through the mechanistic actions of its key ingredients. While the therapeutic effects of Kampo medicine on hot flashes have been inconsistent, it has demonstrated significant efficacy in improving emotional disturbances, sleep disorders, and somatic symptoms, particularly among individuals whose conditions are not driven solely by hormonal imbalances. In the management of osteoporosis, the integration of Kampo medicine with conventional Western treatments not only enhances overall therapeutic outcomes but also contributes to the reduction of adverse effects. One limitation of current research is the lack of randomized controlled trials (RCTs) evaluating the efficacy of Kampo medicine in managing Genitourinary Syndrome of Menopause (GSM), highlighting the need for further investigation in this area. The integration of Kampo medicine into menopausal symptom management may contribute to a more holistic, patient-centered approach that offers both traditional and Western medical options. This integrative model has the potential to support shared decision-making and improve personalized care for menopausal women.

Keywords: menopausal symptoms, Kampo, traditional herbal medicine, key ingredients

1. Introduction

Menopausal symptoms arise as a consequence of ovarian dysfunction and reduced estrogen secretion, leading to autonomic and neuropsychiatric disturbances. These symptoms include hot flushes, night sweats, dizziness, palpitations, sleep disturbances, mood changes, headaches, musculoskeletal pain, atrophic vaginitis, bladder irritability, and general malaise (*1-3*). Moreover, menopause has been linked to an increased risk of osteopenia, osteoporosis, and ischemic heart disease (*4*).

Menopausal symptoms can last for 4–5 years, with 9% of women still experiencing symptoms at the age of 72 (*5*). Hormone therapy is widely recognized as the most effective treatment for menopausal symptoms. However, extensive research has documented its potential risks, including increased incidences of breast, ovarian, and endometrial cancer, as well as a heightened risk of stroke and thromboembolism, particularly with prolonged use (*6-10*). Since the early 2000s, the use of menopausal hormone therapy has exhibited a substantial decline, particularly among women aged 52 to 65, largely attributable to safety concerns following the initial results of the Women's Health Initiative trial (*6*). Consequently, both patients and healthcare professionals are increasingly seeking alternative therapeutic options that demonstrate efficacy while minimizing adverse effects. In the United States, 82% of physicians advocate for herbal therapies as a complementary approach for managing menopausal symptoms (*11*). Traditional Chinese herbal medicine, known for its relatively mild side effects, is a natural therapeutic approach that has been widely utilized in some Asian countries, such as China and Japan. Its popularity is attributable in part to the relatively mild side effects associated with its use.

In Japan, Kampo medicine has been officially

incorporated into the National Health Insurance System, enabling patients to freely choose between Western and Kampo treatments at an affordable cost. Kampo formulations have become the most widely used form of Complementary and Alternative Medicine recommended by physicians in Japan (*12*). The market size for prescribed Kampo formulations has steadily grown, reaching approximately 162 billion yen per year by 2020 (*13*). Given this growing interest in safer and evidence-based alternatives, Kampo medicine has attracted increasing attention for its therapeutic potential in menopausal care. This narrative review aims to systematically summarize the current applications and clinical evidence of Kampo medicine in managing menopausal symptoms across multiple domains, including vasomotor, neuropsychiatric, musculoskeletal, skeletal, and genitourinary systems.

2. Kampo's basic concepts

Kampo medicine is based on a diagnostic framework that integrates three fundamental dichotomies: Yin-You (yin-yang), Kyo-Jitsu (deficiency-excess), and Netsu-Kan (heat-cold), and three essential physiological substances: Ki (Qi), Ketsu (blood), and Sui (fluid) (*14-16*). According to the principles of Kampo medicine, the onset of menopausal disorders is attributed to imbalances in Ki (Qi), Ketsu, and Sui. These elements have historically been referred to as "Blood Path Syndrome", which is characterized by blood stasis and microcirculatory dysfunction. Ketsu stagnation was identified as the most prevalent pathological condition among menopausal women, with a prevalence of 36.5% among cases. This was followed by Ki regurgitation (25.9%) and Ki stagnation (24.8%) as relatively frequent patterns. Among women whose primary menopausal symptoms were headache, hot flushes, and dizziness, the most commonly associated patterns were Sui metabolism disorders (48.8%), Ketsu stagnation (48.1%), and again Sui metabolism disorders (48.0%), respectively (*17*).

According to Kampo theory, the optimal formula should be selected individually based on four traditional diagnostic methods: *i*) visual inspection, *ii*) auscultation, *iii*) palpation and olfaction, and *iv*) inquiry into the patient's subjective symptoms. These methods enable practitioners to ascertain not only the imbalanced substance (Ki, Ketsu, or Sui), but also the predominant pattern among the dichotomies (yin–yang, deficiency–excess, heat–cold), thereby guiding treatment selection. In accordance with these diagnostic principles, 25 commonly used Kampo formulations (Table 1) have been officially standardized for the treatment of menopausal symptoms, as listed in the official compendium of Kampo medicines and their constituent crude drugs published by the Ministry of Health, Labour and Welfare of Japan (*18*).

3. Kampo for menopausal symptoms

A growing body of research supports the efficacy and safety of Kampo medicine in managing a wide range of menopausal symptoms. The following section will review its studies across five key symptom domains. Table 1 and Table 2 summarize Kampo formulations with existing research evidence for each symptom domain, including their herbal components and mechanisms of action from both traditional and modern medical perspectives.

3.1. Kampo for hot flushes

Approximately 60–80% of menopausal women experience hot flushes and sweating, symptoms that typically peak during the late menopausal transition and the initial phase of menopause (*19*). Menopausal hot flashes are primarily attributed to dysregulation of the hypothalamic thermoregulatory center triggered by fluctuating or declining estrogen levels (*20*). This hormonal disturbance is believed to enhance the activity of neuropeptides such as calcitonin gene-related peptide (CGRP), a potent vasodilator (*21*). Elevated CGRP levels increase skin temperature and promote sweating, contributing directly to the onset of hot flashes (*22*). Keishibukuryogan may alleviate vasomotor symptoms by improving peripheral blood flow and lowering plasma CGRP concentrations, thereby modulating the underlying mechanisms of hot flashes (*23*). Notably, in one clinical study, Keishibukuryogan significantly increased blood flow in the toes, which associated with a reduction in upper body hot flashes and a relief of cold sensations in the lower extremities of postmenopausal women, whereas hormone replacement therapy (HRT) reduced peripheral blood flow (*24*). Similarly, Unkeito has been shown to relieve hot flashes and coldness in the lower limbs by improving poor circulation and modulating excessive peripheral blood flow (*25*). EH0202, a herbal supplement, significantly reduces facial flushing by decreasing facial skin surface blood flow, while also exerting lipid-lowering effects (*26*).

In addition to improving peripheral circulation, some Kampo formulations also appear to alleviate hot flashes by modulating inflammation-related thermoregulatory pathways. Both Keishibukuryogan and Kamishoyosan significantly reduce IL-8 levels, a key cytokine involved in thermoregulation (*27*). In addition, keishibukuryogan decreases circulating monocyte chemotactic protein-1 level in postmenopausal women, which is the primary chemokine responsible for the recruitment of monocytes to sites of active inflammation (*27,28*).

Although several Kampo formulations have demonstrated pharmacological activity and some efficacy in alleviating hot flashes and night sweats, current studies still reveal inconsistent therapeutic outcomes (*29,30*).

3.2. Kampo for emotional and sleep disorders

Table 1. Twenty-five standardized Kampo formulations for menopausal symptom treatment

Japanese name	Synonym	Ingredients	Effects	Ref.
Unkeito	Wen-Jing-Tang	*Angelica, Cnidium, Paeonia (lactiflora), Cinnamomum, Paeonia (suffruticosa), Panax, Glycyrrhiza, Ophiopogon, Pinellia, Zingiber, Colla Corii, Evodia*	Improvement of circulation, alleviation of hot flashes and cold limbs, alleviation of depressive symptoms and anxiety, prevention of bone loss, inhibition of osteoclast activity	(*24*) (*39*) (*57*)
Unseiin		*Rehmannia, Angelica, Cnidium, Paeonia, Coptis, Scutellaria, Gardenia, Phellodend*	—	
Orengedokuto	Huang-Lian-Jie-Du-Tang	*Coptis, Scutellaria, Phellodendron, Gardenia*	—	
Keishibukuryogan	Gui-Zhi-Fu-Ling-Wan	*Cinnamomum, Paeonia (lactiflora), Paeonia (suffruticosa), Prunus, Poria*	Improvement of peripheral blood flow, reduction of plasma CGRP levels, alleviation of vasomotor symptoms including hot flashes and cold sensations, alleviation of sleep disturbances, increase of bone mineral content, improvement of calcium metabolism	(*23*) (*24*) (*38*) (*59*)
Keishibukuryogankayokuinin	Keishibukuryoganyokuinin	*Cinnamomum, Paeonia (lactiflora), Paeonia (suffruticosa), Prunus, Poria, Rehmannia, Gardenia*	—	
Koujito		*Atractylodes, Poria, Alisma, Polyporus, Cinnamomum*	—	
Kousosan		*Citrus, Paeonia (lactiflora), Cyperus, Ligusticum, Glycyrrhiza*	—	
Goshakusan		*Paeonia (lactiflora), Glycyrrhiza, Zingiber, Cinnamomum, Jujube*	—	
Saikokaryukotsuboreito		*Bupleurum, Paeonia (lactiflora), Poria, Cinnamomum, Aconite*	Bone protection, anti-inflammatory effects	(*60*)
Saikokeishikankyoto		*Bupleurum, Paeonia (lactiflora), Scutellaria, Pinellia, Zingiber*	—	
San'oshashinto		*Rehmannia, Plantago, Dioscorea, Alisma, Poria*	—	
San'ousan		*Rehmannia, Plantago, Dioscorea, Alisma, Poria, Cinnamomum*	—	
Shimotsuto		*Angelica, Rehmannia, Paeonia (lactiflora), Cnidium, Atractylodes, Poria*	—	
Hachimisoyosan		*Bupleurum, Paeonia (lactiflora), Atractylodes, Poria, Glycyrrhiza, Angelica, Rehmannia, Cnidium*	—	
Kamishoyosan	Jia-Wei-Xiao-Yao-San	*Bupleurum, Paeonia (lactiflora), Atractylodes, Poria, Glycyrrhiza*	Anti-inflammatory effects, modulation of thermoregulatory pathways, anxiolytic effects, reduction of anxiety symptoms, immunomodulation, alleviation of sleep disturbances	(*27*) (*34*) (35-37) (*38*)
Kamishoyosangoshimotsuto	Kamishoyosankasenkyujio	*Bupleurum, Paeonia (lactiflora), Atractylodes, Poria, Glycyrrhiza, Angelica, Rehmannia, Cnidium*	—	

Table 1. Twenty-five standardized Kampo formulations for menopausal symptom treatment (continued)

Japanese name	Synonym	Ingredients	Effects	Ref.
Senkyuchachosan		*Cnidium, Angelica, Rehmannia, Paeonia (lactiflora)*	—	
Tsudosan		*Rhei, Angelica, Cnidium, Paeonia (lactiflora), Citrus*	—	
Tokishakuyakusan		*Angelica, Paeonia (lactiflora), Alisma, Poria, Atractylodes*	Alleviation of sleep disturbances	(*38*)
Tokishakuyakusankaninjin		*Angelica, Paeonia (lactiflora), Alisma, Poria, Atractylodes, Panax*	—	
Tokishakuyakusankabushi		*Angelica, Paeonia (lactiflora), Alisma, Poria, Atractylodes, Aconite*	—	
Nyoshinsan		*Atractylodes, Poria, Alisma, Polyporus, Cinnamomum*	Mood stabilization, improvement of sleep and depressive symptoms	(*45*)
Yokukansan		*Atractylodes, Poria, Angelica, Cnidium, Bupleurum, Glycyrrhiza*	Anxiolytic and hypnotic effects	(*40-42*)
Yokukansankashakuyakuoren		*Atractylodes, Poria, Angelica, Cnidium, Bupleurum, Glycyrrhiza, Paeonia (lactiflora), Coptis*	—	
Yokukansankachinpihange		*Atractylodes, Poria, Angelica, Cnidium, Bupleurum, Glycyrrhiza, Citrus, Pinellia*	Alleviation of sleep disturbances	(*43*)

Table 2. Additional Kampo formulations for menopausal symptoms identified in recent studies

Japanese name	Synonym	Ingredients	Effects	Ref.
EH0202		*Cucurbita, Plantago, Lonicera, Carthamus*	Reduction of facial flushing	(*26*)
Porcine Placental Extract (PPE)		*Extractum Placentae*	Alleviation of depression and anxiety	(*44*)
Hachimijiogan	Ba-Wei-Di-Huang-Wan	*Rehmannia, Cornus, Dioscorea, Poria, Alisma, Paeonia (suffruticosa), Cinnamomum, Aconitum*	Enhancement of calcium metabolism, prevention and treatment of osteoporosis	(*54*)
Kamikihito		*Panax, Astragalus, Atractylodes, Poria, Ziziphus, Polygala, Zingiber, Glycyrrhiza, Angelica, Paeonia (lactiflora), Zizyphus, Saussurea, Cinnamomum, Bupleurum, Ginseng*	Increase of bone mass	(*58*)
Keishibukuryogan and bushi		*Cinnamomum, Paeonia (lactiflora), Paeonia (suffruticosa), Prunus, Poria, Aconitum*	Alleviation of lower back pain	(*74*)
Boiogito		*Sinomenium, Astragalus, Ziziphus, Glycyrrhiza, Zingiber, Atractylodes (lancea)*	Alleviation of joint and muscle pain, improvement of mobility and physical function	(*64,66*)
Keishikaryoujutsubuto		*Cinnamomum, Paeonia (lactiflora), Glycyrrhiza, Zingiber, Ziziphus, Atractylodes (lancea), Poria*	Alleviation of joint and muscle pain	(*64-65*)

The menopausal transition is associated with an elevated risk of mood disorders (*31*), with the incidence of first-onset depression being approximately twice as high as in premenopausal women (*32*). Epidemiological surveys indicate that the incidence of anxiety and depression among perimenopausal women ranges between 21% and 25% (*33*). There is a bidirectional relationship between mood and sleep, and sleep disturbances are increasingly recognized as a core component of menopausal psychological symptoms rather than a secondary complaint. Anxiety and depression frequently coexist with insomnia, and all three are influenced by overlapping neuroendocrine and neurotransmitter mechanisms during the menopausal transition.

Higuchi *et al.* demonstrated that peri-menopausal women with nonspecific symptoms who were treated with Kamishoyosan exhibited significantly lower Hamilton anxiety scores compared to those receiving HRT (*34*). Beyond endocrine mechanisms, immune factors are also involved in the development and aggravation of menopausal symptoms (*35*). Kamishoyosan has been shown to alleviate these symptoms while reducing serum levels of IL-6 and sIL-6R (*36*). It also increases TNF-α concentrations, suggesting that cytokines may influence mood regulation *via* the central nervous system and can be modulated by herbal interventions (*37*). In addition, research has shown that Japanese Kampo formulations, such as Tokishakuyakusan, Kamishoyosan, and Keishibukuryogan, are effective in alleviating sleep disturbances in perimenopausal women, improving sleep onset, reducing sleep interruptions, and enhancing restorative sleep (*38*). Furthermore, the combined use of Unkeito and HRT has been found to significantly reduce scores on the Self-Rating Depression Scale and alleviate both depressive symptoms and anxiety levels, as measured by the State-Trait Anxiety Inventory (*39*).

The Japanese Kampo Medicine Clinical Practice Guidelines recommend Yokukansan for treating menopausal insomnia (*40*). Studies also have shown that it can reduce anxiety and improve sleep quality, likely through modulation of central neurotransmitter systems (*41*). Yokukansan has been shown to enhance the anxiolytic effect of fluvoxamine by downregulating 5-HT_{2A} receptor expression in the prefrontal cortex, suggesting that their combination may provide a synergistic approach for the treatment of anxiety disorders (*42*). YokuKansan-ka-chimpihange is a Kampo compound formula derived from the classical prescription Yokukansan, with the addition of *Citrus reticulata* and *Pinellia*. One polysomnographic study has shown that YokuKansan-ka-chimpihange significantly increases total sleep time in healthy adults and demonstrates a tendency to improve sleep efficiency and reduceP sleep latency (*43*).

Oral administration of porcine placental extract (PPE) over a 24-week period significantly reduced scores on the Simplified Menopausal Index, Zung's Self-Rating Depression Scale, and the State-Trait Anxiety Inventory, indicating notable improvements in anxiety and depressive symptoms (*44*). Nyoshinsan, one of the commonly used Kampo formulations for managing menopausal symptoms, has demonstrated clinical efficacy in alleviating psychiatric manifestations such as nocturnal awakening and depressive mood. Notably, its therapeutic effects appear to be more pronounced in women with a higher body mass index (*45*).

While HRT is effective in relieving vasomotor symptoms, its effects on psychiatric symptoms such as insomnia, anxiety, depression, dizziness, and irritability are limited (*46,47*). Not all climacteric symptoms can be explained by ovarian hypofunction alone (*48,49*), and estrogen therapy has significant limitations in addressing psychological manifestations.

3.3. Kampo for osteoporosis

Osteoporosis is a metabolic bone disease characterized by degenerative changes in bone microarchitecture, leading to increased bone fragility and a higher risk of fractures. It affects more than 200 million people worldwide (*50*), with postmenopausal women being particularly vulnerable due to estrogen deficiency. Estrogen deficiency accelerates trabecular bone loss and induces the production of proinflammatory cytokines such as IL-6, which enhance osteoclast activity and contribute to the development of postmenopausal osteoporosis (*51*). Currently, clinical management of osteoporosis primarily relies on two therapeutic strategies: anti-resorptive agents and bone anabolic agents. However, long-term use of anti-resorptive agents such as bisphosphonates may lead to complications like osteonecrosis of the jaw (*52*) or atypical fractures (*53*), while HRT also carries potential side effects.

Compared to synthetic drugs, Kampo medicines are known for their fewer adverse effects, making them more suitable for long-term use. Hachimi-jio-gan (HJG) has been shown to enhance calcium metabolism (*54*) and demonstrate efficacy in osteoporosis prevention and treatment (*55*). Furthermore, a study in ovariectomized rats found that HJG inhibited bone resorption without significantly affecting bone formation. Notably, combining HJG with alendronate significantly improved trabecular bone mass and microstructure compared to either treatment alone (*56*). Similarly, Unkeito (*57*) has been reported to suppress RANKL-induced osteoclastogenesis, promote osteoclast apoptosis, and prevent bone loss in ovariectomized mice, highlighting its potential as a therapeutic agent for postmenopausal osteoporosis. Kamikihito has been shown to effectively increase bone mass, improve anemia, and reduce menopausal symptom severity in women with osteoporosis (*58*). In an randomized controlled trial (RCT) involving women who had

undergone oophorectomy and entered surgically induced menopause, the combination of Keishibukuryogan and vitamin D3 significantly increased bone mineral content, as well as serum calcium and alkaline phosphatase levels, which shows a therapeutic effect on osteopenia caused by estrogen deficiency (*59*). Saikokaryukotsuboreito can prevent loss of bone volume and suppress serum IL-6 level in a postmenopausal model (*60*).

Kampo medicine offers a promising therapeutic approach for the treatment of postmenopausal osteoporosis, particularly for patients who are intolerant to conventional medications or unwilling to undergo hormone therapy.

3.4. Kampo for somatic symptoms

Some of the most common climacteric symptoms are somatic symptoms, such as muscle and joint pain, which cause limitations in performing daily tasks. Several evidence suggest that changes in or loss of sex hormones may enhance susceptibility to musculoskeletal pain and influence disease progression (*3,61*). These findings indicate a correlation between menopause and the increased incidence of joint pain and osteoarthritis (OA) (*62*).

Approximately 50% of menopausal women report arthralgia (*63*). Traditional herbal medicine has been utilized for centuries to treat various musculoskeletal pain conditions. Keishikaryoujutsubuto and Boiogito have been reported to alleviate menopausal hand joint pain, muscle pain, and stiffness, thereby significantly improving quality of life (*64*). A randomized, placebo-controlled clinical trial has demonstrated the efficacy and safety of Keishikaryoujutsubuto in managing pain associated with knee OA (*65*). Additionally, an RCT investigating the therapeutic effects of Boiogito on knee OA with joint effusion demonstrated that patients in the Boiogito group exhibited significant improvements in stair-climbing ability, as measured by the Knee Society Scoring System functional score (*66*). Sinomenium acutum, a substitute for Fangji in Japan due to concerns about aristolochic acid toxicity. Sinomenium acutum has long been used in traditional Chinese medicine to treat rheumatic diseases (*67*), and its main active compound, sinomenine, has demonstrated anti-inflammatory and analgesic effects in both animal and human models of OA (*66,68,69*).

In traditional Chinese medicine, the placenta is known as Ziheche (processed human placenta) and has been used for centuries in Asian countries to alleviate menopausal symptoms. In Japan, a commonly used pharmaceutical preparation derived from hydrolyzed human placenta is commercially available under the name Laennec (*70*). Recently, PPE has been developed as an oral supplement for therapeutic purposes similar to human placental extract. Oral administration of PPE, especially in combination with menopausal hormone therapy, has shown efficacy in relieving chronic shoulder stiffness and knee pain in postmenopausal women (*71*).

Low back pain is one of the most common pain conditions and tends to worsen during the perimenopausal and postmenopausal periods (*72*). Its causes are multifactorial, including hormonal decline, bone loss, muscle atrophy, and psychological stress. Although hormone therapy is effective for alleviating hot flashes, menopausal hormone therapy and oral contraceptives have been linked to an increased risk of Low back pain (*73*). Kampo medicine offers a unique advantage in that it can be modified based on an individual's menopausal constitution to simultaneously address systemic menopausal symptoms and musculoskeletal complaints. An RCT found that Keishibukuryogan combined with bushi (*Aconiti tuber*) was more effective than Keishibukuryogan alone in relieving nonspecific lumbago in menopausal women, with higher symptom relief rates (*74*).

Kampo formulations has demonstrated clinical efficacy in alleviating menopausal musculoskeletal symptoms. In addition, bioactive components from traditional remedies, such as Sinomenium acutum and PPE, show promise for pain relief and functional improvement.

3.5. Genitourinary Syndrome of Menopause (GSM)

GSM is a clinical condition resulting from decreased estrogen levels following menopause, affecting the genital and lower urinary tract. Common symptoms include vaginal dryness, burning sensations, dyspareunia, urinary frequency, and urgency (*75*). The prevalence of GSM has been documented to be approximately 64.7% one year after menopause, increasing to 84.2% after six years (*76*). Due to the intimate nature of its symptoms, many women may be reluctant to seek medical attention, leading to underreporting and undertreatment of this condition. MHT remains the primary treatment for GSM (*77*). Conversely, Kampo medicine's current scope is confined to the provision of symptomatic relief, and there is an absence of substantial clinical evidence, such as RCTs, specifically addressing GSM. Consequently, further research is warranted to explore Kampo's potential role in the comprehensive management of GSM.

4. Concise overview of key ingredients in the Kampo formulations discussed

In the management of menopausal syndrome, Kampo medicines have demonstrated promising clinical potential due to their multi-component and multi-target characteristics. In this review, we provide a concise overview of the key ingredients identified in the Kampo formulations discussed (Figure 1).

Glycyrrhizae radix and *cinnamomi cortex* exhibited

Estrogen Receptor β-dependent estrogenic activity, and unkeito, kamishoyosan, and nyoshinsan demonstrated estrogenic effects, potentially useful for treating menopausal syndrome (*78*). Cinnamaldehyde, a pivotal active constituent of Keishibukuryogan, has been demonstrated in earlier studies to activate the transient receptor potential ankyrin 1 channel (*79*), thereby promoting thermoregulatory responses such as increased brown adipose tissue activity and elevated rectal temperature. Moreover, cinnamaldehyde exerts anti-inflammatory effects in chondrocytes by inhibiting lipopolysaccharide -induced inflammation and attenuating cartilage degeneration through the suppression of the NF-kappaB signaling pathway (*80*). Glycyrrhizin and geissoschizine methyl ether are two active components of Yokukansan. Geissoschizine methyl ether acts as a partial agonist at serotonin 5-HT1A receptors and an antagonist at 5-HT7 receptors, primarily targeting neurons in the prefrontal cortex, thereby modulating emotional and anxiety-related behaviors (*81-84*). The glycyrrhizin metabolite, 18β-glycyrrhetinic acid, enhances glutamate uptake in the hippocampus by activating astrocytic glutamate transporters, which may contribute to alleviating depressive symptoms and improving sleep quality (*85*). Liquiritigenin, another active compound of *Glycyrrhiza*, exhibits estrogenic agonist activity by stimulating the expression of estrogen-regulated genes, indicating that it possesses characteristics of a selective estrogen receptor modulator (*86*). The lignan components contained in EH0202, such as secoiso and lariciresinol (*87*), exhibit phytoestrogenic activity and may contribute to the regulation of the central thermoregulatory system.

Paeoniflorin and paeonol, bioactive components derived from peony, demonstrate significant therapeutic potential in alleviating menopausal symptoms through multiple mechanisms. Paeoniflorin, an active compound in traditional Kampo formulations such as Unkeito, Tokishakuyakusan, Kamikihito, Keishibukuryogan, and Hachimijiogan, has multiple biological effects. It promotes non-rapid eye movement sleep *via* the adenosine A1 receptor (*88*) and helps improve osteoporosis caused by high-fat, high-carbohydrate diet-induced hyperlipidemia (*89*). Paeoniflorin also directly stimulates 3T3-L1 adipocytes to secrete estradiol, suggesting potential roles in managing ovarian dysfunction in postmenopausal women (*90*). Paeonol alleviates postmenopausal cognitive impairment, anxiety, and depression by upregulating G protein-coupled receptor 30 expression and activating the PI3K/Akt/mTOR signaling pathway with increased hippocampal brain-derived neurotrophic factor levels (*91*). Additionally, it prevents bone loss by suppressing RANKL-induced osteoclastogenesis *via* inhibition of ERK, p38, and NF-kappaB pathways (*92*).

The efficacy of Hachimijiogan in combating osteoporosis is attributable to the synergistic actions of its core components, including catalpol, loganin, and morroniside. Catalpol (*93*) has been shown to support bone formation while limiting bone breakdown. Loganin (*94*) has been demonstrated to promote osteogenesis and balance bone remodeling. Morroniside (*95*) has been shown to protect against inflammation-driven bone loss by modulating key signaling pathways, such as NF-kappaB and MAPK. Saikokaryukotsuboreito is traditionally employed in the treatment of Menopausal symptoms. Among its

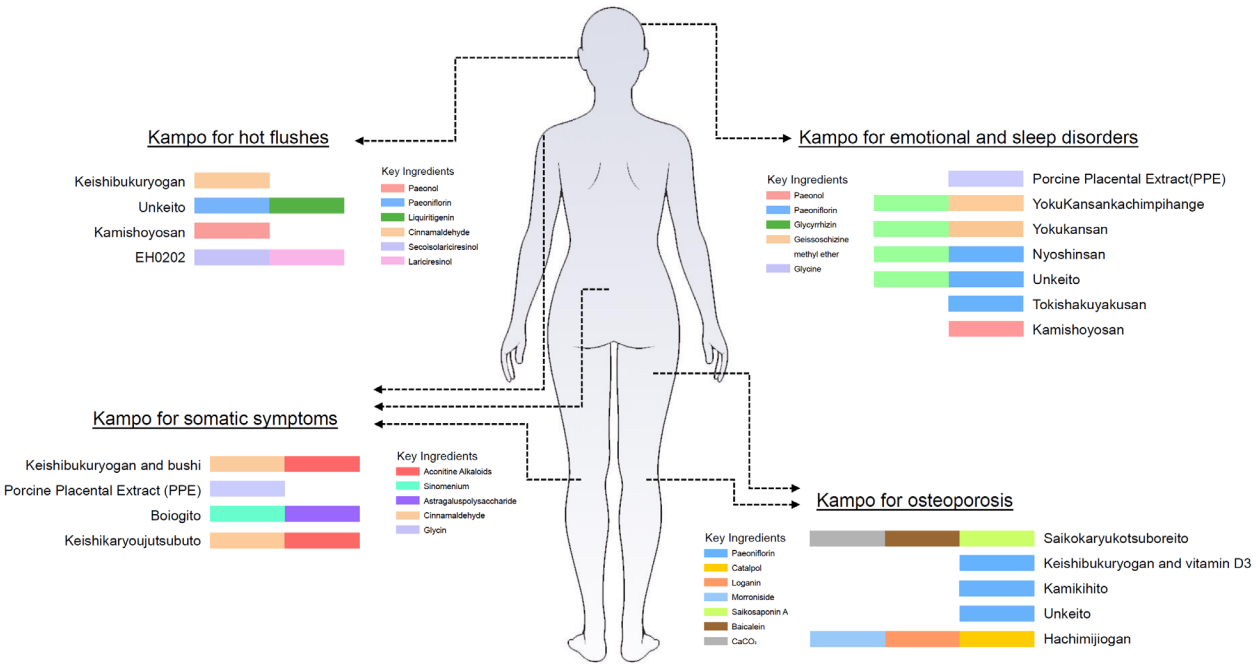

Figure 1. Kampo formulations and key ingredients for menopausal symptoms.

constituents, saikosaponin A, baicalein, and calcium carbonate are considered key contributors to its effects on bone health. Saikosaponin A (*96*) has been shown to mitigate bone loss by inducing ferroptosis in osteoclasts and inhibiting osteoclastogenesis. Baicalein (*97*) inhibits osteoclast differentiation and promotes apoptosis in mature osteoclasts, thereby reducing bone resorption. The use of oyster shell–fortified foods (*98*) has demonstrated efficacy in the prevention and treatment of osteoporosis by enhancing calcium intake and supporting bone mineralization. It is noteworthy that the oyster shell composition is predominantly calcium carbonate, constituting a bioavailable calcium source. Keishikaryoujutsubuto and Keishibukuryogan combined with bushi (*Aconiti tuber*) contain aconitine alkaloids, which are believed to improve peripheral circulation and reduce pain and stiffness (*99*). Boiogito includes sinomenium (*100*) and astragalus polysaccharides (*101*), which exhibit anti-inflammatory and immunomodulatory effects, aiding in the relief of musculoskeletal discomfort.

The efficacy of Kampo medicine in managing menopausal syndrome is substantiated by both formula-level clinical observations and component-level mechanistic evidence. These findings suggest that the therapeutic effects of Kampo formulations are attributable to their multi-component, multi-target actions, offering pharmacological plausibility for their traditional use.

5. Conclusion

Kampo medicine has experienced a resurgence in Japan following its official approval by the Ministry of Health and Welfare in 1976. Today, it is recognized as a principal therapeutic option for managing menopausal symptoms, alongside hormone therapy. Among the approximately 150 Kampo formulations currently in clinical use, Tokishakuyakusan, Kamishoyosan, and Keishibukuryogan are regarded as the most representative and frequently prescribed formulations for alleviating menopausal complaints in women (*38*).

Kampo medicine fundamentally differs from Western medicine in its underlying etiological concepts, diagnostic criteria, patient evaluation methods, and treatment selection strategies. Each system possesses distinct philosophical foundations and clinical approaches, and rather than being mutually exclusive, they may be considered complementary. In the treatment of hot flash and GSM, HRT remains the first-line approach. However, Kampo medicine has demonstrated significant effectiveness in managing emotional and sleep disturbances as well as various somatic symptoms. This may be attributed to Kampo's ability to interpret and treat the multifaceted physical and psychological manifestations of menopause as an integrated syndrome. By selecting from a small number of formulations tailored to the individual's overall symptom pattern, Kampo aligns closely with the heterogeneous and systemic nature of menopausal disorders.

Given the unique diagnostic and therapeutic principles of Kampo, future clinical research should not only pursue high-quality RCTs but also explore ways to incorporate Kampo-specific diagnostic frameworks into study designs. Instead of treating Western and Kampo medicine as opposing paradigms, a patient-centered model that presents both options clearly, along with their respective benefits and potential risks, should be encouraged. This integrative approach has the potential to empower women to make informed decisions and may lead to more personalized and effective management of menopausal health.

Funding: This work was supported by a grant from Qinghai Provincial Department of Science and Technology, Demonstration Study of Natural Population Cohort on the Tibetan Plateau (Grant No.2024-0204-SFC-0019).

Conflict of Interest: The authors have no conflicts of interest to disclose.

References

1. Gracia CR, Freeman EW. Acute consequences of the menopausal transition: The rise of common menopausal symptoms. Endocrinol Metab Clin North Am. 2004; 33:675-689.
2. Maartens LW, Leusink GL, Knottnerus JA, Smeets CG, Pop VJ. Climacteric complaints in the community. Fam Pract. 2001; 18:189-194.
3. Gulati M, Dursun E, Vincent K, Watt FE. The influence of sex hormones on musculoskeletal pain and osteoarthritis. Lancet Rheumatol. 2023; 5:225-238.
4. Benagiano G, Farris M. Why a consensus conference on hormone replacement therapy and the cardiovascular system? Maturitas. 2004; 47:245-253.
5. Rödström K, Bengtsson C, Lissner L, Milsom I, Sundh V, Björkelund C. A longitudinal study of the treatment of hot flushes: The population study of women in Gothenburg during a quarter of a century. Menopause. 2002; 9:156-161.
6. Rossouw JE, Anderson GL, Prentice RL, LaCroix AZ, Kooperberg C, Stefanick ML, Jackson RD, Beresford SA, Howard BV, Johnson KC, Kotchen JM, Ockene J. Risks and benefits of estrogen plus progestin in healthy postmenopausal women: Principal results From the Women's Health Initiative randomized controlled trial. JAMA. 2002; 288:321-333.
7. Lacey JV Jr, Brinton LA, Leitzmann MF, Mouw T, Hollenbeck A, Schatzkin A, Hartge P. Menopausal hormone therapy and ovarian cancer risk in the National Institutes of Health-AARP Diet and Health Study Cohort. J Natl Cancer Inst. 2006; 98:1397-1405.
8. Ziel HK, Finkle WD. Increased risk of endometrial carcinoma among users of conjugated estrogens. N Engl J Med. 1975; 293:1167-1170.
9. Canonico M, Plu-Bureau G, Lowe GDO, Scarabin PY. Hormone replacement therapy and risk of venous

thromboembolism in postmenopausal women: Systematic review and meta-analysis. BMJ. 2008; 336:1227-1231.
10. Renoux C, Dell'aniello S, Garbe E, Suissa S. Transdermal and oral hormone replacement therapy and the risk of stroke: A nested case-control study. BMJ. 2010; 340:c2519.
11. Singh B, Liu XD, Der-Martirosian C, Hardy M, Singh V, Shepard N, Gandhi S, Khorsan R. A national probability survey of American Medical Association gynecologists and primary care physicians concerning menopause. Am J Obstet Gynecol. 2005; 193:693-700.
12. Motoo Y, Yukawa K, Arai I, Hisamura K, Tsutani K. Use of complementary and alternative medicine in Japan: A cross-sectional internet survey using the Japanese version of the international complementary and alternative medicine questionnaire. JMA J. 2019; 2:35-46.
13. General affairs committee, Japan kampo medicines manufacturers association. Annual report on production dynamics in the pharmaceutical industry. *https://www.nikkankyo.org/serv/movement/R02/all.pdf* (accessed April 25, 2025).
14. Terasawa K. Evidence-based reconstruction of Kampo medicine: Part II—the concept of Sho. Evid Based Complement Alternat Med. 2004; 1:119-123.
15. Watanabe S, Toyama T, Sato T, Suzuki M, Morozumi A, Sakagami H, Hamada N. Kampo therapies and the use of herbal medicines in the dentistry in Japan. Medicines (Basel). 2019; 6:34.
16. Arai YC, Makino I, Ikemoto T, Saisu H, Terajima Y, Owari K. Kampo for the treatment of pain in Japan: A review. Pain Ther. 2020; 9:161-170.
17. Ushiroyama T, Sakuma K, Nosaka S. Rate of identification of eight-principle pattern and physiological activity in women with climacteric symptoms in Japanese Kampo medicine. Kampo Med. 2005; 56:779-787.
18. Pharmaceutical and Food Safety Bureau, Ministry of Health, Labour and Welfare. *https://www.mhlw.go.jp/file/06-Seisakujouhou-11120000-Iyakushokuhinkyoku/0000160072.pdf* (accessed April 25, 2025).
19. Freeman EW, Sherif K. Prevalence of hot flushes and night sweats around the world: A systematic review. Climacteric. 2007; 10:197-214.
20. Freedman RR. Physiology of hot flashes. Am J Hum Biol. 2001; 13:453-464.
21. Oliveira MA, Lima WG, Schettini DA, Tilelli CQ, Chaves VE. Is calcitonin gene-related peptide a modulator of menopausal vasomotor symptoms? Endocrine. 2019; 63:193-203.
22. Wilhelms DB, Dock H, Brito HO, Pettersson E, Stojakovic A, Zajdel J, Engblom D, Theodorsson E, Hammar ML, Spetz Holm AE. CGRP is critical for hot flushes in ovariectomized mice. Front Pharmacol. 2018; 9:1452.
23. Chen JT, Shiraki M. Menopausal hot flash and calciotonin gene-related peptide; effect of Keishi-bukuryo-gan, a kampo medicine, related to plasma calciotonin gene-related peptide level. Maturitas. 2003; 45:199-204.
24. Ushiroyama T, Ikeda A, Sakuma K, Ueki M. Comparing the effects of estrogen and an herbal medicine on peripheral blood flow in post-menopausal women with hot flashes: hormone replacement therapy and gui-zhi-fu-ling-wan, a Kampo medicine. Am J Chin Med. 2005; 33:259-267.
25. Ushiroyama T, Sakuma K, Nosaka S. Comparison of effects of vitamin E and wen-jing-tang (unkei-to), an herbal medicine, on peripheral blood flow in post-menopausal women with chilly sensation in the lower extremities: A randomized prospective study. Am J Chin Med. 2006; 34:969-979.
26. Ushiroyama T, Yoshida S, Tadaki K, Ikeda A, Ueki M. Clinical efficacy of EH0202, a Kampo formula, on the health of middle-aged women. Am J Chin Med. 2004; 32:755-770.
27. Yasui T, Matsui S, Yamamoto S, Uemura H, Tsuchiya N, Noguchi M, Yuzurihara M, Kase Y, Irahara M. Effects of Japanese traditional medicines on circulating cytokine levels in women with hot flashes. Menopause. 2011; 18:85-92.
28. Ylä-Herttuala S, Lipton BA, Rosenfeld ME, Särkioja T, Yoshimura T, Leonard EJ, Witztum JL, Steinberg D. Expression of monocyte chemoattractant protein 1 in macrophage-rich areas of human and rabbit atherosclerotic lesions. Proc Natl Acad Sci U S A. 1991; 88:5252-5256.
29. Okuda Y. Clinical efficacy of Saikokeishito in the treatment of climacteric disorder. Jpn J Orient Med. 2016; 67:323-330. (in Japanese)
30. Takamatsu K, Ogawa M, Higuchi T, Takeda T, Hayashi K, Mizunuma H. Effects of Kamishoyosan, a traditional Japanese medicine, on menopausal symptoms: A randomized, placebo-controlled, double-blind clinical trial. Evid Based Complement Alternat Med. 2020; 2020:9285317.
31. Badawy Y, Spector A, Li Z, Desai R. The risk of depression in the menopausal stages: A systematic review and meta-analysis. J Affect Disord. 2024; 357:126-133.
32. Cohen LS, Soares CN, Vitonis AF, Otto MW, Harlow BL. Risk for new onset of depression during the menopausal transition: The Harvard study of moods and cycles. Arch Gen Psychiatry. 2006; 63:385-390.
33. Nagda AL, Datar MC, Naphade NM, Shetty JV. A cross-sectional assessment of depression, anxiety, and cognition in perimenopausal and menopausal women. J Midlife Health. 2023; 14:117-122.
34. Windsor JS, Rodway GW. Sleep disturbance at altitude: Current opinion in pulmonary medicine. 2012; 18:554-560.
35. Brebner K, Hayley S, Zacharko R, Merali Z, Anisman H. Synergistic effects of interleukin-1beta, interleukin-6, and tumor necrosis factor-alpha: Central monoamine, corticosterone, and behavioral variations. Neuropsychopharmacology. 2000; 22:566-580.
36. Kami-shoyo-san, a herbal medicine, reduces plasmainterleukin-6 (lL-6) and soluble I-6 receptorconcentrations in depressive climacteric women. J Trad Med. 2003; 20:150-155.
37. Ushiroyama T, Ikeda A, Sakuma K, Ueki M. Changes in serum tumor necrosis factor (TNF-alpha) with kami-shoyo-san administration in depressed climacteric patients. Am J Chin Med. 2004; 32:621-629.
38. Terauchi M, Hiramitsu S, Akiyoshi M, Owa Y, Kato K, Obayashi S, Matsushima E, Kubota T. Effects of three Kampo formulae: Tokishakuyakusan (TJ-23), Kamishoyosan (TJ-24), and Keishibukuryogan (TJ-25) on Japanese peri- and postmenopausal women with sleep disturbances. Arch Gynecol Obstet. 2011; 284:913-921.
39. Matsuo A, Koike K, Hoshina Y. Study of the efficacy of unkeito for depressive and anxiety symptoms during menopause that are refractory to hormone replacement therapy. Recent Progress of Kampo Medicine in Obstetrics

and Gynecology. 2005; 22:70-74. (in Japanese)
40. Japan Society for Oriental Medicine, EBM Committee. Guidelines for the management and treatment of sleep disorders, 3rd edition. *https://www.jsom.or.jp/medical/ebm/cpg/pdf/Issue/TypeC/20190625.pdf* (accessed April 25, 2025).
41. Mizoguchi K, Ikarashi Y. Multiple psychopharmacological effects of the traditional Japanese Kampo medicine Yokukansan, and the brain regions it affects. Front Pharmacol. 2017; 8:149.
42. Ohno R, Miyagishi H, Tsuji M, Saito A, Miyagawa K, Kurokawa K, Takeda H. Yokukansan, a traditional Japanese herbal medicine, enhances the anxiolytic effect of fluvoxamine and reduces cortical 5-HT2A receptor expression in mice. J Ethnopharmacol. 2018; 216:89-96.
43. Aizawa R, Kanbayashi T, Saito Y, Ogawa Y, Sugiyama T, Kitajima T, Kaneko Y, Abe M, Shimizu T. Effects of Yoku-kan-san-ka-chimpi-hange on the sleep of normal healthy adult subjects. Psychiatry Clin Neurosci. 2002; 56:303-304.
44. Koike K, Yamamoto Y, Suzuki N, Yamazaki R, Yoshikawa C, Takano F, Takuma K, Sugiura K, Inoue M. Efficacy of porcine placental extract on climacteric symptoms in peri- and postmenopausal women. Climacteric. 2013; 16:28-35.
45. Takamatsu K, Fujii E, Mizuno H, *et al.* An investigation of the usefulness of nyoshinsan for climacteric disorder. Recent Progress of Kampo Medicine in Obstetrics and Gynecology. 2003; 20:95-100. (in Japanese)
46. Anarte MT, Cuadros JL, Herrera J. Hormonal and psychological treatment: Therapeutic alternative for menopausal women? Maturitas. 1998; 29:203-213.
47. Welton AJ, Vickers MR, Kim J, Ford D, Lawton BA, MacLennan AH, Meredith SK, Martin J, Meade TW; WISDOM team. Health related quality of life after combined hormone replacement therapy: Randomised controlled trial. BMJ. 2008; 337:a1190.
48. Kaufert PA, Gilbert P, Tate R. The Manitoba Project: A re-examination of the link between menopause and depression. Maturitas. 2008; 61:54-66.
49. Dickins KA, Looby SE. Behavioral and psychological health inequities in income disparate perimenopausal women: A brief report. Menopause. 2020; 28:86-92.
50. Nayak S, Edwards DL, Saleh AA, Greenspan SL. Systematic review and meta-analysis of the performance of clinical risk assessment instruments for screening for osteoporosis or low bone density. Osteoporos Int. 2015; 26:1543-1554.
51. Jilka RL, Hangoc G, Girasole G, Passeri G, Williams DC, Abrams JS, Boyce B, Broxmeyer H, Manolagas SC. Increased osteoclast development after estrogen loss: Mediation by interleukin-6. Science. 1992; 257:88-91.
52. Sarin J, DeRossi SS, Akintoye SO. Updates on bisphosphonates and potential pathobiology of bisphosphonate-induced jaw osteonecrosis. Oral Dis. 2008; 14:277-285.
53. Odvina CV, Zerwekh JE, Rao DS, Maalouf N, Gottschalk FA, Pak CYC. Severely suppressed bone turnover: A potential complication of alendronate therapy. J Clin Endocrinol Metab. 2005; 90:1294-1301.
54. Ikeda R, Mizoguchi K. Hachimijiogan (Ba-Wei-Di-Huang-Wan), a herbal medicine, improves unbalance of calcium metabolism in aged rats. J Ethnopharmacol. 2009; 124:176-181.
55. Hidaka S, Okamoto Y, Nakajima K, Suekawa M, Liu SY. Preventive effects of traditional Chinese (Kampo) medicines on experimental osteoporosis induced by ovariectomy in rats. Calcif Tissue Int. 1997; 61:239-246.
56. Chen H, Wu M, Kubo K ya. Combined treatment with a traditional Chinese medicine, Hachimi-jio-gan (Ba-Wei-Di-Huang-Wan) and alendronate improves bone microstructure in ovariectomized rats. J Ethnopharmacol. 2012; 142:80-85.
57. Fang K, Murakami Y, Kanda S, Shimono T, Dang AT, Ono M, Nishiyama T. Unkeito suppresses RANKL-mediated osteoclastogenesis *via* the Blimp1-Bcl6 and NF-κB signaling pathways and enhancing osteoclast apoptosis. Int J Mol Sci. 2022; 23:7814.
58. Kanai S. The effect of kami-kihi-to on the maintenance of bone mass in patients with osteoporosis. Japanese Journal of Oriental Medicine. 1998; 49:59-66. (in Japanese)
59. Ohta H, Nemoto K. Combined effect of vitamin D3 and TSUMURA Keishibukuryogan on osteopenia following oophorectomy. Kampo Igaku. 1989; 13:173-179. (in Japanese)
60. Hattori T, Fei W, Kizawa T, Nishida S, Yoshikawa H, Kishida Y. The fixed herbal drug composition "Saikokaryukotsuboreito" prevents bone loss with an association of serum IL-6 reductions in ovariectomized mice model. Phytomedicine. 2010; 17:170-177.
61. Blümel JE, Danckers L. International climacteric research: Role of the Collaborative Group for Research of the Climacteric in Latin America (REDLINC). Maturitas. 2011; 70:207.
62. Blümel JE, Chedraui P, Baron G, *et al*. Menopause could be involved in the pathogenesis of muscle and joint aches in mid-aged women. Maturitas. 2013; 75:94-100.
63. Szoeke CEI, Cicuttini F, Guthrie J, Dennerstein L. Self-reported arthritis and the menopause. Climacteric. 2005; 8:49-55.
64. Kogure T, Harada N, Yamamoto K, Tatsumi T. Traditional herbal (kampo) medicine for musculoskeletal symptoms in menopausal women. Traditional & Kampo Medicine. 2016; 3:177-180.
65. Sul JU, Kim MK, Leem J, Jo HG, Yoon SH, Kim J, Lee EJ, Yoo JE, Park SJ, Kim YI, Kim E, Jung IC, Jeon JH, Park YC. Efficacy and safety of gyejigachulbutang (Gui-Zhi-Jia-Shu-Fu-Tang, Keishikajutsubuto, TJ-18) for knee pain in patients with degenerative knee osteoarthritis: A randomized, placebo-controlled, patient and assessor blinded clinical trial. Trials. 2019; 20:140.
66. Majima T, Inoue M, Kasahara Y, Onodera T, Takahashi D, Minami A. Effect of the Japanese herbal medicine, Boiogito, on the osteoarthritis of the knee with joint effusion. Sports Med Arthrosc Rehabil Ther Technol. 2012; 4:3.
67. Liu L, Resch K, Kaever V. Inhibition of lymphocyte proliferation by the anti-arthritic drug sinomenine. Int J Immunopharmacol. 1994; 16:685-691.
68. Kogure T, Tatsumi T, Shigeta T, Fujinaga H, Sato T, Niizawa A. Effect of kampo medicine on pain and range of motion of osteoarthritis of the hip accompanied by acetabular dysplasia: Case report and literature review. Integr Med Insights. 2011; 6:13-17.
69. Fujitsuka N, Tamai M, Tsuchiya K, Iizuka S, Tsuchiya N, Makino B, Hattori T, Kase Y, Isohama Y. Boiogito, a Kampo medicine, improves hydrarthrosis in a rat model of knee osteoarthritis. BMC Complement Altern Med. 2015; 15:451.
70. Japan Bio Products Co., Ltd. LAENNEC. *https://*

jbpglobal.placenta.co.jp/medical_products/laennec/ (accessed April 25, 2025).
71. Koike K, Yamamoto Y, Suzuki N, Yamazaki R, Yoshikawa C, Takano F, Sugiura K, Inoue M. Efficacy of porcine placental extract on shoulder stiffness in climacteric women. Climacteric. 2013; 16:447-452.
72. Wang YXJ. Menopause as a potential cause for higher prevalence of low back pain in women than in age-matched men. J Orthop Translat. 2017; 8:1-4.
73. Heuch I, Heuch I, Hagen K, Storheim K, Zwart JA. Menopausal hormone therapy, oral contraceptives and risk of chronic low back pain: The HUNT Study. BMC Musculoskelet Disord. 2023; 24:84.
74. Ohta H, Makita K. Lumbago with emphasis on nonspecific lumbago, which obstetricians and gynecologists think is the most common form in women. The Journal of Therapy. 1995; 77:1646-1657. (in Japanese)
75. Sarmento ACA, Costa APF, Vieira-Baptista P, Giraldo PC, Eleutério J, Gonçalves AK. Genitourinary syndrome of menopause: Epidemiology, physiopathology, clinical manifestation and diagnostic. Front Reprod Health. 2021; 3:779398.
76. Palma F, Volpe A, Villa P, Cagnacci A, Writing group of AGATA study. Vaginal atrophy of women in postmenopause. Results from a multicentric observational study: The AGATA study. Maturitas. 2016; 83:40-44.
77. Palacios S, Stevenson JC, Schaudig K, Lukasiewicz M, Graziottin A. Hormone therapy for first-line management of menopausal symptoms: Practical recommendations. Womens Health (Lond). 2019; 15:1745506519864009.
78. Wang Z, Kanda S, Shimono T, Enkh-Undraa D, Nishiyama T. The *in vitro* estrogenic activity of the crude drugs found in Japanese herbal medicines prescribed for menopausal syndrome was enhanced by combining them. BMC Complement Altern Med. 2018; 18:107.
79. Mori N, Urata T. Intragastric administration of cinnamaldehyde induces changes in body ettemperature *via* TRPA1. Biosci Biotechnol Biochem. 2024; 88:196-202.
80. Chen P, Ruan A, Zhou J, Huang L, Zhang X, Ma Y, Wang Q. Cinnamic aldehyde inhibits lipopolysaccharide-induced chondrocyte inflammation and reduces cartilage degeneration by blocking the nuclear factor-kappa B signaling pathway. Front Pharmacol. 2020; 11:949.
81. Ikarashi Y, Mizoguchi K. Neuropharmacological efficacy of the traditional Japanese Kampo medicine yokukansan and its active ingredients. Pharmacol Ther. 2016; 166:84-95.
82. Ikarashi Y, Sekiguchi K, Mizoguchi K. Serotonin receptor binding characteristics of geissoschizine methyl ether, an indole alkaloid in Uncaria hook. Curr Med Chem. 2018; 25:1036-1045.
83. Ueki T, Nishi A, Imamura S, Kanno H, Mizoguchi K, Sekiguchi K, Ikarashi Y, Kase Y. Effects of geissoschizine methyl ether, an indole alkaloid in Uncaria hook, a constituent of yokukansan, on human recombinant serotonin 7 receptor. Cell Mol Neurobiol. 2013; 33:129-135.
84. Nishi A, Yamaguchi T, Sekiguchi K, Imamura S, Tabuchi M, Kanno H, Nakai Y, Hashimoto K, Ikarashi Y, Kase Y. Geissoschizine methyl ether, an alkaloid in Uncaria hook, is a potent serotonin $_{1}$A receptor agonist and candidate for amelioration of aggressiveness and sociality by yokukansan. Neuroscience. 2012; 207:124-136.
85. Kawakami Z, Ikarashi Y, Kase Y. Glycyrrhizin and its metabolite 18 beta-glycyrrhetinic acid in glycyrrhiza, a constituent herb of yokukansan, ameliorate thiamine deficiency-induced dysfunction of glutamate transport in cultured rat cortical astrocytes. Eur J Pharmacol. 2010; 626:154-158.
86. Mersereau JE, Levy N, Staub RE, Baggett S, Zogovic T, Chow S, Ricke WA, Tagliaferri M, Cohen I, Bjeldanes LF, Leitman DC. Liquiritigenin is a plant-derived highly selective estrogen receptor beta agonist. Mol Cell Endocrinol. 2008; 283:49-57.
87. Lestari B, Walidah Z, Utomo RY, Murwanti R, Meiyanto E. Supplementation with extract of pumpkin seeds exerts estrogenic effects upon the uterine, serum lipids, mammary glands, and bone density in ovariectomized rats. Phytother Res. 2019; 33:891-900.
88. Chen CR, Sun Y, Luo YJ, Zhao X, Chen JF, Yanagawa Y, Qu WM, Huang ZL. Paeoniflorin promotes non-rapid eye movement sleep *via* adenosine A1 Receptors. J Pharmacol Exp Ther. 2016; 356:64-73.
89. Wang Y, Zhu Y, Lu S, Hu C, Zhong W, Chai Y. Beneficial effects of paeoniflorin on osteoporosis induced by high-carbohydrate, high-fat diet-associated hyperlipidemia *in vivo*. Biochem Biophys Res Commun. 2018; 498:981-987.
90. Kobayashi K, Tang YT, Sasaki K. Paeoniflorin, a constituent of Kami-shoyo-san, suppresses blood glucose levels in postmenopausal diabetic mice by promoting the secretion of estradiol from adipocytes. Biochem Biophys Rep. 2022; 32:101335.
91. Kang WC, Lee YS *vivo*, Park K, Kong CH, Jeon M, Kim MS, Jung SY, Choi JH, Ryu JH. Paeonol alleviates postmenopause-induced neuropsychiatric symptoms through the modulation of GPR30 in ovariectomized mice. J Ethnopharmacol. 2024; 327:118063.
92. Tsai HY, Lin HY, Fong YC, Wu JB, Chen YF, Tsuzuki M, Tang CH. Paeonol inhibits RANKL-induced osteoclastogenesis by inhibiting ERK, p38 and NF-kappaB pathway. Eur J Pharmacol. 2008; 588:124-133.
93. Wu C, Wang N, Xu P, Wang X, Shou D, Zhu Y. Preparation and application of polyvinyl alcohol-decorated cell membrane chromatography for screening anti-osteoporosis components from Liuwei Dihuang decoction-containing serum. J Sep Sci. 2020; 43:2105-2114.
94. Lee CG, Kim DW, Kim J, Uprety LP, Oh KI, Singh S, Yoo J, Jin HS, Choi TH, Park E, Jeong SY. Effects of loganin on bone formation and resorption *in vitro* and *in vivo*. Int J Mol Sci. 2022; 23:14128.
95. Xiao J, Han Q, Yu Z, Liu M, Sun J, Wu M, Yin H, Fu J, Guo Y, Wang L, Ma Y. Morroniside inhibits inflammatory bone loss through the TRAF6-mediated NF-κB/MAPK signalling pathway. Pharmaceuticals (Basel). 2023; 16:1438.
96. Li TQ, Liu Y, Feng C, Bai J, Wang ZR, Zhang XY, Wang XX. Saikosaponin A attenuates osteoclastogenesis and bone loss by inducing ferroptosis. Front Mol Biosci. 2024; 11:1390257.
97. Kim MH, Ryu SY, Bae MA, Choi JS, Min YK, Kim SH. Baicalein inhibits osteoclast differentiation and induces mature osteoclast apoptosis. Food Chem Toxicol. 2008; 46:3375-3382.
98. Ahmed SA, Gibriel AA, Abdellatif AK, Ebied HM. Evaluation of food products fortified with oyster shell for the prevention and treatment of osteoporosis. J Food Sci Technol. 2015; 52:6816-6820.
99. Xu H, Arita H, Hayashida M, Zhang L, Sekiyama H, Hanaoka K. Pain-relieving effects of processed Aconiti

tuber in CCI-neuropathic rats. J Ethnopharmacol. 2006; 103:392-397.
100. Liu L, Riese J, Resch K, Kaever V. Impairment of macrophage eicosanoid and nitric oxide production by an alkaloid from Sinomenium acutum. Arzneimittelforschung. 1994; 44:1223-1226.
101. Chen J, Chen Y, Li Y, Liu Z. Astragalus polysaccharide inhibits Toll-like receptor 4/nuclear factor kappaB p65 pathway in the treatment of knee osteoarthritis in rats. Chin J Tissue Eng Res. 2023; 27:5002-5008.

Received April 28, 2025; Revised June 5, 2025; Accepted June 19, 2025.

**Address correspondence to:*
Yanming Ren, Department of Public Health, Qinghai University ledical College, No. 16 KunlunRd, Xi-ning 810008, China.
E-mail: btyqh@126.com

Peipei Song, Center for Clinical Sciences, Japan Institute for Health Security, Tokyo, 1-21-1 Toyama Shinjuku-ku, Tokyo 162-8655, Japan.
E-mail: psong@jihs.go.jp

Released online in J-STAGE as advance publication June 25, 2025.

Review

DOI: 10.5582/ddt.2025.01059

Quercetin as a multifaceted therapeutic agent in recurrent pregnancy loss: Mechanisms and clinical perspectives

Qing Qi[1,§], Jing Zhou[2,§], Jing Wang[3,4], Yiyuan Zhou[5], Hongmei Sun[6], Ling Wang[7,4,*]

[1] School of Physical Education, Wuhan Business University, Wuhan, Hubei, China;
[2] Department of Obstetrics and Gynecology, Nanfang Hospital, Southern Medical University, Guangzhou, Guangdong, China;
[3] Hainan Women and Children's Medical Center, Haikou, Hainan, China;
[4] Guizhou University of Traditional Chinese Medicine, Guiyang, Guizhou, China;
[5] Department of Obstetrics, The First Affiliated Hospital of Guizhou University of Traditional Chinese Medicine, Guiyang, Guizhou, China;
[6] School of Clinical Medicine, Hexi University, Zhangye, Gansu, China;
[7] Department of Obstetrics and Reproductive Immunology, Shanghai East Hospital, Tongji University School of Medicine, Shanghai, China.

SUMMARY: In recent years, there has been an escalating incidence of recurrent pregnancy loss (RPL), imposing substantial psychosocial and economic burdens on families. Despite extensive investigations, approximately 50% of cases remain idiopathic, underscoring the intricate nature of potential pathogenic mechanisms. Quercetin (QUE), a prevalent flavonoid compound, exhibits potential in the therapeutic modulation of RPL by influencing endocrine, coagulation, oxidative stress, inflammation, and immune responses. This review aims to elucidate the potential role of QUE in RPL, explore its molecular mechanisms, and delineate its therapeutic significance. Herein, we synthesize existing evidence on the impact of QUE in RPL, particularly in traditional Chinese medicine, accentuating areas necessitating further exploration. QUE demonstrates regulatory prowess over RPL by modulating endocrine functions, encompassing thyroid functionality, diabetes, polycystic ovary syndrome, and luteal phase defects. It exhibits anti-inflammatory and antioxidant properties, influences coagulation functions, and affects immune cells such as T cells, T helper cells, macrophages, and natural killer cells. QUE also interacts with maternal-fetal interface cells, including myeloid-derived suppressor cells, stromal cells, and extravillous trophoblast cells, highlighting its multifaceted role in the modulation of RPL. Despite promising preclinical data, clinical trials directly targeting RPL remain limited. We emphasize the need for rigorous human studies to validate QUE's efficacy and safety in pregnancy. By elucidating the mechanistic underpinnings of QUE in treating RPL, this research may contribute to developing targeted interventions for RPL and other adverse pregnancy conditions, ultimately ameliorating reproductive health and well-being for affected individuals and families.

Keywords: endocrine, coagulation, inflammation, oxidative stress, maternal-fetal interface

1. Introduction

Recurrent pregnancy loss (RPL) is defined as the occurrence of two or more consecutive fetal losses with the same sexual partner before 28 weeks of gestation. With the increasing trend of women delaying childbirth and the implementation of policies such as China's "comprehensive two-child" and "three-child" policies, the incidence of RPL has been rising each year (*1*). It has become a significant health issue both nationally and globally. Globally, RPL affects 1–5% of couples, with rising incidence linked to delayed childbearing. The etiology of RPL is complex and diverse, and its clinical manifestations are nonspecific, making the diagnosis and treatment challenging. The treatment of RPL mainly focuses on addressing the causative factors and managing symptoms. The routine use of low molecular weight heparin, either alone or in combination with low-dose aspirin, may be prescribed during early pregnancy for RPL patients with positive thrombophilia screening (PTS), aiming to improve pregnancy outcomes. Assisted reproductive technology can also be utilized to address fertility issues caused by chromosomal abnormalities in RPL patients, among other treatments. However, some of these treatments can be costly and may result in adverse effects such as bleeding, gastrointestinal reactions, liver function abnormalities, and allergies. Moreover, the overall efficacy of these treatments is not always satisfactory. It is important to continue researching and exploring more effective and safer treatment options for RPL to improve patient outcomes and reduce the burden of this condition.

Traditional Chinese medicine (TCM) has a long history and extensive experience in treating RPL. Quercetin (QUE) is a flavonoid compound in everyday vegetables and fruits such as red onions, apples, broccoli, red grapes, and citrus. It is also present in various TCMs like santolina, scutellaria baicalensis, and acacia (*2*). Chemically, it is known as 3,3',4',5,7-pentahydroxyfla vonoids, with a molecular formula of $C_{15}H_{10}O_7$. Figure 1 depicts its structural formula. QUE exhibits favorable therapeutic efficacy, low toxicity, and multiple biological functions. It acts as an antioxidant, anti-inflammatory agent, chelator of iron, and regulator of lipid metabolism (*3,4*). In addition, QUE has been shown to have relatively few toxic side effects. However, in terms of treating RPL, despite the promising research prospects of QUE, clinical trial data directly targeting RPL remains scarce. To address this gap, we can draw inspiration from the ancient and rich repository of TCM. Many of these formulas contain herbs rich in QUE, such as *Cuscuta sinensis* and *Sambucus nigra* (*5,6*). These herbs have a long history of tonifying the kidneys, securing the fetus, and regulating reproductive health, contributing to improved pregnancy outcomes (*7*). In conclusion, investigating the potential role of QUE in RPL and understanding its associated mechanisms could offer new insights into this condition's clinical prevention and treatment.

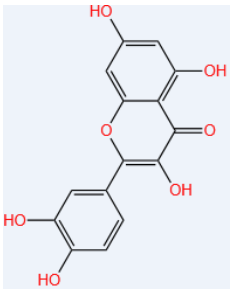

Figure 1. The structural formula of quercetin.

2. Clinical treatment containing QUE

In modern clinical practice, TCMs frequently used to prevent miscarriage include Yi Qi Bu Shen Fang (*8*) and Shou Tai Wan (*9*). Zi Shen Yu Tai pill employs *Cuscuta chinensis* to fortify the kidneys and secure the fetus, with additional herbs like *Taxillus chinensis*, *Dipsacus asperoides*, and *Eucommia ulmoides* to bolster kidney Yang and Qi. *Codonopsis pilosula* and *Atractylodes macrocephala* augment Qi and strengthen the Pi, while *Rehmannia glutinosa* and *Lycium barbarum* nourish the blood and calm the fetus. This formula has been shown to effectively alleviate traditional Chinese medical symptoms during pregnancy and elevate serum progesterone levels (*10,11*). Similarly, Jia Wei Shou Tai pill prominently features *Cuscuta chinensis*, complemented by *Dipsacus asperoides*, *Taxillus chinensis*, and donkey-hide gelatin, to improve levels of progesterone and human chorionic gonadotropin during pregnancy (*12*). In these miscarriage-preventing formulas, *Cuscuta chinensis* and *Taxillus chinensis* often play a crucial role, with QUE identified as a significant active component in these kidney-tonifying herbs through liquid chromatography-mass spectrometry (*13,14*), sparking interest in their potential to enhance pregnancy outcomes.

Innovations upon traditional prescriptions for treating RPL have led scholars to develop the "Bushen-Yiqi-Lixue-Yangtai" (BYLY) compounds used to prevent and treat RPL (*15*). A clinical trial with 480 patients revealed that the combination of Duphaston and BYLY markedly reduced early miscarriage rates compared to BYLY or Duphaston alone, suggesting significant benefits and improved pregnancy outcomes. This regimen incorporates various herbs rich in QUE, such as *Paeonia lactiflora* Pall. and *Cuscuta chinensis*. The mass spectrometry analysis verified that the key component of the compound above is QUE. Besides, network pharmacology studies further identified QUE as a key molecule in BYLY's treatment of RPL, and cellular experiments showed that QUE enhanced the biological function of trophoblast cells under hypoxic conditions. This clinical evidence from widely used herbal medicines underscores QUE's potential as a therapeutic agent for RPL. Table 1 summarises clinical trials involving QUE for the treatment of RPL, where the key component of the primary drugs used in the clinical trials is QUE (*10,15-20*). These clinical studies have limited sample sizes and exhibit heterogeneity in herbal formulations, indicating that QUE's therapeutic use requires more direct clinical validation (*21*).

3. QUE improves endocrine function

Endocrine dysfunction plays a significant role in the occurrence of RPL, with approximately 8% to 12% of endocrine alterations associated with RPL (*22,23*). Although various endocrine factors can cause RPL, many underlying mechanisms remain unclear. Several endocrine disorders have been identified as possible contributors to RPL, including thyroid dysfunction, diabetes, polycystic ovary syndrome (PCOS), and luteal insufficiency. These conditions can adversely affect oocyte quality and endometrial tolerance, increasing the risk of RPL. Additionally, they may induce a prothrombotic state, further elevating the likelihood of experiencing recurrent miscarriage.

3.1. QUE regulates thyroid function

Maternal influences on the production, secretion, and metabolism of thyroid hormone (TH) during pregnancy can significantly increase the incidence of thyroid disease (*24*). Abnormal thyroid function has been found to affect

Table 1. Clinical trials using QUE-containing drugs for the treatment of miscarriage

No.	Research Title	Experimental Design	Sample Size	Medicine	Experimental Period	Results
1	Zishen yutai pill as an adjuvant therapy in threatened Miscarriage: A meta-analysis of 23 randomized controlled trials (*10*)	Meta-analysis	2411	Zishen yutai pill & Western medicine	14d	Significantly improved human chorionic gonadotropin, the total effective rate, progesterone, estradiol, abdominal pain, vaginal bleeding, and fibrinogen
2	The effect of a traditional Chinese quadri-combination therapy and its component quercetin on recurrent pregnancy loss: A clinical trial, network pharmacology, and experiments-based study (*15*)	RCT	480	Duphaston & BYLY	14-28d	The early miscarriage rate was 10.62% in the Duphaston+BYLY group, 29.17% in the BYLY group, and 29.06% in the Duphaston group
3	Clinical Efficacy of Bushen Antai Decoction in Patients with Kidney Deficiency-Type RPL (*16*)	RCT	260	Bushen Antai Decoction & Dydrogesterone	<12 weeks in gestational age	The integrated group reached 93.1%, the pure TCM group 74.4%, and the pure Western medicine group 73.6%
4	Effect of Yiqi Bushen & Progesterone on RPL in Kidney Deficiency Threatened Abortion and Hormone Levels (*17*)	RCT	102	Yiqi Bushen & Progesterone	14d	The research group's fetal protection rate was 93.88%, higher than the control's 79.17%
5	Clinical Observation on the Treatment of RPL-PTS by Bushen Huoxue Recipe (*18*)	RCT	146	Bushen Huoxue Recipe & Low molecular weight heparin.	<12 weeks in gestational age	The integrated group reached 90.9%, the pure TCM group 74.4%, and the pure Western medicine group 52.6%
6	Efficacy of Modified Shoutai Pill in the Treatment of RPL and Its Impact on Coagulation Function and Th17 Cell-Related Factors (*19*)	Retrospective study	120	Modified Shoutai Pill & Progesterone	<12 weeks in gestational age	The research group's effective rate was 90.48%, higher than control's 75.44%
7	Effect of Jiawei Shoutai pills combined with dydrogesterone on pregnancy outcome of kidney-deficiency early threatened abortion after tocolytic therapy (*20*)	RCT	92	Jiawei Shutai Pill & Dydrogesterone	14d	The research group's fetal protection rate was 95.65%, higher than the control's 80.43%

pregnancy outcomes at both endocrine and immune levels and is considered a risk factor for RPL (*25*).

3.1.1. Hyperthyroidism

Hyperthyroidism increases the risk of RPL. Excessive TH in the bloodstream can lead to increased neuromuscular excitability, elevated secretion of norepinephrine and angiotensin, vasospasms, and contractions, ultimately resulting in miscarriage (*26*). QUE has been found to directly inhibit hyperthyroidism by activating the Nrf2 signaling pathway. Furthermore, QUE exhibits antihypertensive effects and acts as an effective angiotensin-converting enzyme inhibitor (ACEI), further mitigating vascular and contractile complications associated with hyperthyroidism. Besides, QUE also influences TH metabolism by inhibiting deiodinases, enzymes critical for TH activation (*27*). These findings highlight the potential therapeutic benefits of QUE in addressing thyroid-related reproductive complications.

3.1.2. Hypothyroidism

Hypothyroidism is often associated with hypoprolactinemia, which can lead to follicular hypoplasia and luteal insufficiency (*28*). This results in inadequate production of steroid hormones, which are necessary to maintain the endometrium during the secretory phase. Insufficient hormonal support can lead to early miscarriage. Studies have shown that QUE exhibits an anti-thyroid effect by inhibiting thyroid cell growth and suppressing the expression of key thyroid-related proteins, including the sodium/iodide symporter, thyroglobulin, thyroid peroxidase, and thyroid-stimulating hormone receptor (*29*). Although no studies have specifically investigated QUE's effects in hypothyroidism models, it is hypothesized that QUE may exacerbate hypothyroidism. Therefore, the severity of hypothyroidism should be carefully evaluated when considering QUE in clinical applications.

3.2. Diabetes

Diabetes, whether in the form of pre-existing diabetes combined with gestational syndrome or gestational diabetes mellitus, is a common metabolic disorder that can have significant impacts on pregnancy outcomes. Insulin resistance (IR) is a characteristic feature of diabetes where the body's response to insulin is reduced, leading to elevated blood glucose levels and compensatory hyperinsulinemia (*30*). Poor control of blood glucose during pregnancy increases the risk and incidence of RPL, as well as adverse clinical outcomes for both the mother and infant (*31*). QUE has been extensively studied for its potential therapeutic effects on diabetes. Numerous studies have reported its antidiabetic activity (*32-35*), primarily due to its ability to improve IR. QUE has shown efficacy in significantly improving insulin sensitivity and glucose uptake. Additionally, QUE has been found to enhance oocyte and embryo quality in diabetic mouse models (*36*) and improve endometrial tolerance (*37*) in the diabetes animal model.

3.3. Polycystic ovarian syndrome (PCOS)

PCOS is an endocrine disorder that serves as a risk factor for RPL. Hyperinsulinemia/IR, high androgen levels, and obesity are the main factors contributing to RPL in individuals with PCOS. Studies have shown the therapeutic effects of QUE in animal models of PCOS (*38,39*). QUE has demonstrated significant attenuation of PCOS-induced IR, sex hormone disorders, and ovulatory abnormalities. In addition to hyperinsulinemia/IR, high androgen levels, and obesity, other factors such as elevated luteinizing hormone (LH) levels, hyperhomocysteinemia, and a prethrombotic state complement reinforce the development of RPL in PCOS. QUE has been found to possess inhibitory effects on LH levels (*40*). Although there are no specific reports on the association between QUE and hyperhomocysteinemia, some studies have indicated that QUE protects against homocysteinemia-induced oxidative stress in rats (*41*). These findings suggest a potential positive role for QUE in managing hyperhomocysteinemia.

3.4. Potential effects of QUE in luteal phase defect (LPD)

LPD is closely associated with miscarriage and is characterized by reduced endometrial secretory responsiveness caused by issues such as post-ovulatory luteal dysplasia, insufficient progesterone secretion, or premature degeneration of the corpus luteum (*42*). LPD leads to a decreased ability of the endometrium to support implantation and maintain pregnancy. Although there are limited reports on the association between QUE and LPD, researchers have conducted studies using a Bu-shen-zhu-yun decoction in rats, significantly improving LPD. It is worth noting that the serum level of QUE was elevated in the treatment group compared to the rats in the control group (*43*), suggesting that QUE may have beneficial effects in improving LPD and potentially reducing the risk of RPL by addressing the underlying factors contributing to LPD.

3.5. Potential effects of QUE in hormone supplementation

The researchers discovered that supplementation of progesterone, progestogen, and human chorionic gonadotropin can reduce the abortion rate in patients with RPL and increase the live birth rate (*44,45*). QUE has been shown to upregulate steroid hormone levels and improve ovarian function (*46*), indicating its potential role in hormone modulation. Notably, reports indicate

that QUE can promote the release of progesterone and progestogen from ovarian granulosa cells (*47,48*) and stimulate progesterone release from preovulatory follicles (*49*). These findings highlight the promising role of QUE in hormonal regulation and its potential as a therapeutic approach for individuals with RPL.

Individuals with a history of RPL undergo comprehensive endocrine evaluations to identify any underlying hormonal abnormalities and address them accordingly. Based on the existing research foundation, it can be speculated that QUE may help regulate endocrine function and reduce the risk of complications associated with RPL (Figure 2).

4. QUE improves coagulation

PTS, characterized by increased blood coagulation and a higher risk of thrombus formation, has gained significant attention in its association with RPL. While there is currently a lack of specific reports on the relationship between QUE and the prethrombotic state, a review of the literature reveals that QUE has demonstrated the ability to inhibit the mRNA level of plasminogen activator inhibitor 1, a key substance involved in the prethrombotic state. This inhibitory effect has been observed in a dose- and time-dependent manner (*50,51*), suggesting a potential role for QUE in inhibiting the process of thrombus formation. In addition, some studies have reported the regulatory role of QUE in coagulation function. For example, in treating patients with COVID-19, QUE can reduce coagulation abnormalities and inhibit thrombosis by inhibiting blood protein disulfide isomerase (*52*). In a neonatal asthma rat model, QUE can protect neonatal asthma by reducing coagulation time and coagulation factor activity (*53*). These findings highlight the potential of QUE as both a preventive and therapeutic agent in modulating coagulation processes and mitigating complications associated with PTS and related conditions.

5. QUE's antioxidant properties

QUE is a potent free radical scavenger among flavonoids. Due to the presence of phenolic hydroxyl groups and double bonds, it exhibits significant antioxidant activity (*54*). The catechol group on the B ring and the hydroxyl group at position three on the A ring collectively contribute to QUE's antioxidant characteristics (*55*). The hydroxyl groups in QUE's structure deactivate free radicals by donating active hydrogen, thereby oxidizing and stabilizing them, preventing unsaturated fatty acid oxidation (*56*). Due to its chemical structure, QUE can scavenge various free radicals, including ROS, RNS, H_2O_2, superoxide, and hydroxyl radicals (*57*). Oxidative stress levels are elevated in the plasma and placentas of patients with RPL (*58*), and researchers speculate that oxidative damage caused by increased production of oxidative substances and weakened antioxidant defenses might contribute to RPL (*59*). Compared to the control group, women with recurrent miscarriages show increased spontaneous chemiluminescence in granulocytes, confirming heightened leukocyte free radical production (*60*). Plasma samples from patients with RPL also show a marked increase in superoxide anion radicals and H_2O_2 (*61*). These findings suggest that QUE may potentially ameliorate oxidative stress in patients with RPL.

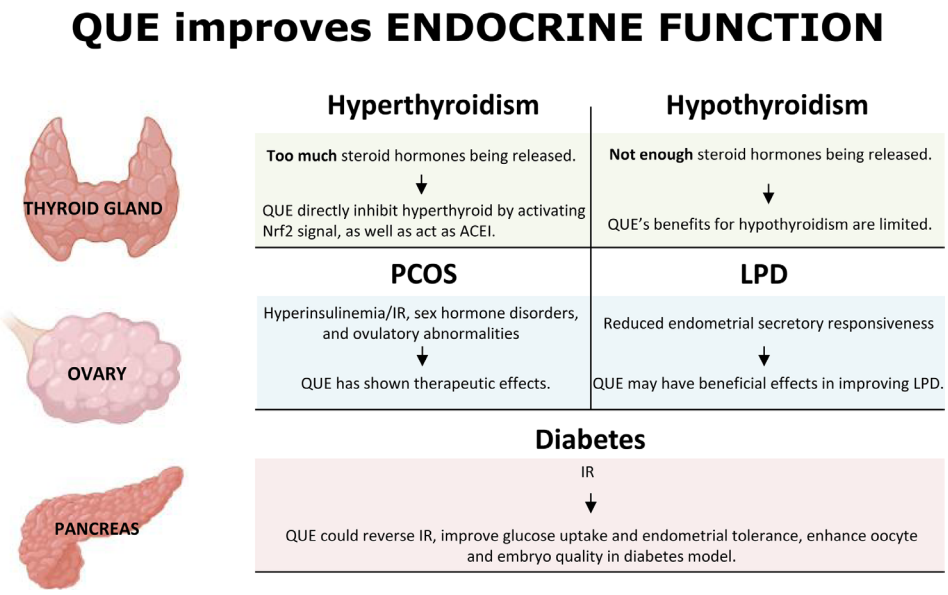

Figure 2. Mechanisms of quercetin in improving endocrine function in various conditions relevant to recurrent pregnancy loss. QUE: quercetin; Nrf2: nuclear factor erythroid 2-related factor 2; ACEI: angiotensin-converting enzyme inhibitor; PCOS: polycystic ovary syndrome; LPD: luteal phase defect; IR: insulin resistance.

6. QUE regulates gut microbiota

Dysbiosis of the gut microbiota is increasingly recognized as a potential risk factor for inflammation and the development of autoimmune and immune-mediated diseases. In patients who have experienced miscarriage, serum levels of interleukin 2 (IL2), IL17A, IL17F, tumor necrosis factor alpha (TNF alpha), and interferon gamma (IFN gamma) are significantly elevated, indicating a predisposition toward inflammation through Th1 and Th17-mediated immunity (*62*). A randomized controlled study analyzing fecal microbiota revealed a marked reduction in microbial diversity and the relative abundance of *Prevotella_1*, *Prevotellaceae_UCG_003*, and *Selenomonas_1* in RPL cases, which leads to a decrease in inducible Tregs and the activation of pro-inflammatory cells. This research further suggests a correlation between reduced gut microbial diversity and increased pro-inflammatory cytokines in miscarriage patients (*63*).

QUE has been reported to enhance gut microbial diversity and restore microbial symbiosis, thereby alleviating colitis in mouse models of *Citrobacter rodentium* infection and dextran sulfate sodium salt-induced colitis (*64,65*). Specifically, QUE supplementation promotes the enrichment of *Bacteroides*, *Bifidobacterium*, *Lactobacillus*, and *Clostridium*, while significantly reducing the abundance of *Fusobacterium* and *Enterococcus*, indicating a profound impact on the composition of the gut microbiota (*66*).

Although no studies have directly investigated the effects of QUE on the gut microbiota of RPL patients, given its ability to restore gut microbial balance and the crucial role of gut microbiota in shaping and regulating the immune system and immune responses, QUE may potentially alleviate RPL by modulating the gut microbiota. While QUE restores gut microbiota in colitis models, its role in RSA-related dysbiosis remains speculative. Future studies should profile fecal microbiota in RSA patients pre/post-QUE intervention.

7. QUE regulates inflammatory responses and immune cells

7.1. QUE's anti-inflammatory properties

Chronic endometritis (CE) is a persistent, mild inflammation of the endometrium. Although a subtle condition, the prevalence of CE is notably higher in women with infertility, implantation failure, and RPL (*67,68*). Women with a history of RPL and untreated CE show a very low live birth rate (7%). However, after treatment and resolution of CE, the sustained pregnancy rate significantly improves (*69*).

Various studies on cell and animal models have demonstrated that QUE possesses anti-inflammatory properties. *In vitro* research on guinea pig epithelial cells revealed that QUE inhibits the production of pro-inflammatory enzymes, such as cyclooxygenase and lipoxygenase (*70*). The anti-inflammatory activity of QUE is primarily attributed to its ability to suppress pro-inflammatory cytokines, such as nuclear factor kappa B, TNF alpha, IL 6, and IL1 beta, and inflammatory mediators like catalase and nitric oxide (*71*). In cases of CE, the overexpression of IL1 beta, IFN gamma, and TNF alpha suggests that QUE may alleviate CE by inhibiting the expression of these pro-inflammatory factors, ultimately improving sustained pregnancy rates.

In vitro studies indicate that QUE exhibits both anti-inflammatory and immune-enhancing effects. However, a double-blind, placebo-controlled, randomized trial revealed that, although daily supplementation with 500 or 1000 mg of QUE for 12 weeks significantly increased plasma QUE levels in adult women in the UK community, it had no impact on innate immune function or inflammatory markers. Further validation is needed to confirm QUE's role as an immune modulator in humans (*72*).

7.2 QUE regulates immune cells

The immune system plays a crucial role in maternal-fetal immune tolerance, which is necessary for a successful pregnancy. Abnormalities in immune cells, specifically T cells, dendritic cells (DCs), macrophages, and natural killer (NK) cells, have been implicated in RPL (Figure 3).

7.2.1. T cells

T-cell receptors stimulate the differentiation of primitive $CD4^+$ T cells into specific subsets, such as T helper 1 (Th1), Th2, Th7, Th17, Th22, and follicular Th cells, each playing a distinct role in pregnancy (*73*). Imbalances in the Th1/Th2 ratio, with an increase in Th1 cells and a decrease in Th2 cells, may contribute to recurrent miscarriage. Th1 cells release pro-inflammatory factors like IFN gamma and TNF beta, promoting inflammation at the maternal-fetal interface (*74*). Maintaining a standard Th17/Treg ratio is essential for a healthy pregnancy. Imbalances in this ratio have been associated with early recurrent miscarriages (*75,76*). Treg cells exhibit anti-inflammatory and immunosuppressive effects through cytokine secretion and contact-dependent inhibition, while Th17 cells release pro-inflammatory factors like IL17, IL6, IL22, and TNF alpha. Existing studies suggest that QUE can improve the balance of Th1/Th2 (*77,78*) and Th17/Treg (*79,80*) ratios in various allergic diseases, indicating its potential benefit in RPL by modulating T cell function.

7.2.2. DCs

DCs, accounting for approximately 1% to 2% of immune cells in the metaphase, serve a dual role as powerful antigen-presenting cells and activators of

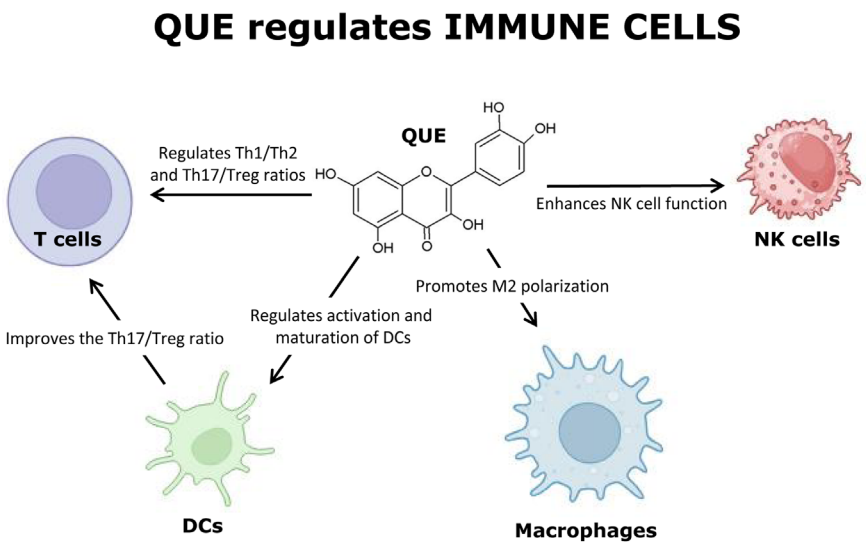

Figure 3. Immunomodulatory effects of QUE on key immune cells in recurrent pregnancy loss. QUE: quercetin; DCs: dendritic cells; NK: natural killer; Th: T helper.

effector T cells to mediate cellular immune responses. Immature DCs can promote immune tolerance by inducing the generation of differentiated Tregs. Research has confirmed the significant role of DCs in maternal recognition of paternal antigens (*81*). In response to specific cytokines like GM-CSF, IL-4, IL-10, TGF beta, and IDO, decidual DCs acquire a tolerogenic phenotype known as tolerogenic DCs. These tDCs are capable of driving Th0 cell differentiation into Tregs. Additionally, DCs have been shown to promote the differentiation and proliferation of endometrial mesenchymal stromal cells and local angiogenesis (*82*). In the relevant literature, QUE has been reported to possess inhibitory effects on the activation and maturation of DCs, thereby exhibiting anti-inflammatory properties and preventing the progression of atherosclerosis (*83*). Based on these existing reports, it can be hypothesized that QUE may inhibit the inflammatory response in RPL by directly acting on DCs. Furthermore, QUE might benefit RPL by influencing T cells through DCs, promoting their differentiation into Tregs, and improving the Th17/Treg ratio.

7.2.3. Macrophages

Macrophages can be categorized into M1 and M2 subtypes, with M1 promoting inflammation and M2 supporting normal pregnancy. The balance between M1 and M2 macrophages is crucial for maintaining pregnancy (*84*). At the maternal-fetal interface, the ratio of M1/M2 macrophages changes during different stages of pregnancy. Initially, M1-type macrophages predominate in the periamputation period, then transition to a mixed population of M1 and M2 macrophages. After the establishment of the placenta, M2-type macrophages become dominant (*85*). An imbalance, with a significant increase in M1-type macrophages or a decrease in M2-type macrophages, can lead to RPL (*86*). QUE has been reported to inhibit M1-type macrophage polarization and promote M2-type macrophage polarization, suggesting its therapeutic potential in inflammatory disorder-related diseases (*87*).

7.2.4. NK cells

NK cells are present in various sites within the female reproductive system, including cNK cells in peripheral blood, trNK cells in tissues, and uNK cells in the uterus, primary immune cells at the maternal-fetal interface, and crucial for early embryonic development. Abnormalities such as excessive aggregation of uNK cells in early pregnancy, abnormal cytotoxicity, or decreased secretion of growth-promoting factors by cNK and metaphase NK cells can contribute to RPL (*88-90*). Although specific reports on the relationship between QUE and NK cells at different sites are limited, existing studies have indicated that QUE can enhance NK cell function (*91,92*). This suggests the potential therapeutic role of QUE in regulating NK cell function and its potential benefit in RPL.

While the existing literature supports the notion that QUE may modulate the function of immune cells, further research is needed to fully understand the mechanisms and evaluate the efficacy of QUE in managing immune cell abnormalities associated with RPL.

8. QUE regulates other cells at the maternal-fetal interface

8.1. Decidual myeloid-derived suppressor cells (MDSCs)

Myeloid-derived suppressor cells are a novel, heterogeneous group of immunosuppressive cells originating from myeloid progenitors and can be subdivided into monocytic and granulocytic subtypes. In the murine decidua, they are second in abundance

only to uterine NK cells (*93*). Various factors, such as estrogen, progesterone, hypoxic conditions, the HLA-G/ILT4 signaling axis, as well as the STAT3 and CXCR2 signaling pathways, collectively promote the differentiation and accumulation of MDSCs at the maternal-fetal interface (*94*). MDSCs maintain immune tolerance at this interface by inhibiting the proliferation of DCs and T cells and by promoting the generation of Tregs (*95*). Research also indicates that QUE can enhance the survival of MDSCs and stimulate the secretion of T cell inhibitory factors *in vitro*, thereby negatively regulating immune responses (*96*). Additionally, the Bushen Antai recipe has been shown to mobilize MDSCs in miscarriage-prone mice, enhancing immune tolerance and angiogenesis at the maternal-fetal interface, thereby alleviating miscarriage-related issues (*97*).

8.2. Decidual stromal cells (DSCs)

DSCs are a significant component of the decidua at the maternal-fetal interface, playing a crucial role in immune regulation through the secretion of various cytokines (*98*). Compared to patients with normal pregnancies, DSCs in RPL patients exhibit accelerated senescence, increased oxidative stress, and inhibited proliferation (*99*). The timely clearance of senescent DSCs is essential for maintaining immune balance at the maternal-fetal interface, as the accumulation of these cells may trigger inflammatory responses and propagate senescence signals, potentially leading to recurrent miscarriage (*100*). Studies have shown that QUE reduces the expression of senescence-associated beta-galactosidase-positive cells and senescence markers in DSCs, thereby facilitating the proper progression of decidualization (*101*). Furthermore, QUE partly regulates the expression of Bcl-2/Bax proteins, inhibiting apoptosis in endometrial cells, which supports successful embryo implantation (*102*). Interestingly, QUE can also activate p53, promoting apoptosis in stromal cells exhibiting a senescent-like phenotype (*103*). However, some studies in rats have indicated that subcutaneous administration of QUE at a dose of 50 mg/kg/day during the peri-implantation period may negatively impact uterine fluid volume and the development of receptivity, thereby potentially impairing embryo implantation (*104*).

8.3. Decidual extravillous trophoblast cells

DSCs regulate the function of extravillous trophoblast cells through various factors (*105*). Extravillous embryonic trophoblast cells play a vital role at the maternal-fetal interface by facilitating embryo anchoring to the maternal decidua, vascular remodeling, and immune modulation (*106*). Insufficient proliferation and invasion of extravillous trophoblast cells into the endometrium are major defects associated with pregnancy complications such as recurrent miscarriage (*107*).

Research has demonstrated that under hypoxia/reoxygenation (H/R) conditions, human trophoblast cell line HTR-8/SVneo experiences oxidative stress, accompanied by a reduction in glutathione levels and a significant decline in trophoblast invasiveness. The addition of QUE notably reduces oxidative stress, inhibits the activation of pro-apoptotic kinases induced by phosphorylation during H/R, and enhances spheroid stem cell formation in HTR-8/SVneo cells, promoting their invasive capacity (*108*). Besides, the pretreatment with QUE has been shown to prevent H/R-induced oxidative stress in trophoblast cell lines (*109*). Oxidative stress induced by placental hypoxia is closely linked to mitochondrial metabolic dysfunction, and QUE can improve mitochondrial function under hypoxic conditions, thereby promoting trophoblast cell fusion (*110,111*).

9. Conclusion

In conclusion, RPL is a common complication of clinical pregnancy with a complex etiology, often involving multiple causative factors. As a natural antioxidant and anti-inflammatory flavonol, QUE is widely found in herbal medicines, fruits, and vegetables. Current literature suggests that QUE may have therapeutic effects on RPL by regulating endocrine, coagulation, oxidation, inflammation, immune responses, and maternal-fetal interface. However, the specific molecular mechanisms of QUE remain unclear. For instance, while various studies on cellular and animal models have demonstrated the anti-inflammatory properties of QUE, an RCT observed no significant impact of QUE supplementation on innate immune function or inflammatory markers. Thus, further validation is required to determine whether QUE mitigates RPL by inhibiting the suppression of inflammation. Similarly, although QUE has been shown to regulate gut microbiota balance, the primary microbiota influenced by QUE does not align with the significant microbial alterations observed in RPL patients. This raises the question of whether QUE affects RPL by modulating gut microbiota, warranting further investigation. Additionally, while QUE can promote the clearance of senescent stromal cells and facilitate decidualization, other studies suggest that subcutaneous injection of QUE during the peri-implantation period may negatively impact embryo implantation. This highlights the need to consider the timing of QUE administration when treating RPL carefully. Due to pharmacokinetic differences, QUE's efficacy in animal models may not translate directly to humans. Dose optimization and placental barrier penetration require further exploration. To confirm the precise role of QUE in the treatment of RPL patients, more extensive and high-quality prospective trials are needed, particularly those focusing on the effects of QUE on endocrine, coagulation, oxidation, inflammation, immune response, and maternal-fetal interface-related reproductive

abnormalities. In the future, more clinical trials will likely explore the application of QUE in RPL patients.

Funding: This work was supported by a grant from the National Natural Science Foundation of China (grant No. 82374243 to L Wang) and the Chinese Association of Integration of Traditional and Western Medicine special foundation for Obstetrics and Gynecology (grant No. FCK-ZSYTW-04 to Q Qi).

Conflict of Interest: The authors have no conflicts of interest to disclose.

References

1. Ying H, Xie H. The challenges and response measures faced by obstetrics under the "Three-Child" fertility policy. Zhongguo Shi Yong Fu Ke Yu Chan Ke Za Zhi. 2023; 39:577-580. (in Chinese)
2. Saadh MJ, Ahmed HH, Chandra M, Al-Hussainy AF, Hamid JA, Mishra A, Taher WM, Alwan M, Jawad MJ, Al-Nuaimi AMA, Alsaikhan F, Farhood B, Akhavan-Sigari R. Therapeutic effects of quercetin in oral cancer therapy: A systematic review of preclinical evidence focused on oxidative damage, apoptosis and anti-metastasis. Cancer Cell Int. 2025; 25:66.
3. Liu L, Barber E, Kellow NJ, Williamson G. Improving quercetin bioavailability: A systematic review and meta-analysis of human intervention studies. Food Chem. 2025; 477:143630.
4. Mehta PA, Nelson A, Loveless S, *et al*. Phase 1 study of quercetin, a natural antioxidant for children and young adults with Fanconi anemia. Blood Adv. 2025; 9:1927-1939.
5. Wei Z, Hong H, Liu W, He K, Wang J, Guo X, Zhang D, Li Q, Yang Z. Quercetin protects goat sperm motility by inhibiting neutrophil extracellular traps and maintaining plasma membrane and acrosome integrity. Vet Sci. 2024; 11:553.
6. Uhl K, Mitchell AE. Elderberry, an ancient remedy: A comprehensive study of the bioactive compounds in three *Sambucus nigra* L. Subspecies. Annu Rev Food Sci Technol. 2024; 15:27-51.
7. Liu Q, Miao C, Lin F, Zhang H, Zhang Q. A case-control retrospective study for the effect of Shoutai Wan on IVF-ET pregnancy outcome. Medicine. 2024; 103:e36846.
8. Yang SL, Niu TT, Li XL, Li DJ, Li MQ, Wang HY. Bu-Shen-Yi-Qi formula impairs cytotoxicity of NK cells by up-regulating IDO expression in trophoblasts. Gynecol Endocrinol. 2018; 34:675-679.
9. Yang K, Zeng L, Li Y, Wu L, Xiang W, Wu X, Wang G, Bao T, Huang S, Yu R, Zhang G, Liu H. Uncovering the pharmacological mechanism of Shou Tai Wan on recurrent spontaneous abortion: A integrated pharmacology strategy-based research. J Ethnopharmacol. 2024; 323:117589.
10. Maharajan K, Xia Q, Duan X, Tu P, Zhang Y, Liu K. Therapeutic importance of Zishen Yutai Pill on the female reproductive health: A review. J Ethnopharmacol. 2021; 281:114523.
11. Chen X, Shi Y, Li H, Gong F, Yao C, Bai H, Fan Y, Shi D, Qu Q, Diao F, Zhu Y, Yang D. Effects of the Zishen Yutai Pill on live births compared with placebo among infertile women with frozen-thawed embryo transfer cycle: A multicentre double-blind randomized controlled trial. Phytomedicine. 2024; 135:156072.
12. Di X, Duan Z, Ma Y, Song X, Hao Y, Li G, Tan Z, Lou Y, Lin X. Jiawei Shoutai Pill promotes decidualization by regulating the SGK1/ENaC pathway in recurrent spontaneous abortion. J Ethnopharmacol. 2024; 318:116939.
13. Yuan J, Li L, Cai Z, Wu N, Chen C, Yin S, Liu S, Wang W, Mei Y, Wei L, Liu X, Zou L, Chen H. Qualitative analysis and componential differences of chemical constituents in Taxilli Herba from different hosts by UFLC-Triple TOF-MS/MS. Molecules. 2021; 26:6373.
14. Wang M, Xu XY, Wang HD, Wang HM, Liu MY, Hu WD, Chen BX, Jiang MT, Qi J, Li XH, Yang WZ, Gao XM. A multi-dimensional liquid chromatography/high-resolution mass spectrometry approach combined with computational data processing for the comprehensive characterization of the multicomponents from *Cuscuta chinensis*. J Chromatogr A. 2022; 1675:463162.
15. Zhou J, Li L, Pan X, Wang J, Qi Q, Sun H, Li C, Wang L. The effect of a traditional Chinese quadri-combination therapy and its component quercetin on recurrent spontaneous abortion: A clinical trial, network pharmacology and experiments-based study. Front Pharmacol. 2022; 13:965694.
16. Han C, Sun Z, Song Y. Clinical efficacy of Bushen Antai Decoction in patients with Kidney Deficiency-Type RPL. Zhong Cheng Yao Za Zhi. 2019; 41:5. (in Chinese)
17. Wang P. Effect of Yiqi Bushen & Progesterone on RPL in Kidney Deficiency threatened abortion and hormone levels. Si Chuan Zhong Yi Za Zhi. 2022; 40:3. (in Chinese)
18. Xie H. Clinical observation on the treatment of RPL-PTS by Bushen Huoxue Recipe. Jiangxi University of Traditional Chinese Medicine, 2023. (Thesis)
19. Zhang Y, Shao L, Fan H, Lv K, Zhao Q, Jiang L. Efficacy of modified Shoutai pill in the treatment of RPL and its impact on coagulation function and Th17 cell-related factors. Zhong Yi Yao Xue Bao Za Zhi. 2024; 52:61-66. (in Chinese)
20. Zhao Z, Zhang J, Li Y. Effect of Jiawei Shoutai pills combined with dydrogesterone on pregnancy outcome of kidney-deficiency early threatened abortion after tocolytic therapy. Hu Nan Zhong Yi Za Zhi. 2023; 39:20-23. (in Chinese)
21. Khamineh Y, Ghiasvand M, Panahi-Alanagh S, Rastegarmand P, Zolghadri S, Stanek A. A narrative review of quercetin's role as a bioactive compound in female reproductive disorders. Nutrients. 2025; 17:1118.
22. Mu F, Wang M, Zeng X, Liu L, Wang F. A predictive model of pregnancy loss using pre-pregnancy endocrine and immunological parameters in women with abnormal glucose/lipid metabolism and previous pregnancy loss. Endocrine. 2024; 86:441-450.
23. Wen X, Dong P, Liu J, Wang SJ, Li J. Role of immune inflammation in recurrent spontaneous abortions. J Inflamm Res. 2024; 17:9407-9422.
24. Chan SY, Marsh MS, Gilbert J, Boelaert K, Evans C, Dhillon-Smith R, Royal College of O, Gynaecologists. Management of thyroid disorders in pregnancy: Green-top guideline No. 76. BJOG. 2025; 132:130-161.
25. Zhou Y, Wang Y, Yu T, Li Y, Mi M, Su J, Ge J. Subclinical hypothyroidism during pregnancy and the impact of levothyroxine therapy on pregnancy outcomes in women. PeerJ. 2025; 13:e19343.
26. Dong AC, Morgan J, Kane M, Stagnaro-Green A,

Stephenson MD. Subclinical hypothyroidism and thyroid autoimmunity in recurrent pregnancy loss: A systematic review and meta-analysis. Fertil Steril. 2020; 113:587-600.
27. Yamanouchi H, Minami Y, Kajiya K. Evaluation and validation of angiotensin-converting enzyme inhibitory activity of moringa oleifera, quercetin, and isoquercetin: A comparative study of fluorescence and absorbance measurement methods. Food Res Int. 2025; 202:115768.
28. Brown EDL, Obeng-Gyasi B, Hall JE, Shekhar S. The thyroid hormone axis and female reproduction. Int J Mol Sci. 2023; 24:9815.
29. Giuliani C, Di Dalmazi G, Bucci I, Napolitano G. Quercetin and thyroid. Antioxidants (Basel, Switzerland). 2024; 13:1202.
30. Accili D, Deng Z, Liu Q. Insulin resistance in type 2 diabetes mellitus. Nat Rev Endocrinol. 2025; 21:413-426.
31. Hinojal I, Chimenea A, Antinolo G, Garcia-Diaz L. Impact of continuous glucose monitoring on pregnancy outcomes in women with pregestational diabetes. Acta Diabetol. 2025. doi: 10.1007/s00592-024-02439-2.
32. Basaldua-Maciel V, Guzman-Flores JM, Reyes-Chaparro A, Martinez-Esquivias F. Therapeutic potential of quercetin in type 2 diabetes based on a network pharmacology study. Curr Top Med Chem. 2025. doi: 10.2174/0115680266361598250212030220.
33. Farhadi F, Sharififar F, Jafari M, Rahimi VB, Askari N, Askari VR. Hallmarks of quercetin benefits as a functional supplementary in the management of diabetes mellitus-related maladies: From basic to clinical applications. Curr Drug Metab. 2024; 25:653-669.
34. Lin F, Zhou W, Yuan X, Liu S, He Z. Mechanistic study of quercetin in the treatment of hepatocellular carcinoma with diabetes *via* MEK/ERK pathway. Int Immunopharmacol. 2024; 142:113194.
35. Yi R, Liu Y, Zhang X, Sun X, Wang N, Zhang C, Deng H, Yao X, Wang S, Yang G. Unraveling quercetin's potential: A comprehensive review of its properties and mechanisms of action, in diabetes and obesity complications. Phytother Res. 2024; 38:5641-5656.
36. Rashidi Z, Khosravizadeh Z, Talebi A, Khodamoradi K, Ebrahimi R, Amidi F. Overview of biological effects of quercetin on ovary. Phytother Res. 2021; 35:33-49.
37. Bolouki A, Zal F, Mostafavi-Pour Z, Bakhtari A. Protective effects of quercetin on uterine receptivity markers and blastocyst implantation rate in diabetic pregnant mice. Taiwan J Obstet Gynecol. 2020; 59:927-934.
38. Li M, Cui Y, Wu X, Yang X, Huang C, Yu L, Yi P, Chen C. Integrating network pharmacology to investigate the mechanism of quercetin's action through AKT inhibition in co-expressed genes associated with polycystic ovary syndrome and endometrial cancer. Int J Biol Macromol. 2025; 297:139468.
39. Yuan J, Li Z, Yu Y, Wang X, Zhao Y. Natural compounds in the management of polycystic ovary syndrome: A comprehensive review of hormonal regulation and therapeutic potential. Front Nutr. 2025; 12:1520695.
40. Eleyan M, Ibrahim KA, Mohamed RA, Hussien M, Zughbur MR, Aldalou AR, Masad A, El-Rahman HAA, Abdelgaid HA. Quercetin diminishes the apoptotic pathway of magnetite nanoparticles in rats' ovary: Antioxidant status and hormonal profiles. Environ Anal Health Toxicol. 2024; 39:2024025-2024020.
41. Ortiz-Salguero C, Romero-Bernal M, Gonzalez-Diaz A, Doush ES, Del Rio C, Echevarria M, Montaner J. Hyperhomocysteinemia: Underlying links to stroke and hydrocephalus, with a focus on polyphenol-based therapeutic approaches. Nutrients. 2024; 17:40.
42. Collins LC, Gatta LA, Dotters-Katz SK, Kuller JA, Schust DJ. Luteal phase defects and progesterone supplementation. Obstet Gynecol Surv. 2024; 79:122-128.
43. Jiang X, Zhou H, Shi M, Zhou B, Liu B, Yuan Y, Shan J, Xu J, Xie T. Bu-shen-zhu-yun decoction promotes synthesis and secretion of FSHβ and LHβ in anterior pituitary cells *in vitro*. Biomed Pharmacother. 2018; 102:494-501.
44. Zhao Y, D'Souza R, Gao Y, Hao Q, Kallas-Silva L, Steen JP, Guyatt G. Progestogens in women with threatened miscarriage or recurrent miscarriage: A meta-analysis. Acta Obstet Gynecol Scand. 2024; 103:1689-1701.
45. Wang B, Gao M, Yao Y, Shen H, Li H, Sun J, Wang L, Zhang X. Enhancing endometrial receptivity: The roles of human chorionic gonadotropin in autophagy and apoptosis regulation in endometrial stromal cells. Reprod Biol Endocrinol. 2024; 22:37.
46. Chen Y, Zhao Y, Miao C, Yang L, Wang R, Chen B, Zhang Q. Quercetin alleviates cyclophosphamide-induced premature ovarian insufficiency in mice by reducing mitochondrial oxidative stress and pyroptosis in granulosa cells. J Ovarian Res. 2022; 15:138.
47. Tarko A, Štochmaľová A, Harrath AH, Kotwica J, Baláži A, Sirotkin AV. Quercetin can affect porcine ovarian cell functions and to mitigate some of the effects of the environmental contaminant toluene. Res Vet Sci. 2023; 154:89-96.
48. Shen M, Li T, Feng Y, Wu P, Serrano BR, Barcenas AR, Qu L, Zhao W. Effects of quercetin on granulosa cells from prehierarchical follicles by modulating MAPK signaling pathway in chicken. Poult Sci. 2023; 102:102736.
49. Mahmoud AA, Elfiky AM, Abo-Zeid FS. The anti-androgenic effect of quercetin on hyperandrogenism and ovarian dysfunction induced in a dehydroepiandrosterone rat model of polycystic ovary syndrome. Steroids. 2022; 177:108936.
50. Olave NC, Grenett MH, Cadeiras M, Grenett HE, Higgins PJ. Upstream stimulatory factor-2 mediates quercetin-induced suppression of PAI-1 gene expression in human endothelial cells. J Cell Biochem. 2010; 111:720-726.
51. Urano T, Sano Y, Suzuki Y, Okada M, Sano H, Honkura N, Morooka N, Doi M, Suzuki Y. Evaluation of thrombomodulin/thrombin activatable fibrinolysis inhibitor function in plasma using tissue-type plasminogen activator-induced plasma clot lysis time. Res Pract Thromb Haemost. 2024; 8:102463.
52. Manjunath SH, Thimmulappa RK. Antiviral, immunomodulatory, and anticoagulant effects of quercetin and its derivatives: Potential role in prevention and management of COVID-19. J Pharm Anal. 2022; 12:29-34.
53. Zhu S, Wang H, Zhang J, Yu C, Liu C, Sun H, Wu Y, Wang Y, Lin X. Antiasthmatic activity of quercetin glycosides in neonatal asthmatic rats. 3 Biotech. 2019; 9:189.
54. Yang D, Wang T, Long M, Li P. Quercetin: Its main pharmacological activity and potential application in clinical medicine. Oxid Med Cell Longev. 2020; 2020:8825387.
55. Abruzzese V, Matera I, Martinelli F, Carmosino M, Koshal P, Milella L, Bisaccia F, Ostuni A. Effect of quercetin on ABCC6 transporter: Implication in HepG2 migration. Int J Mol Sci. 2021; 22:3437.
56. Zhao L, Wang H, Du X. The therapeutic use of quercetin in ophthalmology: Recent applications. Biomed Pharmacother. 2021; 137:111371.
57. Dagher O, Mury P, Thorin-Trescases N, Noly PE, Thorin

E, Carrier M. Therapeutic potential of quercetin to alleviate endothelial dysfunction in age-related cardiovascular diseases. Front Cardiovasc Med. 2021; 8:658400.
58. Zhang X, Gao J, Yang L, Feng X, Yuan X. Oxidative stress and its role in recurrent pregnancy loss: Mechanisms and implications. J Mol Histol. 2024; 56:55.
59. Fang T, Ji X, Su Z, Zhang A, Zhu L, Tang J, Mai Z, Lin H, Ouyang N, Chen H. Risk factors associated with pregnancy outcomes in patients with recurrent pregnancy loss after treatment. BMC Pregnancy Childbirth. 2024; 24:827.
60. Safronova VG, Matveeva NK, Avkhacheva NV, Sidel'nikova VM, Van'ko LV, Sukhikh GT. Changes in regulation of oxidase activity of peripheral blood granulocytes in women with habitual abortions. Bull Exp Biol Med. 2003; 136:257-260.
61. Al-Sheikh YA, Ghneim HK, Alharbi AF, Alshebly MM, Aljaser FS, Aboul-Soud MAM. Molecular and biochemical investigations of key antioxidant/oxidant molecules in Saudi patients with recurrent miscarriage. Exp Ther Med. 2019; 18:4450-4460.
62. Yao Y, Ye Y, Chen J, Zhang M, Cai X, Zheng C. Maternal-fetal immunity and recurrent spontaneous abortion. Am J Reprod Immunol. 2024; 91:e13859.
63. Liu Y, Chen H, Feng L, Zhang J. Interactions between gut microbiota and metabolites modulate cytokine network imbalances in women with unexplained miscarriage. NPJ Biofilms Microbiomes. 2021; 7:24.
64. Dong Y, Hou Q, Lei J, Wolf PG, Ayansola H, Zhang B. Quercetin alleviates intestinal oxidative damage induced by H(2)O(2) *via* modulation of GSH: *In vitro* screening and *in vivo* evaluation in a colitis model of mice. ACS Omega. 2020; 5:8334-8346.
65. Hong Z, Piao M. Effect of quercetin monoglycosides on ooxidative stress and gut microbiota diversity in mice with dextran sodium sulphate-induced colitis. Biomed Res Int. 2018; 2018:8343052.
66. Lin R, Piao M, Song Y. Dietary quercetin increases colonic microbial diversity and attenuates colitis severity in citrobacter rodentium-infected mice. Front Microbiol. 2019; 10:1092.
67. Kimura F, Takebayashi A, Ishida M, *et al*. Review: Chronic endometritis and its effect on reproduction. J Obstet Gynaecol Res. 2019; 45:951-960.
68. Bouet PE, El Hachem H, Monceau E, Gariepy G, Kadoch IJ, Sylvestre C. Chronic endometritis in women with recurrent pregnancy loss and recurrent implantation failure: Prevalence and role of office hysteroscopy and immunohistochemistry in diagnosis. Fertil Steril. 2016; 105:106-110.
69. McQueen DB, Bernardi LA, Stephenson MD. Chronic endometritis in women with recurrent early pregnancy loss and/or fetal demise. Fertil Steril. 2014; 101:1026-1030.
70. Kim HP, Mani I, Iversen L, Ziboh VA. Effects of naturally-occurring flavonoids and biflavonoids on epidermal cyclooxygenase and lipoxygenase from guinea-pigs. Prostaglandins Leukot Essent Fatty Acids. 1998; 58:17-24.
71. Yang D, Liu X, Liu M, Chi H, Liu J, Han H. Protective effects of quercetin and taraxasterol against H(2)O(2)-induced human umbilical vein endothelial cell injury *in vitro*. Exp Ther Med. 2015; 10:1253-1260.
72. Heinz SA, Henson DA, Nieman DC, Austin MD, Jin F. A 12-week supplementation with quercetin does not affect natural killer cell activity, granulocyte oxidative burst activity or granulocyte phagocytosis in female human subjects. Br J Nutr. 2010; 104:849-857.
73. Wang W, Sung N, Gilman-Sachs A, Kwak-Kim J. T helper (Th) cell profiles in pregnancy and recurrent pregnancy losses: Th1/Th2/Th9/Th17/Th22/Tfh. Front Immunol. 2020; 11:2025.
74. Ansariniya H, Zare F, Mosaffa N, Idali F, Shabani M, Hadinedoushan H. Immunologic deviations in recurrent spontaneous abortion mouse model. Am J Reprod Immunol. 2022; 88:e13631.
75. Muyayalo KP, Li ZH, Mor G, Liao AH. Modulatory effect of intravenous immunoglobulin on Th17/Treg cell balance in women with unexplained recurrent spontaneous abortion. Am J Reprod Immunol. 2018; 80:e13018.
76. AbdulHussain G, Azizieh F, Makhseed Ma, Raghupathy R. Effects of progesterone, dydrogesterone and estrogen on the production of Th1/Th2/Th17 cytokines by lymphocytes from women with recurrent spontaneous miscarriage. J Reprod Immunol. 2020; 140:103132.
77. Cheng J, Zhang M, Zheng Y, Wang J, Wang Q. Integrative analysis of network pharmacology and proteomics to identify key targets of Tuomin-Zhiti-Decoction for allergic rhinitis. J Ethnopharmacol. 2022; 296:115448.
78. Ke X, Chen Z, Wang X, Kang H, Hong S. Quercetin improves the imbalance of Th1/Th2 cells and Treg/Th17 cells to attenuate allergic rhinitis. Autoimmunity. 2023; 56:2189133.
79. Yang Y, Zhang X, Xu M, Wu X, Zhao F, Zhao C. Quercetin attenuates collagen-induced arthritis by restoration of Th17/Treg balance and activation of Heme Oxygenase 1-mediated anti-inflammatory effect. Int Immunopharmacol. 2018; 54:153-162.
80. Wei CB, Tao K, Jiang R, Zhou LD, Zhang QH, Yuan CS. Quercetin protects mouse liver against triptolide-induced hepatic injury by restoring Th17/Treg balance through Tim-3 and TLR4-MyD88-NF-κB pathway. Int Immunopharmacol. 2017; 53:73-82.
81. Robertson SA, Care AS, Moldenhauer LM. Regulatory T cells in embryo implantation and the immune response to pregnancy. J Clin Invest. 2018; 128:4224-4235.
82. Tagliani E, Erlebacher A. Dendritic cell function at the maternal-fetal interface. Expert Rev Clin Immunol. 2011; 7:593-602.
83. Lin W, Wang W, Wang D, Ling W. Quercetin protects against atherosclerosis by inhibiting dendritic cell activation. Mol Nutr Food Res. 2017; 61:1700031.
84. Kadomoto S, Izumi K, Mizokami A. Macrophage polarity and disease control. Int J Mol Sci. 2021; 23:144.
85. Li D, Zheng L, Zhao D, Xu Y, Wang Y. The role of immune cells in recurrent spontaneous abortion. Reprod Sci. 2021; 28:3303-3315.
86. Tsao FY, Wu MY, Chang YL, Wu CT, Ho HN. M1 macrophages decrease in the deciduae from normal pregnancies but not from spontaneous abortions or unexplained recurrent spontaneous abortions. J Formos Med Assoc. 2018; 117:204-211.
87. Tsai CF, Chen GW, Chen YC, Shen CK, Lu DY, Yang LY, Chen JH, Yeh WL. Regulatory effects of quercetin on M1/M2 macrophage polarization and oxidative/antioxidative balance. Nutrients. 2021; 14:67.
88. Zhao Y, Chen X, Zhang T, Chan LK, Liu Y, Chung JP-W, Kwong J, Li TC. The use of multiplex staining to measure the density and clustering of four endometrial immune cells around the implantation period in women with recurrent miscarriage: Comparison with fertile controls. J Mol Histol. 2020; 51:593-603.
89. Liu H, Lin XX, Huang XB, Huang DH, Song S, Chen

YJ, Tang J, Tao D, Yin ZN, Mor G, Liao AH. Systemic characterization of novel immune cell phenotypes in recurrent pregnancy loss. Front Immunol. 2021; 12:657552.
90. Taima A, Fukui A, Yamaya A, Yokota M, Fukuhara R, Yokoyama Y. A semen-based stimulation method to analyze cytokine production by uterine CD56bright natural killer cells in women with recurrent pregnancy loss. J Reprod Immunol. 2020; 142:103206.
91. Heinz SA, Henson DA, Nieman DC, Austin MD, Jin FX. A 12-week supplementation with quercetin does not affect natural killer cell activity, granulocyte oxidative burst activity or granulocyte phagocytosis in female human subjects. Br J Nutr. 2010; 104:849-857.
92. Saeed M, Naveed M, Arain M, Arif M, Abd El-Hack M, Alagawany M, Siyal F, Soomro R, Sun CJ. Quercetin: Nutritional and beneficial effects in poultry. World's Poult Sci J. 2017; 73:355-364.
93. Ahmadi M, Mohammadi M, Ali-Hassanzadeh M, Zare M, Gharesi-Fard B. MDSCs in pregnancy: Critical players for a balanced immune system at the feto-maternal interface. Cell Immunol. 2019; 346:103990.
94. Zhao AM, Xu HJ, Kang XM, Zhao AM, Lu LM. New insights into myeloid-derived suppressor cells and their roles in feto-maternal immune cross-talk. J Reprod Immunol. 2016; 113:35-41.
95. Pang B, Hu C, Li H, Nie X, Wang K, Zhou C, Yi H. Myeloid derived suppressor cells: Escorts at the maternal-fetal interface. Front Immunol. 2023; 14:1080391.
96. Ma Z, Xia Y, Hu C, Yu M, Yi H. Quercetin promotes the survival of granulocytic myeloid-derived suppressor cells *via* the ESR2/STAT3 signaling pathway. Biomed Pharmacother. 2020; 125:109922.
97. Liu Z, Geng Y, Huang Y, Hu R, Li F, Ding J, Ma W, Dong H, Song K, Xu X, Wu X, Song Y, Zhang M. Bushen Antai recipe alleviates embryo absorption by enhancing immune tolerance and angiogenesis at the maternal-fetal interface *via* mobilizing MDSCs in abortion-prone mice. Phytomedicine. 2024; 123:155164.
98. Zhu H, Hou CC, Luo LF, Hu YJ, Yang WX. Endometrial stromal cells and decidualized stromal cells: Origins, transformation and functions. Gene. 2014; 551:1-14.
99. Liu X, Wei X, Wu J, Xu Y, Hu J, Qin C, Chen C, Lin Y. CBLL1 promotes endometrial stromal cell senescence *via* inhibiting PTEN in recurrent spontaneous abortion. FASEB J. 2024; 38:e23833.
100. Zhao X, Hu Y, Xiao W, Ma Y, Shen D, Jiang Y, Shen Y, Wang S, Ma J. Efficacy of mesenchymal stromal cells in the treatment of unexplained recurrent spontaneous abortion in mice: An analytical and systematic review of meta-analyses. PLoS One. 2023; 18:e0294855.
101. Kusama K, Yamauchi N, Yoshida K, Azumi M, Yoshie M, Tamura K. Senolytic treatment modulates decidualization in human endometrial stromal cells. Biochemical and biophysical research communications. Biochem Biophys Res Commun. 2021; 571:174-180.
102. Wang X, Yan Y, Yang L, Li M, Zhong X. Effect of quercetin on the expression of Bcl-2/Bax apoptotic proteins in endometrial cells of lipopolysaccharide-induced-abortion. J Tradit Chin Med. 2016; 36:737-742.
103. Delenko J, Xue X, Chatterjee PK, Hyman N, Shih AJ, Adelson RP, Safaric Tepes P, Gregersen PK, Metz CN. Quercetin enhances decidualization through AKT-ERK-p53 signaling and supports a role for senescence in endometriosis. Reprod Biol Endocrinol. 2024; 22:100.
104. Shahzad H, Giribabu N, Karim K, Kassim N, Muniandy S, Kumar KE, Salleh N. Quercetin interferes with the fluid volume and receptivity development of the uterus in rats during the peri-implantation period. Reprod Toxicol. 2017; 71:42-54.
105. Li X, Shi J, Zhao W, Huang X, Cui L, Liu L, Jin X, Li D, Zhang X, Du M. WNT16 from decidual stromal cells regulates HTR8/SVneo trophoblastic cell function *via* AKT/beta-catenin pathway. Reproduction. 2022; 163:241-250.
106. Pan D, Liu Q, Du L, Yang Y, Jiang G. Polarization disorder of decidual NK cells in unexplained recurrent spontaneous abortion revealed by single-cell transcriptome analysis. Reprod Biol Endocrinol. 2022; 20:108.
107. Wang XH, Xu S, Zhou XY, Zhao R, Lin Y, Cao J, Zang WD, Tao H, Xu W, Li MQ, Zhao SM, Jin LP, Zhao JY. Low chorionic villous succinate accumulation associates with recurrent spontaneous abortion risk. Nat Commun. 2021; 12:3428.
108. Ebegboni VJ, Balahmar RM, Dickenson JM, Sivasubramaniam SD. The effects of flavonoids on human first trimester trophoblast spheroidal stem cell self-renewal, invasion and JNK/p38 MAPK activation: Understanding the cytoprotective effects of these phytonutrients against oxidative stress. Biochem Pharmacol. 2019; 164:289-298.
109. Ebegboni VJ, Dickenson JM, Sivasubramaniam SD. Antioxidative effects of flavonoids and their metabolites against hypoxia/reoxygenation-induced oxidative stress in a human first trimester trophoblast cell line. Food Chem. 2019; 272:117-125.
110. Chen Y, Zhao Y, Miao C, Yang L, Wang R, Chen B, Zhang Q. Quercetin alleviates cyclophosphamide-induced premature ovarian insufficiency in mice by reducing mitochondrial oxidative stress and pyroptosis in granulosa cells. J Ovarian Res. 2022; 15:138.
111. Yoshida K, Kusama K, Shinohara G, Sato S, Yoshie M, Tamura K. Quercetin stimulates trophoblast fusion *via* the mitochondrial function. Sci Rep. 2024; 14:287.

Received June 6, 2025; Revised June 25, 2025; Accepted June 28, 2025.

[§]These authors contributed equally to this work.

**Address correspondence to:*
Ling Wang, Department of Obstetrics and Reproductive Immunology, Shanghai East Hospital, Tongji University School of Medicine, No. 1800 Yuntai Road, Shanghai 200100, China.
E-mail: dr.wangling@vip.163.com

Released online in J-STAGE as advance publication June 29, 2025.

Original Article

DOI: 10.5582/ddt.2025.01043

Abortion adverse events associated with adalimumab, etanercept, ustekinumab, and dupilumab during pregnancy: A pharmacovigilance study based on FDA adverse event reporting system

Qian Liu[1,§], Yang Wang[2,§], Panwei Hu[1,*], Peizhi He[1,*]

[1] Department of Obstetrics and Gynecology, Shuguang Hospital Affiliated to Shanghai University of Traditional Chinese Medicine, Shanghai, China;
[2] Reproductive Medicine Center, Shuguang Hospital Affiliated to Shanghai University of Traditional Chinese Medicine, Shanghai, China.

SUMMARY: Biologics are essential for managing immune-related inflammatory diseases during pregnancy to prevent disease progression and adverse pregnancy outcomes. However, data on the safety of biologics in a broader population are limited. This study aims to evaluate abortion-related adverse events (AEs) associated with adalimumab, etanercept, ustekinumab, and dupilumab, using data from the FDA Adverse Event Reporting System (FAERS) database. A disproportionality analysis was performed using the Reporting Odds Ratio (ROR) and Bayesian Confidence Propagation Neural Network (BCPNN) to identify signals of abortion-related AEs. The time-to-onset profiles were assessed by analyzing the description and Weibull shape parameters (WSPs) for these events. Sensitivity analyses were also conducted, including drug–drug interaction studies, logistic regression, and a similar retrospective analysis using data from the Japanese Adverse Drug Event Report (JADER) database. Disproportionality analysis revealed specific signals for abortion-related AEs associated with adalimumab, etanercept, and ustekinumab. The drug–drug interaction analysis indicated that these biologics, particularly without methotrexate or prednisolone, increase the risk of abortion-related AEs. Logistic regression identified several factors influencing outcomes. The time-to-onset analysis revealed that dupilumab had an earlier onset of 62.5 days, while etanercept had a later onset at 184 days. WSPs analysis revealed that signals for adalimumab, ustekinumab, and dupilumab exhibited early failure-type features, indicating a decreasing risk of abortion-related AEs over time. In conclusion, adalimumab, etanercept, and ustekinumab are associated with an increased risk of abortion-related adverse pregnancy outcomes, though the signals remain relatively weak. Further large-scale studies are needed to provide more definitive evidence.

Keywords: disproportionality analysis, spontaneous abortion, FAERS, biologics, pharmacovigilance

1. Introduction

Immune-related inflammatory disorders impose significant challenges on pregnant populations. In 2019, the age-standardized rates of autoimmune diseases were 89.51 (95% CI: 71.94 to 110.35) per 100,000 women of childbearing age and 85.78 (95% CI: 68.72 to 106.37) per 100,000 in sexually mature adults (*1*). Biologic therapies, including anti-tumor necrosis factor (anti-TNF) agents and anti-interleukin (IL)-12/23 or IL-4/IL-13 antibodies, are widely used to treat immune-mediated inflammatory diseases. Biologics targeting tumor necrosis factor (TNF), such as adalimumab and etanercept, have shown significant promise in managing autoimmune inflammatory diseases (*2*). Patients with spontaneous abortion and preeclampsia/eclampsia exhibit markedly elevated levels of inflammatory cytokines like TNF-α and IL-4 (*3*). These immune-related inflammatory diseases upregulate immunomodulatory and anti-inflammatory factors, which can disrupt syncytialization, adhesion, and hormonal functions of the trophectoderm (*4*). Since the embryo functions as a semi-allograft to the mother, maternal immune tolerance is crucial for sustaining pregnancy. Among the various factors, the balance between Th1 and Th2 cytokines plays a critical role in maintaining immune equilibrium at the maternal-fetal interface (*5-7*). This raises the question of whether biologics targeting T Helper Cells 1 (Th1) (TNF, IL-12/23, IFN-γ) or T Helper Cells 2 (Th2) (IL-4, IL-13, IL-5) cytokines affect the immune balance at this interface during pregnancy. These biologics, which vary in their ability to cross the placental barrier (*8*), may have distinct impacts on pregnancy outcomes, warranting further investigation.

Intrauterine growth restriction, spontaneous abortion, and preterm birth are common adverse outcomes

associated with anti-TNF-α drugs during pregnancy (*9*). Until 2007, the use of etanercept was advised against during pregnancy (*10*); however, its use has since been approved up to gestational weeks 30-32 and throughout pregnancy from 2016 onward (*11*). A recent systematic review of 13 clinical studies involving 68 pregnant patients indicated that dupilumab has demonstrated efficacy in treating atopic dermatitis without clear evidence of adverse pregnancy or neonatal outcomes (*12*). Ustekinumab, which crosses the placental barrier in mid to late pregnancy (*13*), has fetal concentrations higher than maternal levels. However, there is currently no definitive evidence linking ustekinumab to increased risks of adverse pregnancy or neonatal outcomes (*13,14*). Continued use of biologics during pregnancy is recommended for patients with inflammatory bowel disease (IBD) or inflammatory rheumatic diseases to prevent relapse, control symptoms, and minimize complications and disease progression (*15*). Discontinuation of ustekinumab or vedolizumab in these patients may lead to IBD relapse (*16*).

The long-term safety of biotherapy remains a topic of ongoing debate. Antibodies do not cross the placental barrier until mid-gestation (*17*). However, medication withdrawal typically occurs during the first trimester or as soon as pregnancy is confirmed. Pregnant patients with immune-mediated chronic inflammatory diseases face the dilemma of whether the benefits of biological therapy outweigh potential harms to pregnancy outcomes.

The FAERS database contains spontaneous adverse event reports submitted to the FDA, supporting post-marketing safety monitoring and providing insights into the real-world usage of drugs and biologics (*18*). Currently, there is a lack of extensive, comprehensive, and systematic research on the association between biologics and miscarriage, largely due to the high-risk nature of pregnant women. Therefore, a pharmacovigilance study was conducted to examine the relationship between various biological agents and pregnancy loss by analyzing real-world data from the FDA's FAERS. Specifically, this study focused on pregnant women using different biologics, systematically evaluating adverse event signals through descriptive statistics, disproportionality analysis, adverse reaction induction time, logistic regression, and other methods. In summary, this study provides further evidence for the use of biologics in pregnant women with chronic immune-inflammatory diseases, aiming to control disease progression and improve pregnancy outcomes.

2. Materials and Methods

2.1. Data sources

FAERS (the FDA Adverse Event Reporting System) is a database maintained by the FDA that collects and analyzes reports of adverse events associated with drugs and therapeutic biologics. Data for several biologics (adalimumab, etanercept, ustekinumab, and dupilumab) were extracted from the FAERS database for the period from January 2004 to December 2024. This retrospective pharmacovigilance study utilized disproportionality analysis to assess adverse events related to these biologics. Each reported adverse event in the database was mapped to a Preferred Term (PT). The PTs associated with abortion or pregnancy loss were identified from the following categories: "Termination of pregnancy and risk of abortion" (SMQ, Standardized MedDRA Query), "Pregnancy, puerperium and perinatal conditions" (SOC, System Organ Class), "Abortions and stillbirth" (HLGT, High-Level Group Term), and "Abortion-related conditions and complications" (HLT, High-Level Term), based on the Medical Dictionary for Regulatory Activities (MedDRA/J 26.1) English version. Initially, all drugs linked to these adverse events were identified, with several biologics, excluding contraceptive medications or devices, ranking among the top. Following this, abortion-related adverse events (AEs) caused by TNF inhibitors, IL12/23 inhibitors, or IL4 inhibitors were analyzed within a specific population (pregnant women (*19*) aged 15-55 years) from the FAERS database.

2.2. Analysis procedures

The sample range was determined based on relevant literature (*20,21*), with the age range (15-55 years) selected to focus on the reproductive age group of pregnant women. Only drugs identified as "PS" (Primary Suspect Drug) were included in the analysis. Disproportionality analysis, a validated method in pharmacovigilance databases, was employed for this research (*22*). The primary statistical tools used for signal detection were the Reporting Odds Ratio (ROR) (*23*) and Bayesian Confidence Propagation Neural Network (BCPNN) (*24*), with Information Component (IC) values to identify adverse reaction signals. A signal was deemed present if the number of AEs exceeded three and the lower boundary of the 95% Confidence Interval (CI) for the ROR (ROR_{025}) was > 1 or the lower boundary of the 95% CI for the IC (IC_{025}) was > 0 (*25*). The equations and parameters are listed in Table S1 (*https://www.ddtjournal.com/action/getSupplementalData.php?ID=264*).

Time to onset was defined as the period between the start of treatment and the occurrence of abortion events (Event onset date (EVENT_DT) – Therapy start date (START_DT)). To prevent distortion of results, list-wise deletion was applied to missing data and instances where the treatment start date exceeded the AE onset date. The analysis of time-to-onset data included the use of median duration, quartiles, and Weibull shape parameters (WSPs) (*26*). The differences in time to onset for abortion-related

AEs compared to non-abortion-related AEs for each biologic were assessed simultaneously.

2.3. Sensitivity analysis

To account for potential confounding factors, adjustments were made for age, weight, time-to-onset, and different medications in both univariate and multivariate logistic regression analyses. Potential covariates were screened as well. Additionally, drug-drug interactions (DDI) between methotrexate and biologics were used as a positive control, while DDI between prednisolone and biologics served as a negative control, to mitigate signal bias caused by polypharmacy. The Ω-shrinkage model, in combination with the BCPNN method, was employed to analyze DDI signals (*27*). The Japanese Adverse Drug Event Report (JADER) database, a pharmacovigilance database managed by the Pharmaceuticals and Medical Devices Agency (PMDA) of Japan, has been publicly accessible since 2012. It is used to collect and analyze AEs occurring in clinical settings post-marketing of drugs (*28*). To further validate the reliability of the findings, the same analysis was performed using the JADER database for verification purposes.

2.4. Ethical approval of studies and informed consent

Ethical review is not required as the study analyzed de-identified and publicly available FAERS or JADER data. These databases serve as the primary global system for spontaneous reporting of adverse drug events and are freely accessible to the public. The study conformed to the provisions of the Declaration of Helsinki (as revised in 2013, https://wma.net/what-we-do/medical-ethics/declaration-of-helsinki).

2.5. Statistical analysis

Statistical analyses were conducted using Microsoft Excel 2019 and R statistical software version 4.3.0. The Mann-Whitney *U* test was employed to compare AEs related to miscarriage with other AEs caused by biologics. Logistic regression was used for sensitivity analyses.

3. Results

3.1. Clinical characteristics

From Q1 2004 to Q4 2024, after data cleaning and deduplication in the FAERS database, a total of 18,627,667 cases were included (Figure 1). Among these, 124,927 cases occurred in pregnant women of childbearing age. Among biologics targeting Th1 or Th2 type cytokines, positive signals for abortion-related AEs were observed with adalimumab, etanercept, ustekinumab, and dupilumab. A total of 5,076 abortion-related AEs were reported, with adalimumab, etanercept, ustekinumab, and dupilumab identified as the "primary suspect" (PS) in 151, 225, 3, and 6 cases, respectively. Descriptive statistics regarding age, weight, reporting country, and outcomes of these cases are provided in Table 1. The number of reported cases for adalimumab (39.2%) and etanercept (58.4%) was significantly higher. This can be attributed to the time of their market approval: Adalimumab was approved in the US in 2002, and etanercept in 1998, while ustekinumab and dupilumab were launched in 2009 and 2017, respectively. Most of patients with abortion-related AEs were between 25 and 45 years old: Adalimumab (89.4%), etanercept (88%), ustekinumab (100%), and dupilumab (66.6%). The majority of patients had a weight between 45 and 65 kg: Adalimumab (23.1%), etanercept (12.4%), ustekinumab (66.7%), and dupilumab (16.7%). The top three reporting countries were the US, France, the UK, and Germany. In terms of outcomes, aside from other outcomes (OT), hospitalization (HO) was the most common, with rates of adalimumab (8.6%), etanercept (4.4%), and dupilumab (66.6%). Excluding "NA" values, the top 20 diseases treated with these drugs are presented in Figure 2.

3.2. Disproportionality analysis for biologics-related abortion AEs

The total number of abortion-related AEs involving adalimumab and etanercept was the highest, with adalimumab (1,077 cases), etanercept (455 cases), ustekinumab (91 cases), and dupilumab (131 cases). The signal values and associations between each drug and abortion-related AEs are shown in Figure 3: Adalimumab (ROR (95% CI) = 1.32 (1.24–1.42), IC (IC_{025}) = 0.37 (0.28)), etanercept (ROR (95% CI) = 1.13 (1.03–1.24), IC (IC_{025}) = 0.17 (0.03)), and ustekinumab (ROR (95% CI) = 1.29 (1.05–1.60), IC (IC_{025}) = 0.35 (0.04)) exhibited positive signal values, while dupilumab (ROR (95% CI) = 1.13 (0.95–1.35), IC (IC_{025}) = – 0.08) displayed a negative signal. At the PT level, all drugs showed positive signal values for the term "Abortion spontaneous": Adalimumab (ROR (95% CI) = 1.49 (1.39–1.59), IC (IC_{025}) = 0.53 (0.43)), etanercept (ROR (95% CI) = 1.32 (1.19–1.46), IC (IC_{025}) = 0.38 (0.23)), ustekinumab (ROR (95% CI) = 1.54 (1.23–1.92), IC (IC_{025}) = 0.59 (0.27)), and dupilumab (ROR (95% CI) = 1.35 (1.12–1.62), IC (IC_{025}) = 0.41 (0.14)). Furthermore, adalimumab showed positive signals for several additional abortion-related AEs: Abortion (ROR (95% CI) = 1.46 (1.14–1.88), IC (IC_{025}) = 0.53 (0.16)), Hemorrhage in pregnancy (ROR (95% CI) = 1.73 (1.31–2.29), IC (IC_{025}) = 0.76 (0.35)), and Post-abortion hemorrhage (ROR (95% CI) = 2.28 (1.11–4.69), IC (IC_{025}) = 1.13 (0.13)). These results suggest that different biologics are associated with positive signals for a limited number of AEs, as depicted in Figures 4A and 4B.

Pregnancy loss is closely related to abnormal

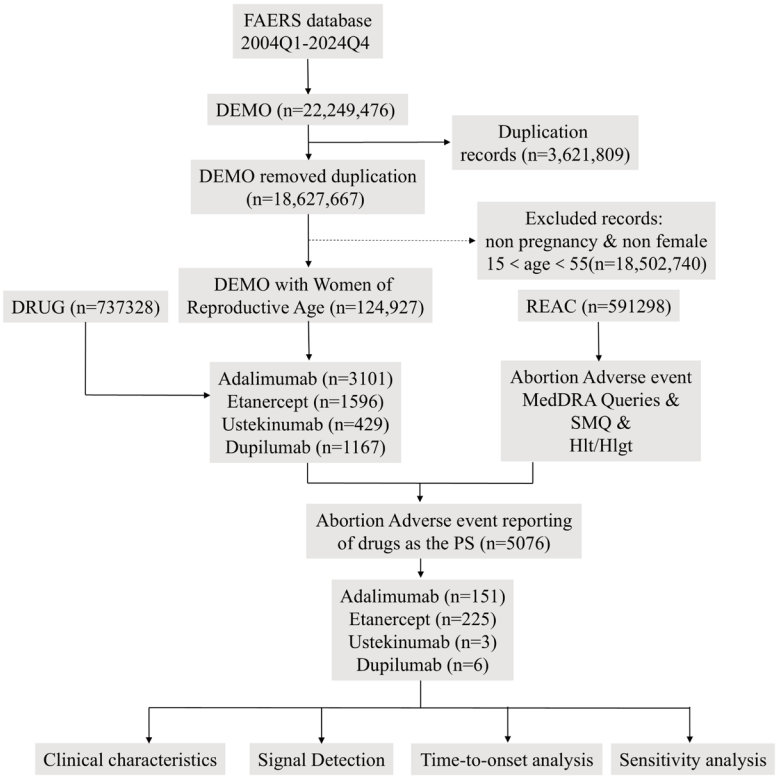

Figure 1. The flow chart of the study.

embryonic development, with the elimination of such embryos often manifesting as miscarriage. While this study focused on miscarriage-related AEs, the top 10 most frequently reported adverse reactions during pregnancy were also examined for the biologics in question. These included: Spontaneous abortion (1,519 cases), live birth (531 cases), pregnancy (456 cases), fetal death (332 cases), premature delivery (206 cases), preeclampsia (174 cases), premature labor (158 cases), gestational diabetes (149 cases), normal newborn (145 cases), and ectopic pregnancy (128 cases) (Figure 5A). Etanercept had the highest number and proportion of reports for abortion-related AEs (225 cases, 14.11%), followed by adalimumab (151 cases, 4.87%), dupilumab (6 cases, 0.51%), and ustekinumab (3 cases, 0.7%) (Figure 5B). This distribution may be influenced by the differing market availability timelines of the drugs, which could affect the baseline number of reports. The number of AEs caused by biologics in women of childbearing age during pregnancy, with a focus on death as the outcome indicator, is shown in Figure 5C. The proportion of death with the outcome of "live birth" was the highest, at 6.59%, while the proportion of death with the outcome of "abortion spontaneous" was 0.13%. The pregnancy process inherently carries risks to both the mother and fetus. Although the likelihood of maternal death due to abortion-related AEs is low, it highlights the potential risks of embryonic loss, endometrial dysfunction, and broader maternal health complications.

3.3. Time to onset of abortion-related adverse event

The time to onset of abortion-related AEs induced by these biologics was analyzed and presented in Figure 6. It was found that dupilumab had the earliest median time for inducing abortion-related AEs, whereas etanercept had the latest median time, with the broadest range. The median time to onset and interquartile range were as follows: Adalimumab: 460 days (146–1,150 days), etanercept: 558 days (184–1,432 days), ustekinumab: 281 days (120–953 days), and dupilumab: 185 days (62.5–324 days).

The WSP analysis was conducted to assess the change ratio in the incidence rate of AEs. As shown in Table 2, based on the shape parameter values, the Weibull distribution types for each drug were as follows: Adalimumab, ustekinumab, and dupilumab were categorized as "Early failure," indicating that the incidence rate of abortion-related AEs induced by these drugs decreases over time. In contrast, etanercept had a shape parameter β of 0.93, which, although classified within the "Random failure" model, still showed tendencies towards the "Early failure" pattern. A comparative analysis of the time to onset of abortion-related and non-abortion-related AEs induced by these biologics revealed that the time to onset of abortion-related AEs induced by adalimumab was significantly longer than that for non-abortion-related AEs, with a significant difference ($p = 0.009$). Conversely, the time to onset of abortion-related AEs induced by etanercept was

Table 1. Characteristics of abortion-related AEs associated with biologics

FAERS	Cases, N (%)			
Characteristic	Adalimumab	Etanercept	Ustekinumab	Dupilumab
Total cases	151 (39.2%)	225 (58.4%)	3 (0.8%)	6 (1.6%)
Gender				
Female	151 (100%)	225 (100%)	3 (100%)	6 (100%)
Age				
≥15&<25	15 (10%)	23 (10.2%)	0	1 (16.7%)
≥25&<45	135 (89.4%)	198 (88%)	3 (100%)	4 (66.6%)
≥45&≤55	1 (0.6%)	4 (1.8%)	0	1 (16.7%)
Reported countries (Top3)				
1	US 33 (21.8%)	US 102 (45.3%)	FRA 2 (66.6%)	US 2 (33.3%)
2	GER 12 (7.9%)	UK 21 (9.3%)	US 1 (33.3%)	FRA 1 (16.6%)
3	UK 10 (6.6%)	GER 15 (6.6%)	-	GER 1 (16.6%)
Outcomes				
OT	137 (90.7%)	208 (92.4%)	3 (100%)	4 (66.6%)
HO	13 (8.6%)	10 (4.4%)	-	2 (33.3%)
CA		4 (1.7%)		-
DS		1 (0.4%)		
LT		1 (0.4%)		
Weight				
<45	2 (1.3%)	1 (0.4%)	0	0
≥45&<65	35 (23.1%)	28 (12.4%)	2 (66.7%)	1 (16.7%)
≥65&<80	17 (11.3%)	9 (4%)	1 (33.3%)	0
≥80	10 (6.6%)	9 (4%)	0	1 (16.7%)
JADER	Cases, N (%)			
Characteristic	Adalimumab	Etanercept	Ustekinumab	Dupilumab
Total cases	9 (32.1%)	13 (46.4%)	5 (17.9%)	1 (3.6%)
Gender/Female	9 (100%)	13 (100%)	5 (100%)	1 (100%)
Reported person				-
Physician	5 (55.6%)	10 (76.9%)	3	
consumer	1 (11.1%)	0	0	
pharmacist	2 (22.2%)	0	2	
Medical professionals	1 (11.1%)	3 (33.1%)	0	
Outcomes				
recovery	4 (44.4%)	4 (30.8%)	1 (20.0%)	
sequela	0		2 (40.0%)	
unknow	5 (55.6%)	9 (69.2%)	2 (40.0%)	

FAERS: FDA Adverse Event Reporting System, JADER: Japanese Adverse Drug Event Report, OT: Other, HO: Hospitalization - Initial or prolonged, CA: Congenital Anomaly, DS: Disability, LT: Life - Threatening.

significantly shorter than for non-abortion-related AEs ($p < 0.01$). For the other two biologics, the differences were not statistically significant.

3.4. Sensitivity analysis

To mitigate potential confounding factors, logistic regression analyses were performed, with age, weight, time to onset, and each drug as independent variables and the occurrence of the target AEs as the dependent variable. The variables were categorized as follows: AGE (age) into four groups: < 23 years, 23-35 years, 35-45 years, and > 45 years; WT (weight) into three groups: < 50 kg, 50-80 kg, and > 80 kg; TIME (time of onset) into three groups: < 1 year, 1-2 years, and > 2 years; and each drug: Adalimumab, etanercept, ustekinumab, and dupilumab. Using the "< 23 years old" group as the reference for age, the risk of abortion-related AEs was significantly increased in the 23-35 years old group (OR = 1.62 [1.12-2.38, $p = 0.012$]), increased but not significantly in the 35-45 years old group (OR = 1.28 [0.87-1.92, $p = 0.228$]), and decreased but not significantly in the > 45 years old group (OR = 0.49 [0.11-1.51, $p = 0.269$]). For time to onset, the risk of abortion was significantly increased in the 1-2 years group (OR = 1.65 [1.24-2.18, $p < 0.001$]) and even more so in the > 2 years group (OR = 2.26 [1.84-2.77, $p < 0.001$]). Compared to the adalimumab group (reference), the risk of abortion was significantly lower in the ustekinumab group (OR = 0.73 [0.57-0.92, $p = 0.010$]), while no significant differences were observed in the other two groups (Figure 7A). After adjusting for other risk factors (Figure 7B), the risk of abortion in the 23-35 years age group was significantly higher than in the reference group (< 23 years old) (OR = 0.73 [0.57-0.92, $p = 0.010$]), while no significant differences

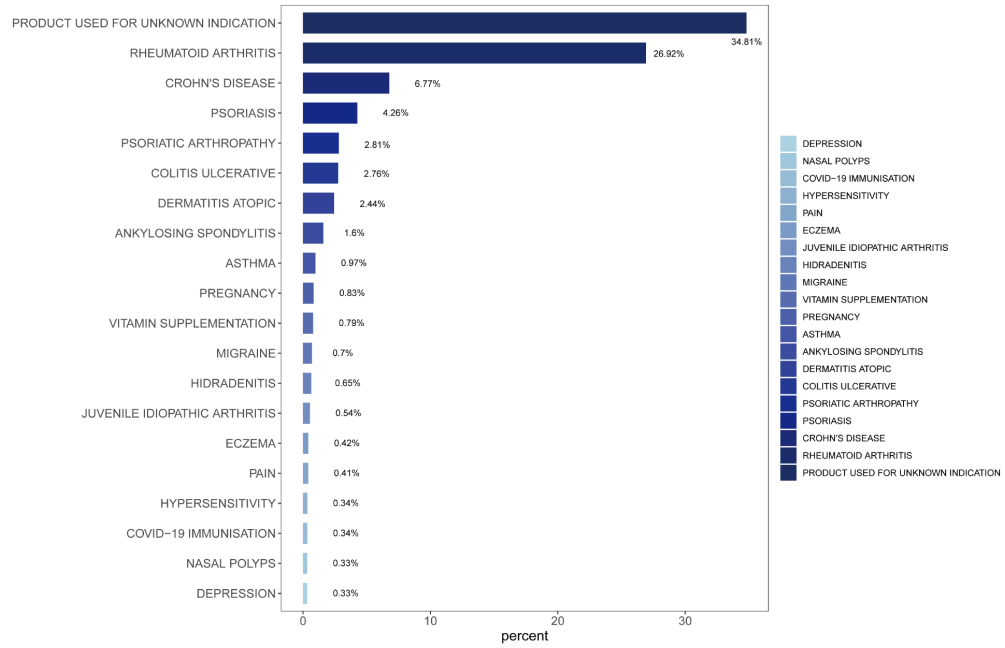

Figure 2. Top 20 diseases treated with these biologics as reported in the FAERS database.

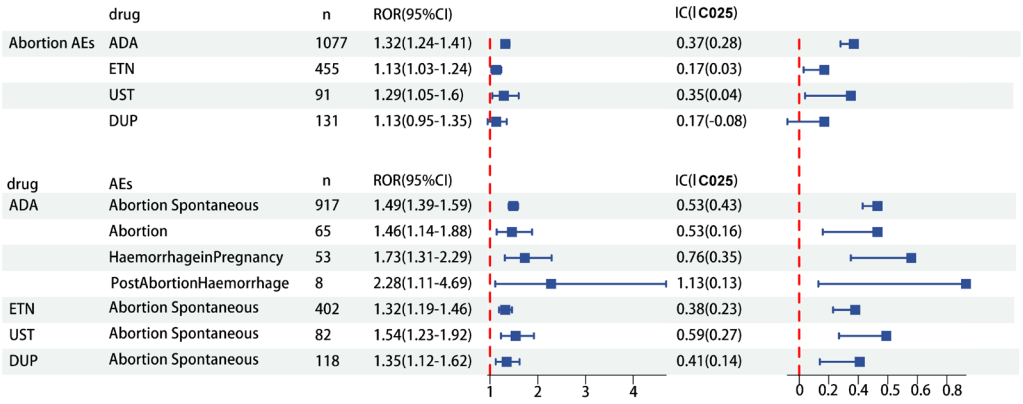

Figure 3. Abortion-related AEs among different biologics.

were observed in the 35-45 and > 45 years age groups compared to the reference group. Weight differences did not significantly influence the outcome. The risk of abortion was significantly higher in the 1-2 years group (OR = 1.65 [1.24-2.19, $p = 0.001$]) and even more so in the > 2 years group (OR = 2.30 [1.86-2.83, $p < 0.001$]). Compared to the adalimumab group, the risk of abortion was significantly lower in the ustekinumab group (OR = 0.72 [0.56-0.92, $p = 0.011$]) and significantly higher in the dupilumab group (OR = 1.97 [1.23-3.13, $p = 0.004$]). The covariates selected by on the stepwise method are presented in Table S2 (*https://www.ddtjournal.com/action/getSupplementalData.php?ID=264*). The covariates that have a notably influence on the model include AGE ≥ 23 years and < 35 years, time to onset ≥ 1 year, and the two drugs ustekinumab and dupilumab.

Methotrexate and prednisolone are commonly used to treat autoimmune inflammatory diseases. Methotrexate is associated with pregnancy loss and teratogenicity (*29*), while prednisolone is used to support pregnancy, particularly in patients with recurrent miscarriages (*30*). A sensitivity analysis was conducted to assess the combination of biologics with methotrexate or prednisolone. The association between the combination of adalimumab and methotrexate and abortion was statistically significant, with the combination potentially reducing the risk of abortion (IC: -2.65 (-2.97 to -2.30), Ω: 0.02) (Table 3). Adalimumab alone was associated with an increased risk of abortion (IC: 0.74 (0.65 to 0.84)). Methotrexate alone may reduce the risk of abortion (IC:

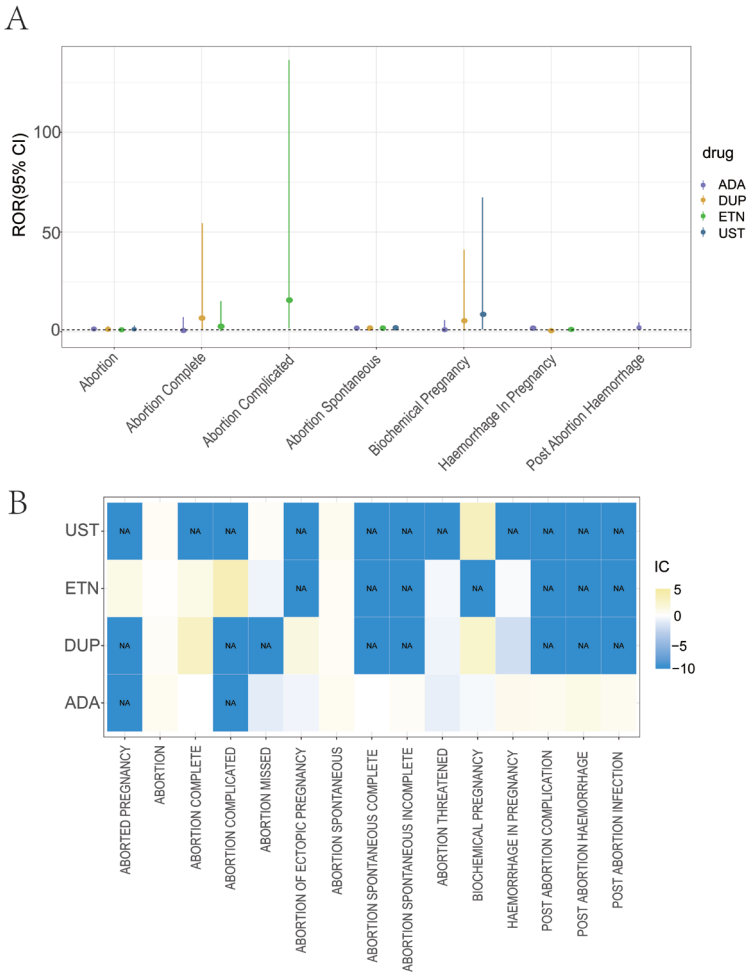

Figure 4. The associations between Abortion-related AEs and different biologics. (A) Forest plots of RORs of different biologics. **(B)** Heatmap showing the associations between biologics and abortion-related AEs. ADA, Adalimumab; ETN, Etanercept; UST, Ustekinumab; DUP, Dupilumab.

-1.01 (-1.29 to -0.71)), though not to the extent observed with the combination of both drugs. A disproportionality analysis of methotrexate in the FAERS database at the PT level for pregnant women is shown in Table S3 (*https://www.ddtjournal.com/action/getSupplementalData.php?ID=264*). Among the AEs related to abortion, "INDUCED ABORTION FAILED" was the only positive event (ROR: 13.67 (7.92 to 23.61)). Given its known teratogenic risks, the use of methotrexate in pregnant populations is highly cautioned. Even so, the analysis in the FAERS database is inconsistent with existing literature. In summary, adalimumab is significantly associated with abortion-related AEs. The combination of adalimumab and prednisolone may reduce the risk of abortion (IC: -2.51 (-2.89 to -2.07), Ω: 0.02), whereas the use of prednisolone alone is associated with abortion-related AEs (IC: 0.79 (0.69 to 0.88)). For other biologics, the risk of abortion is higher in non-combined use with prednisolone compared to combination therapy, except for dupilumab. Additionally, there is insufficient data on the combination of ustekinumab and dupilumab with prednisolone and methotrexate. These findings support the reliability of the association between the studied biologics and abortion-related AEs.

A similar investigation was conducted on abortion-related AEs reports in pregnant women of childbearing age from the post-marketing period of these drugs through Q2 2024 in the JADER database (Figure 7C). The number of cases involved was relatively small, including adalimumab (9 cases), etanercept (13 cases), ustekinumab (5 cases), and dupilumab (1 case). The risk assessment results were as follows: Adalimumab: ROR (95% CI) = 2.48 (1.28–4.79), IC (IC025) = 1.29 (– 0.38); Etanercept: ROR (95% CI) = 2.22 (1.28–3.85), IC (IC025) = 1.14 (– 0.53); Ustekinumab: ROR (95% CI) = 10.09 (4.14–24.58), IC (IC025) = 3.29 (1.61). The signal values for adalimumab, etanercept, and ustekinumab were positive. However, only adalimumab and etanercept had sufficient sample sizes for further analysis. Positive signal values for the PT "Abortion spontaneous " were observed: Adalimumab: ROR (95% CI) = 4.7 (2.09–10.57), IC (IC025) = 2.2 (0.52); Etanercept: ROR (95% CI) = 3.98 (1.97–8.05), IC (IC025) = 1.96 (0.28). These results are generally consistent with the findings from the

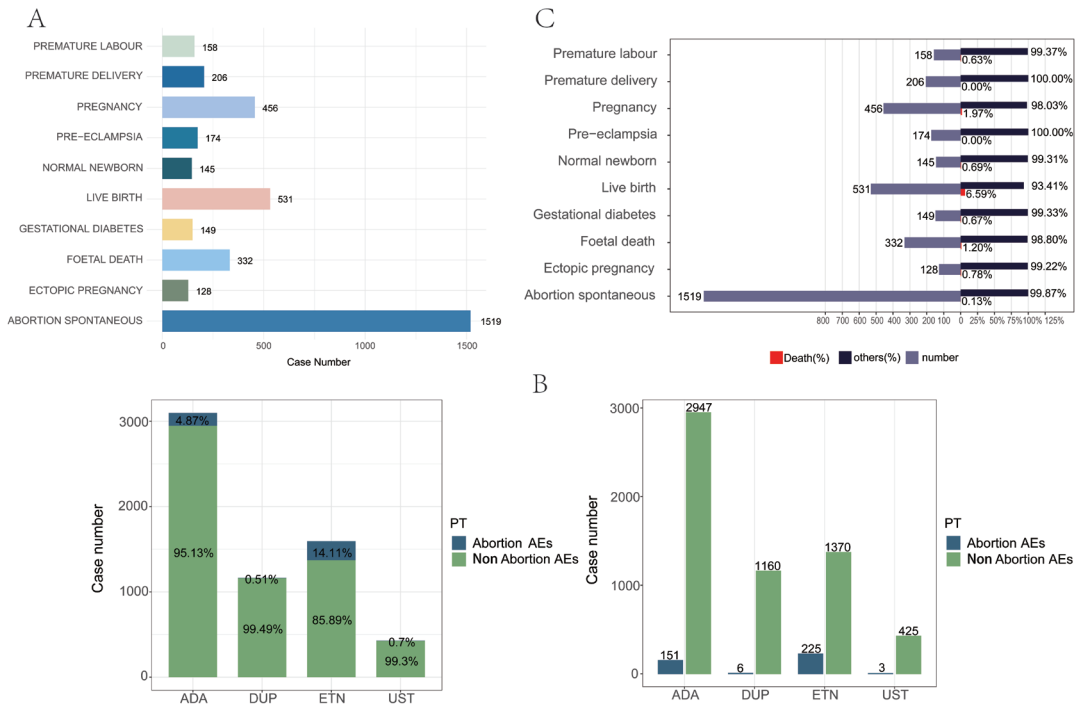

Figure 5. Comparison and outcomes of Abortion-related AEs caused by biologics versus other adverse events. (A) The number of reported cases of the first ten types of these biologics related abortion- AEs. **(B)** The bar chart shows the percentage and number of different biologics abortion AEs and non-abortion-related AEs of different biologics in the FAERS database from Q1 2004 to Q4 2024. **(C)** Death cases and their proportion in biologics concomitantly with abortion AEs. ADA, Adalimumab; ETN, Etanercept; UST, Ustekinumab; DUP, Dupilumab. The vertical axis represents PT. PT, preferred term.

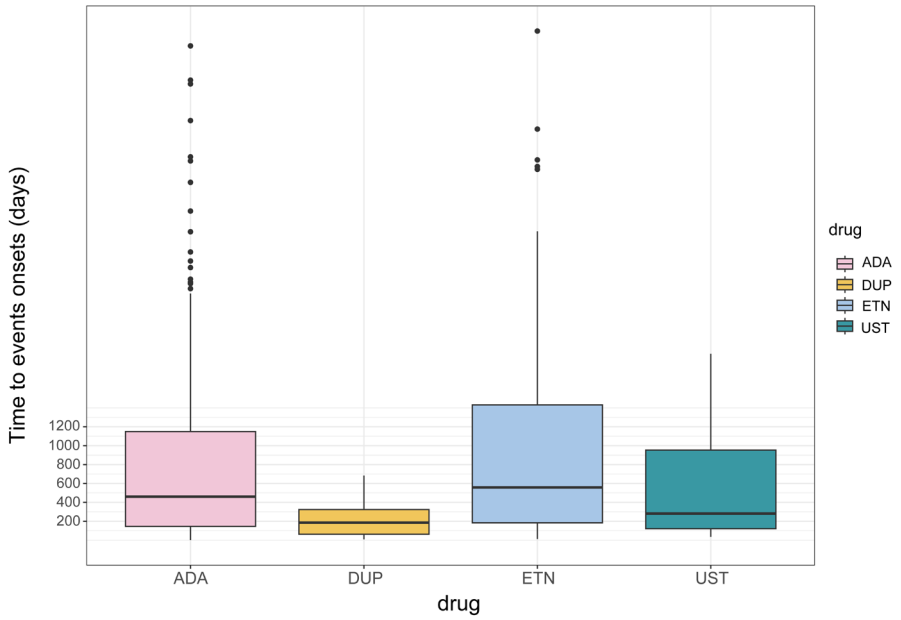

Figure 6. Time to onset of abortion-related AEs. ADA, Adalimumab; ETN, Etanercept; UST, Ustekinumab; DUP, Dupilumab.

FAERS database study.

4. Discussion

The pregnancy represents a high-risk period for pharmacological treatments, particularly for women with chronic inflammatory rheumatic, gastroenterological, or dermatological diseases. During this time, pharmacokinetics and pharmacodynamics undergo significant alterations, presenting potential risks to fetal development. This poses a crucial concern in treatment decisions. Pregnant women often face the challenge of balancing the benefits and risks of pharmacotherapy, which necessitates collaborative decision-making with

Table 2. The WSP analysis for Time-to-onset of different biologics

Database	Adalimumab		Etanercept		Ustekinumab		Dupilumab	
	Abortion AEs	Non Abortion AEs	Abortion AEs	Non Abortion AEs	Abortion AEs	Non Abortion AEs	Abortion AEs	Non Abortion AEs
case reports	622	1036	276	500	48	138	40	162
Median(d)	460	394	558	920	281	395	185	119
(25%-75%)	(146-1150)	(140-809)	(184-1432)	(374-1425)	(120-953)	(133-924)	(62.5-324)	(46-330)
p	0.009		< 0.001		0.408		0.708	
Scale parameter:α	752.57	615.20	868.52	1323.81	597.43	667.58	229.355867	240.53
(95% CI)	(680.35-824.79)	(572.72-657.68)	(750.43-986.61)	(1207.32-1440.30)	(389.73-769.13)	(533.34-801.82)	(158.77-299.94)	(193.63-287.43)
Shape parameter:β	0.86	0.93	0.91	1.04	0.91	0.87	1.05	0.84
(95% CI)	(0.81-0.92)	(0.86-0.94)	(0.83-1.00)	(0.98-1.12)	(0.71-1.12)	(0.76-0.99)	(0.79-1.32)	(0.74-0.93)
Type	Early failure	Early failure	Random failure	Random failure	Random failure	Early failure	Random failure	Early failure

physicians and pharmacists(*31*). This study employed the ROR and BPCNN methods to investigate abortion-related adverse signals linked to adalimumab, etanercept, ustekinumab, and dupilumab in pregnant populations, utilizing data from the FAERS and JADER databases. Among the reported conditions, rheumatoid arthritis (RA, 26.92%), Crohn's disease (6.77%), psoriasis (4.46%), psoriatic arthropathy (2.81%), ulcerative colitis (2.76%), atopic dermatitis (2.44%), ankylosing spondylitis (1.6%), and asthma (0.97%) comprised nearly half of the cases. Notably, "Abortion spontaneous" was the most frequently reported AE across all AEs in pregnant women using these biologics.

Adalimumab and etanercept had a higher number of reported cases due to their earlier release compared to other biologics. Studies have shown that 88.3% of patients with RA are aged between 25 and 45 years, which aligns with the typical childbearing age. Women are more likely to develop RA than men, with conditions such as menopause, postpartum status, and anti-estrogen therapy potentially increasing the risk for RA (*32*). RA also tends to peak between the ages of 50 and 54 years (*33*). The age distribution for IBDs like Crohn's disease and ulcerative colitis follows a bimodal pattern, peaking around ages 20-30 and 50-70 (*34,35*). Atopic dermatitis typically begins in early childhood (*36*) and has a higher incidence in women (10.2%) than men (5.8%) (*37*). The onset of psoriasis is concentrated in two age brackets: 30-39 and 60-69 years, with women tending to develop it slightly earlier than men (*38*). Ankylosing spondylitis is more common in men, particularly between the ages of 18 and 35 (*39*), though it often experiences diagnostic delays in women. The age distribution of these immune-related inflammatory disorders aligns with the age group of women under study. In the sensitivity analysis, both univariate and multivariate logistic regression revealed that compared to the < 23 age group, the signals for abortion-related AEs were more pronounced in the 23-35 age group. Women aged 25 to 45 years, a group with higher fertility demands, may be more exposed to biological treatments, which raises the question of whether the age distribution of cases correlates with active drug interventions in women with strong fertility desires. Factors such as the sensitivity of the reproductive system, the placental barrier's permeability to drugs, and the combined effects of drugs and diseases on pregnancy were considered in relation to the age distribution of cases (*40*).

Pregnant women with chronic autoimmune inflammatory diseases may face significant challenges in controlling active disease, ensuring endometrial receptivity, and weighing the benefits and risks of pharmacological treatment. The impact of diseases such as RA and Crohn's disease on pregnancy outcomes is largely determined by the loss of disease control, a concern also applicable to atopic diseases (*32,40,41*). Adequate disease control before and during pregnancy is

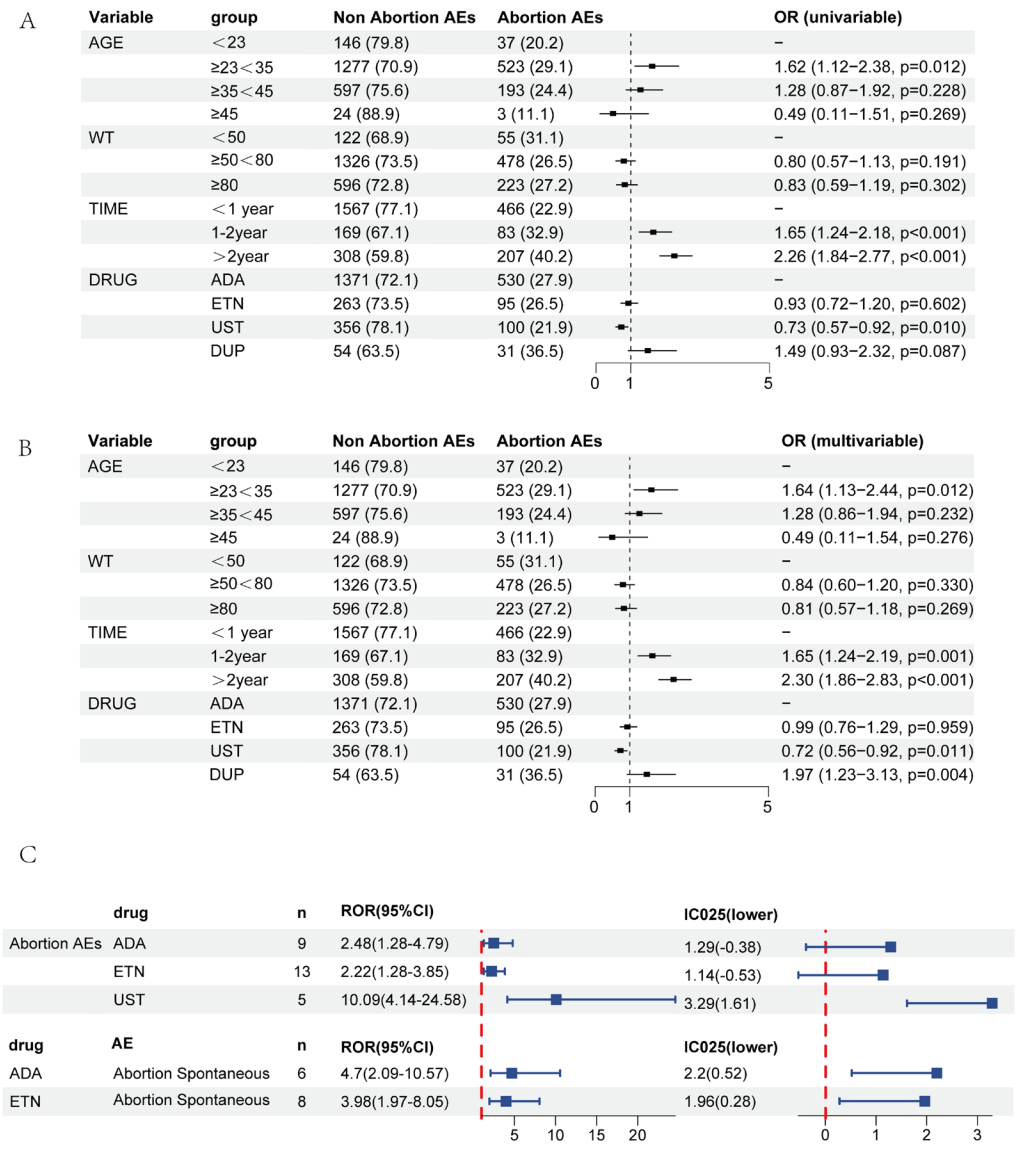

Figure 7. Logistic regression model for detecting influences on the results of outcomes and analysis of JADER databases. (A) Univariate logistic regression for age, weight, time-to-onset, and the effects of different drugs on AEs. **(B)** Multivariate logistic regression for age, weight, time-to-onset, and the effects of different drugs on abortion-related AEs. WT, weight; ADA, Adalimumab; ETN, Etanercept; UST, Ustekinumab; DUP, Dupilumab. **(C)** Abortion-related AEs among different biologics in the JADER database.

crucial. Inflammatory responses undergo distinct phases during pregnancy (*42*). Early pregnancy inflammation, at mild levels, supports endometrial decidualization, trophoblast invasion, and the formation of placental and embryonic structures (*43,44*). However, chronic autoimmune inflammatory diseases like RA, IBD, psoriasis, and ankylosing spondylitis can disrupt cytokine and chemokine signaling in embryonic trophoblast cells. Adalimumab, ustekinumab, and dupilumab are fully human monoclonal antibodies that exert their effects by neutralizing tumor necrosis factor-alpha (TNF-α), blocking the signaling of IL-12 and IL-23, and dual-blocking the signaling of IL-4 and IL-13, respectively (*16,40*). Etanercept, a fusion protein, inhibits TNF-α activity and signaling by preventing its interaction with natural receptors (*4*). These biologics target different cytokines or receptors to modulate inflammatory responses and treat a variety of autoimmune and inflammatory diseases. In the preliminary screening results of biologics associated with abortion-related AEs, these drugs ranked among the top, but relevant research on their safety during pregnancy remains limited.

As research advances, the use of biologics during pregnancy has shifted from cautious hesitation (*45*) to more optimistic support (*16*). This is based on the conclusions derived from subsequent research that reported the safety and lower risk of spontaneous abortion associated with the use of the evoked above biologics during pregnancy. Respectively, a case studies have supported the therapeutic benefits of adalimumab in patients with potential spontaneous abortions (*46*); During pregnancy, the use of etanercept relatively safe

Table 3. DDI interactions between biologics and methotrexate/prednisolone

Durg1	Drug2	N of Abortion with Drug1&Drug2/N of all AEs with Drug1&Drug2	Drug1&Drug2 IC(IC025-IC975)	Ω(Ω025-Ω075)	N of Abortion with Drug1/N of all AEs with Drug1	Drug1 IC (IC025-IC975)	N of Abortion with Drug2/N of all AEs with Drug2	Drug2 IC (IC025-IC975)
Adalimumab	Methotrexate	75/11092	-2.65 (-2.97–-2.3)	0.02 (-0.04-0.08)	984/13851	0.74 (0.65-0.84)	100/4746	-1.01 (-1.29–-0.71)
Adalimumab	Prednisone	49/6567	-2.51 (-2.89–-2.07)	0.02 (-0.057-0.104)	1002/13685	0.79 (0.69-0.88)	44/1873	-0.85 (-1.27–-0.4)
Etanercept	Methotrexate	59/10208	-2.88 (-3.23–-2.48)	-3.88 (-4.72–-3.03)	413/4831	1.01 (0.86-1.16)	89/4767	-1.18 (-1.48–-0.87)
Etanercept	Prednisone	26/5283	-3.11 (-3.62–-2.5)	-4.08 (-5.35–-2.80)	427/5051	0.99 (0.84-1.14)	44/1908	-0.88 (-1.3–-0.43)
Ustekinumab	Methotrexate	1/4913	-7.7 (-8.75–-4.67)	0.03 (-0.07-0.12)	90/1265	0.75 (0.42-1.05)	108/5773	-1.18 (-1.45–-0.89)
Dupilumab	Prednisone	3/13	2.44 (-0.31-2.96)	1.66 (-2.09-5.42)	127/2726	0.13 (-0.13-0.39)	108/10270	-2.01 (-2.28–-1.72)

(*47*); it has also identified that the safety of ustekinumab during pregnancy is higher than that of TNF-α inhibitors (*48*). A review and meta-analysis estimated that among patients with psoriasis using adalimumab, etanercept, ustekinumab, and other biologics during early pregnancy, the prevalence of abortion was 15.3%, and the rate of congenital malformations in live births was approximately 3.0%. This suggests that the pregnancy risks associated with biologic treatment in patients with psoriasis are not significant (*49*). However, spontaneous abortion remains one of the most common adverse pregnancy outcomes associated with TNF-α inhibitors (*9*). Additionally, there have been recommendations to prohibit the clinical use of etanercept and adalimumab from the mid-pregnancy period to the end of pregnancy (*15*). A multicenter retrospective cohort study indicated that exposure to dupilumab during 2–24 weeks of gestation may be linked to an increased risk of adverse pregnancy outcomes, including abortion or embryonic abnormalities, although no statistically significant effects were found. Dupilumab use during pregnancy was also associated with improved atopic dermatitis and a very low risk of adverse pregnancy outcomes (*50*). Fully human monoclonal antibodies like adalimumab, dupilumab, and ustekinumab have half-lives ranging from 9 to 23 days, while Fc fusion proteins such as etanercept have shorter half-lives of 4 to 13 days (*11*). These biologics cross the placenta, with transfer rates gradually increasing from mid-pregnancy through to after 30 weeks of gestation, when fetal or cord serum levels may match or exceed maternal levels (*4*). Previous studies may generate bias in their results due to different kinds of Immune-related inflammatory diseases, limitations in sample size, and variations in administration methods. The present study selectively included women of childbearing age who were pregnant, excluding those with abortion-related AEs. The overall signal for all abortion-related AEs induced by each drug, along with signals for individual PTs, was within the positive range. However, the ROR and IC values indicated a weak association between the drugs and abortion-related AEs. These findings are consistent with previous research. Despite this, the unique characteristics of the pregnant population necessitate a thorough assessment, rational medication use, and vigilant monitoring. Forest plots and heatmaps were employed to depict the degree of association between the drugs and abortion-related AEs. Both "abortion" and "Abortion spontaneous" were observed with each drug. Ustekinumab and dupilumab showed relatively stronger associations with "biochemical pregnancy," whereas etanercept and adalimumab were more strongly associated with "abortion complicated" or "abortion complete". While the overall number of abortion-related AEs was highest in the pregnant population, severe outcomes such as death were rare. Time-to-onset analysis revealed that adalimumab and etanercept

had relatively longer durations, while ustekinumab and dupilumab had shorter ones. Weibull analysis indicated that the incidence of abortion-related AEs generally declined over time, suggesting that prolonged treatment may correlate with reduced risk. Logistic regression in the sensitivity analysis revealed that the risk of AEs increased for events occurring between 1 and 2 years, or after 2 years, compared to those occurring within 1 year. Long-term drug use may lead to cumulative effects, heightening the risk of AEs. These findings offer insights into the latency period of drug-induced AEs in clinical practice, but further long-term prospective observational data are needed for confirmation.

The positive signal strength of abortion-related AEs associated with the same biologics in women of childbearing age, as observed in the JADER database, aligns closely with findings from the FAERS database and prior literature. However, small sample sizes continue to introduce significant confounding factors and biases. Treatment guidelines for RA caution against the use of methotrexate during pregnancy, regardless of dose, recommending its discontinuation at least three months prior to conception (*15*). The therapeutic benefits of prednisolone in recurrent miscarriages or spontaneous abortions primarily pertain to antiphospholipid syndrome treatment, and its effects on pregnancy outcomes and embryonic development are complex and not universally applicable (*51,52*). During the data mining process, these drugs are often administered in combination. The signal for abortion-related AEs from methotrexate in the FAERS database does not align with literature findings, likely due to the explicit prohibition of its use in pregnant populations. However, adalimumab, etanercept, ustekinumab, and dupilumab still exhibit a positive association with abortion-related AEs, independent of their use alongside methotrexate or prednisolone.

Several limitations are inherent in this retrospective database study. Both the FAERS and Open FDA databases are subject to natural reporting bias, with significant information loss in spontaneous anonymous reporting systems. As such, causality between biologics and pregnancy loss cannot be definitively established through pharmacovigilance studies alone (*53*). Furthermore, most of the studies referenced in this analysis were conducted in the US and Europe, while the JADER database has a limited sample size and lacks global representation. With the limitations of the database information exceptions, clinical studies on the association between biologics and spontaneous abortions are extremely rare currently. Most of existing research has expressed doubts and uncertainties regarding their safety during pregnancy. However, in recent years, their reputation has improved somewhat. The last limitation is whether the biologics or the disease itself is the "culprit" of spontaneous abortion. Clinical research on different biologics for treating various diseases has yielded different conclusions. For example, some studies have found that conditions such as RA (*4,54*), psoriasis (*55,56*), ankylosing spondylitis (*57*), and atopic dermatitis (*58*) basically do not increase the risk of miscarriage. The positive results of another study on psoriasis may be related to the older age of the sample population (*59*). However, Crohn's disease and ulcerative colitis may increase the risk of miscarriage (*60,61*). In summary, this overview is consistent with the findings of a recent registry linkage study in Norway (*62*). Therefore, the key issue we need to address in subsequent research is to further clarify the complex interactions between drugs, diseases during pregnancy. Larger, prospective, randomized clinical trials are necessary to validate these findings and support these hypotheses. In clinical studies, efforts should be made to standardize disease activity and treatment duration as much as possible, while also establishing comprehensive control groups.

In conclusion, the study performed a disproportionality analysis of four biologics used during pregnancy and their association with abortion-related AEs. The results are consistent with existing literature: biologics are linked to an increased risk of adverse pregnancy outcomes such as miscarriage, although the association remains relatively weak. This conclusion necessitates confirmation through large-scale, prospective studies.

Acknowledgements

We thank FAERS for the availability of the data. We thank Bullet Edits Limited for the linguistic editing and proofreading of the manuscript.

Funding: This research was funded by the National Natural Science Foundation of China grant number (82305284).

Conflict of Interest: The authors have no conflicts of interest to disclose.

References

1. Cao F, Pan HF, Hou S. A novel metric of autoimmune disease burden and its estimated incidence across different stages in life cycle of women. Autoimmun Rev. 2024; 23:103671.
2. van Loo G, Bertrand MJM. Death by TNF: a road to inflammation. Nat Rev Immunol. 2023; 23:289-303.
3. Jenkins C, Roberts J, Wilson R, MacLean MA, Shilito J, Walker JJ. Evidence of a T(H) 1 type response associated with recurrent miscarriage. Fertil Steril. 2000; 73:1206-1208.
4. Romanowska-Prochnicka K, Felis-Giemza A, Olesinska M, Wojdasiewicz P, Paradowska-Gorycka A, Szukiewicz D. The Role of TNF-alpha and Anti-TNF-alpha Agents during Preconception, Pregnancy, and Breastfeeding. Int J Mol Sci. 2021; 22:2922.
5. Liu M, Zhen X, Song H, Chen J, Sun X, Li X, Zhou J, Yan G, Ding L, Sun H. Low-dose lymphocyte immunotherapy

rebalances the peripheral blood Th1/Th2/Treg paradigm in patients with unexplained recurrent miscarriage. Reprod Biol Endocrinol. 2017; 15:95.
6. Mor G, Cardenas I, Abrahams V, Guller S. Inflammation and pregnancy: the role of the immune system at the implantation site. Ann N Y Acad Sci. 2011; 1221:80-87.
7. Spence T, Allsopp PJ, Yeates AJ, Mulhern MS, Strain JJ, McSorley EM. Maternal Serum Cytokine Concentrations in Healthy Pregnancy and Preeclampsia. J Pregnancy. 2021; 2021:6649608.
8. Guinn D, Kratz K, Baisden K, Ridge S, McClymont S, Fletcher EP, Johnson T, Wang YM. On placental and lactational transfer of IgG-based therapeutic proteins - Current understanding and knowledge gaps from a clinical pharmacology perspective. Clin Transl Sci. 2024; 17:e70049.
9. Dai FF, Hu M, Zhang YW, Zhu RH, Chen LP, Li ZD, Huang YJ, Hu W, Cheng YX. TNF-alpha/anti-TNF-alpha drugs and its effect on pregnancy outcomes. Expert Rev Mol Med. 2022; 24:e26.
10. Romero-Mate A, Garcia-Donoso C, Cordoba-Guijarro S. Efficacy and safety of etanercept in psoriasis/psoriatic arthritis: an updated review. Am J Clin Dermatol. 2007; 8:143-155.
11. Gotestam Skorpen C, Hoeltzenbein M, Tincani A, *et al*. The EULAR points to consider for use of antirheumatic drugs before pregnancy, and during pregnancy and lactation. Ann Rheum Dis. 2016; 75:795-810.
12. Chopra CR, Sharma M, Gill MS, Del Balso V, Sakka N, Abu-Hilal M. Maternal, Fetal, and Labour Outcomes of Dupilumab Use for Atopic Dermatitis During Pregnancy: A Systematic Review. J Cutan Med Surg. 2025; 29:51-55.
13. Watson N, Wu K, Farr P, Reynolds NJ, Hampton PJ. Ustekinumab exposure during conception and pregnancy in patients with chronic plaque psoriasis: a case series of 10 pregnancies. Br J Dermatol. 2019; 180:195-196.
14. Gorodensky JH, Bernatsky S, Afif W, Filion KB, Vinet E. Ustekinumab Safety in Pregnancy: A Comprehensive Review. Arthritis Care Res (Hoboken). 2023; 75:930-935.
15. Wise J. Rheumatic diseases should be actively treated in pregnancy, new guidelines say. BMJ. 2016; 532:i312.
16. Seow CH, Ma C. Keep calm and carry on-managing non-TNF antagonist biologics in pregnancy. Aliment Pharmacol Ther. 2021; 53:450-451.
17. Kachikis A, Englund JA. Maternal immunization: Optimizing protection for the mother and infant. J Infect. 2016; 72 Suppl:S83-90.
18. Joshi A, Gawey L, Saadi C, Naidoo P, Rick JW, Park SY, Cogen AL, Daveluy SD, Hsiao JL, Shi VY. Postmarketing safety surveillance of adalimumab, secukinumab, and infliximab in hidradenitis suppurativa: an analysis of the FDA adverse events reporting system (FAERS) database. J Am Acad Dermatol. 2025; 92:1434-1435.
19. Sakai T, Mori C, Ohtsu F. Potential safety signal of pregnancy loss with vascular endothelial growth factor inhibitor intraocular injection: A disproportionality analysis using the Food and Drug Administration Adverse Event Reporting System. Front Pharmacol. 2022; 13:1063625.
20. Zhou J, Wei Z, Lai W, Liu M, Wu X. The safety profile of usage of glucagon-like peptide-1 receptor agonists in pregnancy: A pharmacovigilance analysis based on the Food and Drug Administration Adverse Event Reporting System. Br J Clin Pharmacol. 2025; 91:1272-1280.
21. Xu H, Xu N, Wang Y, Zou H, Wu S. A disproportionality analysis of low molecular weight heparin in the overall population and in pregnancy women using the FDA adverse event reporting system (FAERS) database. Front Pharmacol. 2024; 15:1442002.
22. Liu Y, Liu Y, Fan R, Kehriman N, Zhang X, Zhao B, Huang L. Pharmacovigilance-based drug repurposing: searching for putative drugs with hypohidrosis or anhidrosis adverse events for use against hyperhidrosis. Eur J Med Res. 2023; 28:95.
23. Liu H, Zou Y, Zhang Q, Zhao J, Wu J, Li X, Cheng Y, Wei H, Li H, Cao S. Pharmacovigilance insights into medication-induced risk of dural arteriovenous fistula. Int J Surg. 2025; 111:1847-1859.
24. Noren GN, Hopstadius J, Bate A. Shrinkage observed-to-expected ratios for robust and transparent large-scale pattern discovery. Stat Methods Med Res. 2013; 22:57-69.
25. Liu J, Xue L, Zeng F, Liu Y, Zhu Y, Zhou J, Zhang J, Chen H. Exploring the potential association between stimulant or atomoxetine use and suicidal or self-injurious behaviors in children with attention deficit hyperactivity disorder: real-world insights from the FAERS database. Eur Child Adolesc Psychiatry. 2025. doi: 10.1007/s00787-025-02694-w.
26. Shu Y, He X, Wu P, Liu Y, Ding Y, Zhang Q. Gastrointestinal adverse events associated with semaglutide: A pharmacovigilance study based on FDA adverse event reporting system. Front Public Health. 2022; 10:996179.
27. Zhang S, Yan MM, Zhao H, Qiu XY, Zhu D. Rhabdomyolysis associated with concomitant use of colchicine and statins in the real world: identifying the likelihood of drug-drug interactions through the FDA adverse event reporting system. Front Pharmacol. 2024; 15:1445324.
28. Inaba I, Kondo Y, Iwasaki S, Tsuruhashi S, Akaishi A, Morita K, Oniki K, Saruwatari J, Ishitsuka Y, Irie T. Risk Evaluation for Acute Kidney Injury Induced by the Concomitant Use of Valacyclovir, Analgesics, and Renin-Angiotensin System Inhibitors: The Detection of Signals of Drug-Drug Interactions. Front Pharmacol. 2019; 10:874.
29. Weber-Schoendorfer C, Diav-Citrin O. Methotrexate in pregnancy: still many unanswered questions. RMD Open. 2023; 9:e002899.
30. Bulletti C, Flamigni C, Giacomucci E. Reproductive failure due to spontaneous abortion and recurrent miscarriage. Hum Reprod Update. 1996; 2:118-136.
31. Lynch MM, Amoozegar JB, McClure EM, Squiers LB, Broussard CS, Lind JN, Polen KN, Frey MT, Gilboa SM, Biermann J. Improving Safe Use of Medications During Pregnancy: The Roles of Patients, Physicians, and Pharmacists. Qual Health Res. 2017; 27:2071-2080.
32. Finckh A, Gilbert B, Hodkinson B, Bae SC, Thomas R, Deane KD, Alpizar-Rodriguez D, Lauper K. Global epidemiology of rheumatoid arthritis. Nat Rev Rheumatol. 2022; 18:591-602.
33. Zhang Z, Gao X, Liu S, Wang Q, Wang Y, Hou S, Wang J, Zhang Y. Global, regional, and national epidemiology of rheumatoid arthritis among people aged 20-54 years from 1990 to 2021. Sci Rep. 2025; 15:10736.
34. Ali RA. The positive influences of increasing age at diagnosis of inflammatory bowel disease on disease prognostication in asian perspective. Intest Res. 2015; 13:4-5.
35. Quezada SM, Steinberger EK, Cross RK. Association

of age at diagnosis and Crohn's disease phenotype. Age Ageing. 2013; 42:102-106.
36. Weidinger S, Beck LA, Bieber T, Kabashima K, Irvine AD. Atopic dermatitis. Nat Rev Dis Primers. 2018; 4:1.
37. Bylund S, Kobyletzki LB, Svalstedt M, Svensson A. Prevalence and Incidence of Atopic Dermatitis: A Systematic Review. Acta Derm Venereol. 2020; 100:adv00160.
38. Iskandar IYK, Parisi R, Griffiths CEM, Ashcroft DM, Global Psoriasis A. Systematic review examining changes over time and variation in the incidence and prevalence of psoriasis by age and gender. Br J Dermatol. 2021; 184:243-258.
39. Wang R, Ward MM. Epidemiology of axial spondyloarthritis: an update. Curr Opin Rheumatol. 2018; 30:137-143.
40. Shakuntulla F, Chiarella SE. Safety of Biologics for Atopic Diseases During Pregnancy. J Allergy Clin Immunol Pract. 2022; 10:3149-3155.
41. Torres J, Mehandru S, Colombel JF, Peyrin-Biroulet L. Crohn's disease. Lancet. 2017; 389:1741-1755.
42. Kalagiri RR, Carder T, Choudhury S, Vora N, Ballard AR, Govande V, Drever N, Beeram MR, Uddin MN. Inflammation in Complicated Pregnancy and Its Outcome. Am J Perinatol. 2016; 33:1337-1356.
43. Joswig A, Gabriel HD, Kibschull M, Winterhager E. Apoptosis in uterine epithelium and decidua in response to implantation: evidence for two different pathways. Reprod Biol Endocrinol. 2003; 1:44.
44. Calleja-Agius J, Jauniaux E, Pizzey AR, Muttukrishna S. Investigation of systemic inflammatory response in first trimester pregnancy failure. Hum Reprod. 2012; 27:349-357.
45. Lund T, Thomsen SF. Use of TNF-inhibitors and ustekinumab for psoriasis during pregnancy: A patient series. Dermatol Ther. 2017; 30. doi: 10.1111/dth.12454.
46. Zhong Z, Wang Y, Wang G, Zhou F. Case Report: TNF-Alpha Inhibitors to Rescue Pregnancy in Women With Potential Pregnancy Loss: A Report of Ten Cases. Front Immunol. 2022; 13:900537.
47. Carman WJ, Accortt NA, Anthony MS, Iles J, Enger C. Pregnancy and infant outcomes including major congenital malformations among women with chronic inflammatory arthritis or psoriasis, with and without etanercept use. Pharmacoepidemiol Drug Saf. 2017; 26:1109-1118.
48. Meyer A, Miranda S, Drouin J, Weill A, Carbonnel F, Dray-Spira R. Safety of Vedolizumab and Ustekinumab Compared With Anti-TNF in Pregnant Women With Inflammatory Bowel Disease. Clin Gastroenterol Hepatol. 2025; 23:144-153 e122.
49. Sanchez-Garcia V, Hernandez-Quiles R, de-Miguel-Balsa E, Gimenez-Richarte A, Ramos-Rincon JM, Belinchon-Romero I. Exposure to biologic therapy before and during pregnancy in patients with psoriasis: Systematic review and meta-analysis. J Eur Acad Dermatol Venereol. 2023; 37:1971-1990.
50. Avallone G, Cavallo F, Tancredi A, *et al*. Association between maternal dupilumab exposure and pregnancy outcomes in patients with moderate-to-severe atopic dermatitis: A nationwide retrospective cohort study. J Eur Acad Dermatol Venereol. 2024; 38:1799-1808.
51. Tektonidou MG, Andreoli L, Limper M, *et al*. EULAR recommendations for the management of antiphospholipid syndrome in adults. Ann Rheum Dis. 2019; 78:1296-1304.
52. Bramham K, Thomas M, Nelson-Piercy C, Khamashta M, Hunt BJ. First-trimester low-dose prednisolone in refractory antiphospholipid antibody-related pregnancy loss. Blood. 2011; 117:6948-6951.
53. Meng L, Huang J, Qiu F, Shan X, Chen L, Sun S, Wang Y, Yang J. Peripheral Neuropathy During Concomitant Administration of Proteasome Inhibitors and Factor Xa Inhibitors: Identifying the Likelihood of Drug-Drug Interactions. Front Pharmacol. 2022; 13:757415.
54. Skomsvoll JF, Ostensen M, Irgens LM, Baste V. Obstetrical and neonatal outcome in pregnant patients with rheumatic disease. Scand J Rheumatol Suppl. 1998; 107:109-112.
55. Broms G, Haerskjold A, Granath F, Kieler H, Pedersen L, Berglind IA. Effect of Maternal Psoriasis on Pregnancy and Birth Outcomes: A Population-based Cohort Study from Denmark and Sweden. Acta Derm Venereol. 2018; 98:728-734.
56. Bobotsis R, Gulliver WP, Monaghan K, Lynde C, Fleming P. Psoriasis and adverse pregnancy outcomes: a systematic review of observational studies. Br J Dermatol. 2016; 175:464-472.
57. Giovannopoulou E, Gkasdaris G, Kapetanakis S, Kontomanolis E. Ankylosing Spondylitis and Pregnancy: A Literature Review. Curr Rheumatol Rev. 2017; 13:162-169.
58. Sanchez-Garcia V, De-Miguel-Balsa E, Ramos-Rincon JM, Belinchon-Romero I. Safety of Dupilumab Therapy for Atopic Dermatitis during Pregnancy: A Systematic Review and Meta-analysis. Acta Derm Venereol. 2025; 105:adv41307.
59. Bandoli G, Johnson DL, Jones KL, Lopez Jiminez J, Salas E, Mirrasoul N, Van Voorhees AS, Chambers CD. Potentially modifiable risk factors for adverse pregnancy outcomes in women with psoriasis. Br J Dermatol. 2010; 163:334-339.
60. Pedersen N, Bortoli A, Duricova D, *et al*. The course of inflammatory bowel disease during pregnancy and postpartum: a prospective European ECCO-EpiCom Study of 209 pregnant women. Aliment Pharmacol Ther. 2013; 38:501-512.
61. Broms G, Granath F, Linder M, Stephansson O, Elmberg M, Kieler H. Birth outcomes in women with inflammatory bowel disease: effects of disease activity and drug exposure. Inflamm Bowel Dis. 2014; 20:1091-1098.
62. Magnus MC, Morken NH, Wensaas KA, Wilcox AJ, Haberg SE. Risk of miscarriage in women with chronic diseases in Norway: A registry linkage study. PLoS Med. 2021; 18:e1003603.

Received May 11, 2025; Revised June 25, 2025; Accepted June 26, 2025.

[§]These authors contributed equally to this work.

**Address correspondence to:*
Panwei Hu, Peizhi He, Department of Obstetrics and Gynecology, Shuguang Hospital Affiliated to Shanghai University of Traditional Chinese Medicine, 528 Zhangheng Road, Shanghai, China.
E-mail: 1551791779@qq.com (Panwei Hu), hpz1849@shutcm.edu.cn (Peizhi He)

Released online in J-STAGE as advance publication June 29, 2025.

Original Article

DOI: 10.5582/ddt.2025.01041

Immune modulation and improved systemic performance of phosphate-functionalized nanogels for antifungal therapy

Theresa Vogel[1,§], Yidong Yu[2,3,§], Thorsten Keller[1], Atsushi Miyashita[4], Lisa Munakata[5], Ryo Suzuki[5], Andreas Beilhack[3], Jürgen Groll[1], Kazuhisa Sekimizu[6,*], Krystyna Albrecht[1,*]

[1] Department for Functional Materials in Medicine and Dentistry, Institute of Functional Materials and Biofabrication, University of Würzburg, Würzburg, Germany;
[2] JSPS International Research Fellow (Endowed Course "Drug Discoveries by Silkworm Models", Faculty of Pharmaceutical Sciences, Teikyo University, Tokyo, Japan;
[3] Department of Internal Medicine II, Center for Experimental Molecular Medicine, Würzburg University Hospital, Würzburg, Germany;
[4] Institute of Medical Mycology, Teikyo University, Tokyo, Japan;
[5] Laboratory of Drug and Gene Delivery Research, Faculty of Pharmaceutical Sciences, Teikyo University, Tokyo, Japan;
[6] Endowed Course "Drug Discoveries by Silkworm Models", Faculty of Pharmaceutical Sciences, Teikyo University, Tokyo, Japan.

SUMMARY: Phosphate functionalization of nanogels (NGs), originally designed to enhance interactions with fungal pathogens, also significantly influences their immune interactions and systemic behaviour. In this study, we investigated how phosphate-modified NGs perform as antifungal carriers *in vivo* using the silkworm model. We found that phosphate functionalization promotes faster internalization by granulocytes—immune cells functionally similar to mammalian neutrophils—highlighting a trade-off between antifungal activity and immune uptake. In parallel, phosphate-functionalized NGs exhibited prolonged circulation, more consistent biodistribution patterns, and reduced batch variability compared to unmodified NGs. These features contributed to superior and more reproducible *in vivo* antifungal efficacy when delivering itraconazole. Importantly, the biodistribution profiles observed in silkworms aligned well with previous mammalian data, further validating silkworms as an efficient, cost-effective model for early-stage evaluation of nanocarrier systems. Our findings underscore the importance of tuning surface functionalization to balance immune interaction and therapeutic performance, providing valuable insights for optimizing systemic antifungal nanotherapies.

Keywords: antifungal delivery, surface functionalization, silkworm, antimicrobial nanocarriers

1. Introduction

Invasive fungal infections lead to over 2.5 million deaths worldwide each year, posing a major public health challenge further aggravated by the scarcity of effective therapeutic options (*1,2*). Despite the existence of antifungal drugs, their clinical efficacy is often hampered by severe side effects, emerging drug resistance, and limited efficacy (*3*), which underscores a pressing need for improved therapeutic strategies. Nanoparticles (NPs) as drug delivery systems (DDS) offer a promising solution by enhancing local drug concentration, improving bioavailability, and reducing toxicity (*4*). Among NPs, nanoparticulate hydrogels, commonly referred to as nanogels (NGs), are particularly appealing as DDS due to their unique combination of high water content, excellent biocompatibility, versatile chemical properties, and ability to provide controlled drug release (*5*).

Recent advances in NG research have shown potential in delivering antifungal drugs effectively. Our initial research demonstrated that redox-sensitive poly(glycidol) (PG)-based NGs could effectively deliver the model antifungal drug itraconazole (NG-ITZ) to the human fungal pathogen *Aspergillus fumigatus in vitro* under protein-free conditions (*6*). More recently, we found that phosphate functionalization of NGs through quenching with phosphoric acid 2-hydroxyethyl acrylate (PHA), facilitated their interaction with *A. fumigatus* under protein-rich conditions (*7*), likely due to the interaction between the phosphate functional group with chitosan in the fungal cell wall (*8,9*). Furthermore, NG×PHA loaded with itraconazole (NG×PHA-ITZ) exhibited superior therapeutic effects in a silkworm (*Bombyx mori*) model of *A. fumigatus* infection compared to the free drug (*7*). These results suggest NG×PHA's potential for systemic

antifungal delivery.

While these findings are promising, they raise additional questions regarding the interactions of NGs with mammalian cells, especially regarding potential cytotoxicity. Although empty NGs and NG×PHA are non-cytotoxic, NG-ITZ and NG×PHA-ITZ exhibit weak cytotoxicity in mammalian cell lines (*6,7*), suggesting that host cells may internalize the drug-loaded NGs—an observation that warrants further investigation. Understanding these interactions is crucial, as the biodistribution of NP-based drug carriers is a key factor influencing their safety and efficacy for clinical applications (*10*). To facilitate systemic antifungal delivery, it is also important to study the biodistribution patterns of NG×PHA within an *in vivo* context.

Conventional preclinical biodistribution studies typically rely on mammalian models, such as mice (*11-14*). However, these mammalian models face significant obstacles, including increasing ethical and regulatory scrutiny and substantial costs. To overcome these challenges during the early stages of nanocarrier development, we utilized the silkworm as an alternative model for preliminary *in vivo* evaluation of antifungal drug-loaded NG×PHA (*7*). The silkworm model delivers several key advantages for preliminary studies, such as minimizing ethical concerns, lowering costs (*15*) and demonstrating effectiveness in the early-stage discovery and development of antimicrobial agents (*16,17*). Furthermore, our previous work demonstrated that the silkworm model can reliably assess the biodistribution and elimination of surface-functionalized gold nanoparticles (AuNPs), providing valuable insights into how surface modifications influence *in vivo* behaviour (*18*).

In this study, we expanded the use of silkworms to compare the cellular interactions and biodistribution of unmodified NGs with NG×PHA, focusing on the impact of phosphate functionalization. We hypothesized that this animal model not only supports the preliminary *in vivo* evaluation of therapeutic effects but also uncovers potential benefits or risks associated with candidate nanocarriers during early development. By using this model, we aim to gain insights into how phosphate functionalization affects NG interactions with host cells and biodistribution, potentially guiding further refinements in NG design for antifungal therapy.

2. Methods

2.1. Synthesis of linear poly(glycidol)

The synthesis of linear poly(glycidol) (PG) with 60 repeating units was carried out following established protocols and characterized accordingly (*7,19,20*). Briefly, the monomer ethoxy ethyl glycidyl ether (EEGE) was synthesized from ethyl vinyl ether and glycidol (*19*). Under inert conditions, the polymerization of EEGE was performed in bulk at 60°C overnight using potassium tert-butoxide as an initiator. The reaction was terminated by the addition of methanol. Subsequently, the obtained poly(EEGE) was deprotected under acidic conditions in tetrahydrofuran (THF), followed by dialysis (for 3 days with 4 water changes per day, using a molecular weight cut-off [MWCO] of 3.5 kDa) and lyophilization, resulting in the formation of linear PG.

2.2. Thiol functionalization of linear PG

Thiol functionalization of linear PG was performed using STEGLICH esterification according to a published method (*21*). Briefly, PG was dissolved in anhydrous *N*,*N*-dimethylformamide (DMF), and 1.1 equivalents of *N*,*N*'-dicyclohexylcarbodiimide (DCC) and 4-dimethylamino pyridine (DMAP) were added. Subsequently, 0.5 equivalents of 3,3′-dithiodipropionic acid (DTPA) in degassed DMF were introduced to the reaction mixture at 0°C. The mixture was stirred at room temperature (RT) overnight. After the formation of the hydrogel, it was washed sequentially with DMF, $CHCl_3$, tetrahydrofuran (THF), EtOH, and water. Then, 0.5 equivalents of tris-(2-carboxyethyl)-phosphine hydrochloride (TCEP·HCl) were added, and the pH of the solution was adjusted to 6-7 with triethylamine (TEA). The reduction was completed after stirring at RT for 4 h. Finally, the thiol-functionalized linear PG (PG-SH) was dialyzed (for 3 days with 4 water changes per day, MWCO = 3.5 kDa) and lyophilized.

2.3. Fluorescence labeling of PG-SH

Fluorescence labeling of PH-SH was performed according to a published method (*6,22*). PG-SH was dissolved in 1× PBS buffer (9 mg/mL). After adding 900 mg of TCEP·HCl, the pH was adjusted to 6 with TEA and the solution was degassed with Argon for 20 min. The labeling reaction was initiated by adding 2 mg of Rhodamine Red C2 maleimide (dissolved in anhydrous DMF at 10 mg/mL). Following an additional 10 min of Argon degassing and overnight stirring at RT, the labeled PG-SH was purified *via* dialysis (3 days, with 4 water changes per day, MWCO = 3.5 kDa) and then lyophilized.

2.4. Synthesis of nanogels *via* nanoprecipitation

Nanogels (NGs) were prepared using a nanoprecipitation technique involving linear PG-SH (with or without fluorescent labeling) in acetone, as previously described (*6,7*). Briefly, 6 mg of the respective polymer was dissolved in water (6 mg/90 µL) and precipitated in 48 mL of acetone with an automatic pipette (Eppendorf®-Xplorer). After 30 min, 30 µL of alloxan monohydrate solution in water (32 mg/mL) was added. The oxidation was halted by adding 4 mL of Milli-Q water after another 30 min.

The nanogels were separated from the precipitation solution by centrifugation at 4000× *g*, at RT for 60 min. The samples were washed five times with water by centrifugation (16162× *g*, RT, 5 min [3×], 2.5 min [2×]). The particle size, zeta-potential, and particle concentration of the NGs were then measured.

2.5. Phosphate functionalization of nanogels

NGs were functionalized by incorporating a quenching step into the previously described synthesis procedure (*7*). After the oxidation step, the pH of the solution was adjusted to 8-9 using TEA. Subsequently, 50 µL of quencher (PHA in acetone at 0.283 mg/mL, 3.49 mmol) was added. Quenching was conducted at RT for 30 min. Following this step, the washing and characterization procedures were carried out as described earlier.

2.6. Rearing of silkworms (*Bombyx mori*)

Silkworm eggs (strain: Kinsyu × Showa) were purchased from Ehime-Sanshu (Ehime, Japan). After hatching, the larvae were reared at 27°C and nourished with an artificial diet (Silkmate 2S, Nosan Corporation, Japan) until the fourth instar. Upon reaching the fifth instar, the larvae were switched to an antibiotic-free diet (Artificial diet for silkworm larvae, Type A, Sysmex Corporation, Japan) for two days (1 g diet/silkworm/day). On the third day of the fifth instar, silkworms were used for experiments unless otherwise specified.

2.7. Collection of hemolymph from silkworms

On the third day of the fifth instar, hemolymph was collected from silkworms under sterile conditions. For surface disinfection, silkworms were soaked in 70% EtOH for 10 min at RT, followed by a brief air-drying period. Hemolymph was then collected by cutting one of the abdominal legs. To prevent melanization, N-phenylthiourea (PTU; 0.1 M in 100% DMSO) was immediately added to the collected hemolymph to achieve a final concentration of 1 mM (*23*). The hemolymph was then centrifuged at 16162 × g, for 1 min at 4°C to pellet the hemocytes. The supernatant was used as a culture medium (*i.e.*, cell-free hemolymph) on the same day of collection or stored at -20°C for further use.

For MIC (minimal inhibitory concentration) determination or characterization of protein corona formation, a larger volume of cell-free hemolymph was required. In this case, silkworms were fed for four days, and hemolymph was collected on the fifth day of the fifth instar.

2.8. Interaction of NGs with primary adherent hemocytes from silkworms

On the third day of the fifth instar, hemolymph was collected from silkworms as described earlier. PTU was added, and 250 µL of hemolymph was immediately transferred into a glass-bottom dish (ø 35 mm [dish]; ø 14 mm [cover slip; poly-lysine coated]; Matsunami, Osaka, Japan), and the cells were allowed to settle for 30 min at RT. Subsequently, the hemolymph was removed, and the cells were washed twice with TC-100 insect medium containing 8% heat-inactivated fetal bovine serum (FBS), 40 IU/mL of penicillin-streptomycin, and 0.1% w/v PTU (250 µL medium per wash). The adherent hemocytes, consisting of granulocytes and plasmatocytes, were obtained (*24*).

Following the second wash, fresh TC-100 medium containing 4×10^9 particles of the desired NG type was added to each dish (250 µL/dish). The samples were co-incubated at 27°C for 1, 3, 6, or 24 h. After co-incubation, the samples were washed five times with 300 µL of Dulbecco's phosphate-buffered saline (DPBS[-]) per wash. Calcein-AM staining was then performed according to the manufacturer's protocol, using a 1 mM stock solution in 100% DMSO with a final concentration of 0.667 µM in 300 µL DPBS(-) per dish. Staining was done in the dark at 27°C for 15 min, followed by three washes as described above. Finally, 100 µL of DPBS(-) was added to each sample, which was then subjected to microscopic examination using a Leica DMI 6000 B fluorescence microscope.

2.9. Biodistribution experiments

To study the biodistribution of NG or the free dye RhoRC2 in silkworms following systemic administration (*i.e.*, intra-hemolymph injection), seven time points were selected: immediately post-injection (0 h), 15 min, 1 h, 3 h, 6 h, 15 h, and 24 h post-injection. For the later time points (15 h and 24 h), silkworms were fed for two days and injected on the third day of the fifth instar. For the other time points, silkworms were fed for two days and fasted for one day prior to the injection. The body weight of individual silkworms (2.1 ± 0.1 g) was recorded prior to injection. Hemolymph and tissue collection occurred on the fourth day of the fifth instar for all seven time points.

A total of 8×10^9 particles of the desired NG batch (or 1.2 µg of the free dye RhoRC2) in 50 µL of DPBS(-) were injected into the hemolymph of individual silkworms as previously described (*25*). The silkworms were incubated at 27°C until dissection. Hemolymph and tissue collection (midgut, Malpighian tubules, hindgut, and fat body) was performed as described earlier and in the Appendix A. Supplementary information (*https://www.ddtjournal.com/action/getSupplementalData.php?ID=257*) (see section "Standard curves of each fluorescently labeled NG batch and the free dye RhoRC2 in distinct silkworm tissues"), respectively. To obtain sufficient tissue homogenates for measuring fluorescent intensity in technical triplicates, hemolymph

and respective tissues from 3-5 silkworms were pooled together (defined as 1 biological replicate). Unless otherwise specified, biological duplicates per NG batch were subjected to measurement. Tissue homogenization was carried out as described in the Appendix A. Supplementary information (*https://www.ddtjournal.com/action/getSupplementalData.php?ID=257*) (see section "Standard curves of each fluorescently labeled NG batch and the free dye RhoRC2 in distinct silkworm tissues"). 100 µL of hemolymph (containing hemocytes) or tissue homogenate was used for measuring fluorescent intensity in technical triplicates.

Using GraphPad Prism (v. 8.4.3), non-linear fitting was applied to model the retention kinetics and estimate Terminal half-lives ($t_{1/2}$). A one-phase decay model was used for RhoRC2-NG and free RhoRC2 dye to represent a single, continuous decay process. In contrast, a two-phase decay model was applied for RhoRC2-NG×PHA, reflecting both an initial rapid decline and a slower terminal phase in retention. To assess batch consistency within each NG type, an extra sum-of-squares F test was performed, comparing the decay rate parameters across the three batches. Data are presented as the mean ± SEM for each time point, based on all six replicates (biological duplicates x technical triplicates).

In general, the results on tissue retention are shown as percentages of initial dose (ID) injected per milligram of tissue (% of ID / mg tissue), calculated as follows:

$$\frac{\%\ \text{of ID}}{mg_{tissue}} = \frac{p_{100\mu L}}{p_{ID} \cdot \%h} \quad (1)$$

where p_{ID} is 8×10^9 particles or 1.2 µg of the free dye (initial dose), $p_{100\mu L}$ is the number of particles or amount of the free dye (ng) in 100 µL of the tissue homogenate (estimated based on respective standard curves, see Appendix B (*https://www.ddtjournal.com/action/getSupplementalData.php?ID=258*). Summary of raw data and standard curves), *%h* is the percentage of tissue in the homogenate, calculated as follows:

$$\%h = \frac{w_{tissue}}{w_{tissue} + w_{saline}} \quad (2)$$

where w_{tissue} is the weight of the collected tissue, w_{saline} is the weight or volume of saline added for homogenization (density = 1 mg/µL). Data are summarized in the Appendix C (*https://www.ddtjournal.com/action/getSupplementalData.php?ID=259*). Summary of tissue retention data and collectively presented in Figure 4.

3. Results

3.1. Synthesis of phosphate-functionalized, fluorescently labelled NGs for cellular interaction and biodistribution studies

NGs were synthesized from thiol-functionalized poly(glycidol) (PG-SH) *via* nanoprecipitation (Figure 1A) (*6,7*). To achieve phosphate functionalization, we added a quenching step with PHA into the synthesis to introduce a phosphoric acid functional group, resulting in NG×PHA (Figures 1A-1B) (*7*). For tracking cellular interactions and biodistribution, we pre-labeled PG-SH with the maleimide-functionalized dye Rhodamine Red C2 (RhoRC2) prior to NG synthesis (Figure 1C). For biodistribution experiments, we selected RhoRC2 due to its structural similarity to rhodamine B, which has been used for NP biodistribution research in mice (*13*) and for studying xenobiotics in silkworms (*26*). RhoRC2 shares a comparable excitation/emission spectrum to rhodamine B (~560/580 nm) and forms covalent bonds with PG-SH. We synthesized and characterized three batches of RhoRC2-NG and RhoRC2-NG×PHA (Table S1, Appendix A. Supplementary information, *https://www.ddtjournal.com/action/getSupplementalData.php?ID=257*).

3.2. Enhanced interaction of granulocytes with phosphate-functionalized NGs compared to unmodified NGs

First, we co-incubated both NG types with *A. fumigatus* in protein-rich (cell-free hemolymph collected from silkworms) and protein-free (RPMI-1640) media. In protein-rich conditions, only RhoRC2-NG×PHA interacted with the fungus, while both NG types adhered to the fungus in protein-free conditions (Figure S1, Appendix A. Supplementary information, *https://www.ddtjournal.com/action/getSupplementalData.php?ID=257*), consistent with our previous findings (*7*).

After confirming the interaction between NG×PHA with *A. fumigatus*, we assessed how NGs interacted with host cells. To align with our subsequent biodistribution studies in the silkworm model, we selected primary adherent hemocytes isolated from silkworm hemolymph (*24*) as representative host cells. These hemocytes, which include granulocytes and plasmatocytes and constitute over 50% of circulating hemocytes (*24,27*), play a crucial role in the initial cellular response to foreign materials (*28*). Their key role in immune defence makes them well-suited for *in vitro* studies designed to mimic the *in vivo* environment following systemic NG administration.

To assess interactions with host cells, we incubated primary adherent hemocytes from hemolymph with both NG types and the free dye RhoRC2 for either 1, 3, 6, or 24 h (Figure 2; Figures S2-S4, Appendix A. Supplementary information, *https://www.ddtjournal.com/action/getSupplementalData.php?ID=257*). Cell viability, assessed with Calcein-AM staining post co-incubation, remained unaffected. Free dye was primarily detected extracellularly, indicating that the intracellular RhoRC2 signal resulted from the cellular NG uptake. Round-shaped granulocytes internalized RhoRC2-NG×PHA more rapidly than RhoRC2-NG, with marked uptake noted after 3 h of co-incubation (Figure 2).

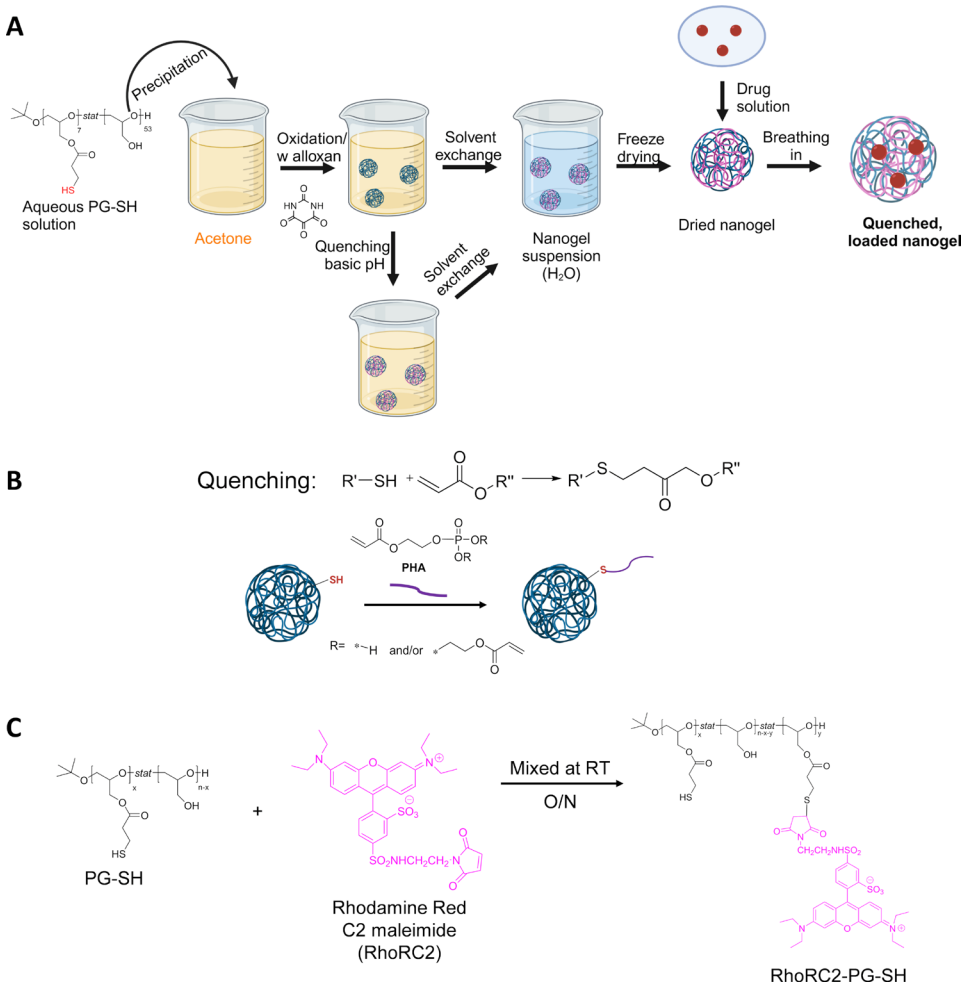

Figure 1. (**A**) Scheme of nanogel (NG) synthesis *via* inverse nanoprecipitation, including functionalization *via* quenching and drug loading steps (image reproduced from Vogel *et al*. 2024 (*7*) under the Creative Commons CC-BY-NC license). (**B**) Detailed illustration of the quenching step (image adapted from Vogel *et al*. 2024 (*7*); icons were created with BioRender under a publication license). (**C**) Fluorescent labeling of PG-SH with Rhodamine Red C2 maleimide. PG-SH: thiol-functionalized poly(glycidol); PHA: phosphoric acid 2-hydroxyethyl acrylate; RT: room temperature; O/N: overnight.

Discrete uptake of RhoRC2-NG by granulocytes was noted after 6 h (Figure S3, *https://www.ddtjournal.com/action/getSupplementalData.php?ID=257*), which became more apparent after 24 h (Figure S4, *https://www.ddtjournal.com/action/getSupplementalData.php?ID=257*). Plasmatocytes (elongated cells) exhibited minimal uptake in both cases.

Notably, both NG types are likely degraded within granulocytes due to ester hydrolysis under the acidic conditions (*19*), although RhoRC2 remains detectable due to its pH stability (*29*).

3.3. Prolonged circulation of phosphate-functionalized NGs in silkworm hemolymph

After completing the *in vitro* study, we conducted *in vivo* biodistribution experiments. We systemically administered RhoRC2-NG, RhoRC2-NG×PHA, or free dye RhoRC2 to silkworms At seven time points within 24 h – 0 h (immediately after injection), 15 min, 1 h, 3 h, 6 h, 15 h, and 24 h – we collected hemolymph (the silkworm equivalent of vertebrate blood (*30*)) and four tissue types (midgut, Malpighian tubules, hindgut, and fat body).

To prevent NG pelleting, we analyzed hemolymph without centrifugation. Using RhoRC2 signals (Figure 3), we estimated NG half-lives in hemolypmh, defined as the time for plasma concentration to drop by 50% during the terminal phase (*31*). Both the free dye RhoRC2 (Figure 3C) and RhoRC2-NG (Figure 3A) followed a one-phase decay model, with half-lives of 3.5 h and 2.0-6.6 h, respectively, indicating relatively rapid clearance from the hemolymph. In contrast, RhoRC2-NG×PHA (Figure 3B) exhibited a two-phase decay model, characterized by an initial rapid decline followed by a prolonged terminal phase with half-lives ranging from 9.5 to 19.9 h. This extended half-life of RhoRC2-NG×PHA may result from faster uptake by granulocytes, as demonstrated in *in vitro* co-culture experiments where RhoRC2-NG×PHA showed more pronounced intracellular accumulation than RhoRC2-NG, persisting for at least 6 h (Figure 2, Figures S2-S3). Interestingly,

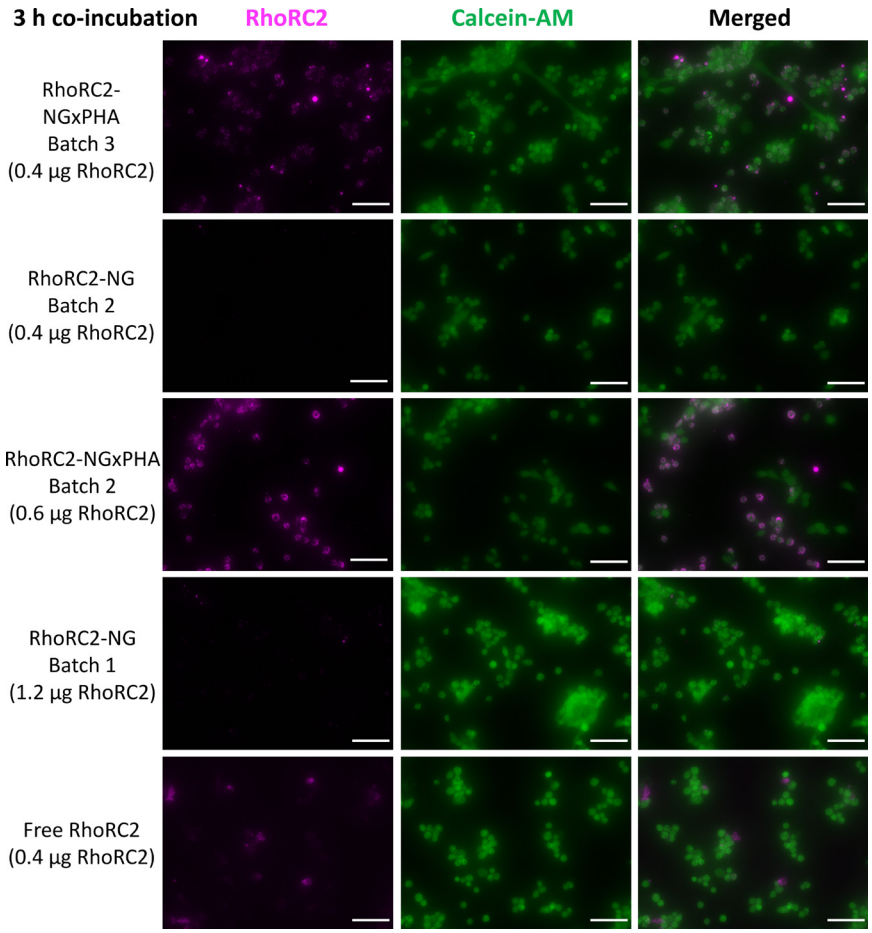

Figure 2. Co-incubation of two distinct NG types with primary adherent hemocytes (granulocytes and plasmatocytes) collected from silkworms for 3 h at 27°C in 250 µL TC-100 medium containing 8% FBS. Two batches of each NG type, as indicated in Table S1 (Appendix A. Supplementary information, *https://www.ddtjournal.com/action/getSupplementalData.php?ID=257*), were used. A total of 4×10^9 particles from each batch were added to respective wells for co-incubation. Given the slightly variations in estimated RhoRC2 loading among the batches, the amount of RhoRC2 in each well was indicated in parentheses. Free dye was used as a control. Following co-incubation, hemocytes were stained with Calcein-AM to confirm their viability. Scale bars = 50 µm.

while the free dye stabilized at approximately 40% of its initial signal by 24 h post injection, both NG types decreased to approximately 10-20%. These findings suggest that, despite initial differences in retention, NGs undergo more efficient clearance from circulation than the free dye during the terminal phase.

3.4. Tissue-specific retention of NGs in silkworms

Tissue retention analysis revealed that both NG types (Figures 4A-4B) predominantly localized in the midgut (akin to the mammalian small intestine (*32*), which also metabolizes exogenous compounds like the liver (*33*)) and the hindgut (comparable to the mammalian large intestine (*34*)). Smaller amounts accumulated in the fat body (responsible for energy storage, metabolism, and partial detoxification, often likened to the mammalian liver (*15*)). The Malpighian tubules (similar to mammalian kidneys (*15*)) showed the least retention. In contrast, the free dye displayed a distinct retention pattern, with primary accumulation in the Malpighian tubules and minimal retention in the hindgut (Figure 4C).

Given the hemolymph retention profiles (Figure 3), we focused our tissue retention analysis on two time points: 3 h post-injection to capture early biodistribution, and 24 h to assess longer-term retention and potential tissue accumulation. At 3 h, RhoRC2-NG (Figure 4A) accumulated significantly more in the midgut than in the fat body and Malpighian tubules. Similarly, RhoRC2-NG×PHA (Figure 4B) displayed greater retention in the midgut than in the fat body, Malpighian tubules, and hindgut. By 24 h, RhoRC2-NG continued to show higher retention in the midgut relative to the other two tissues. However, RhoRC2-NG×PHA no longer exhibited significant differences between the midgut and fat body or hindgut, although retention in the midgut remained higher than in the Malpighian tubules. The free dye (Figure 4C) displayed a distinct retention profile, with significantly higher accumulation in the Malpighian tubules compared to the midgut at 3 h. This difference disappeared by 24 h, indicating clearance over time. Overall, comparisons between tissue types at these time points revealed a clear trend: both NG types preferentially accumulated in the midgut early on, while

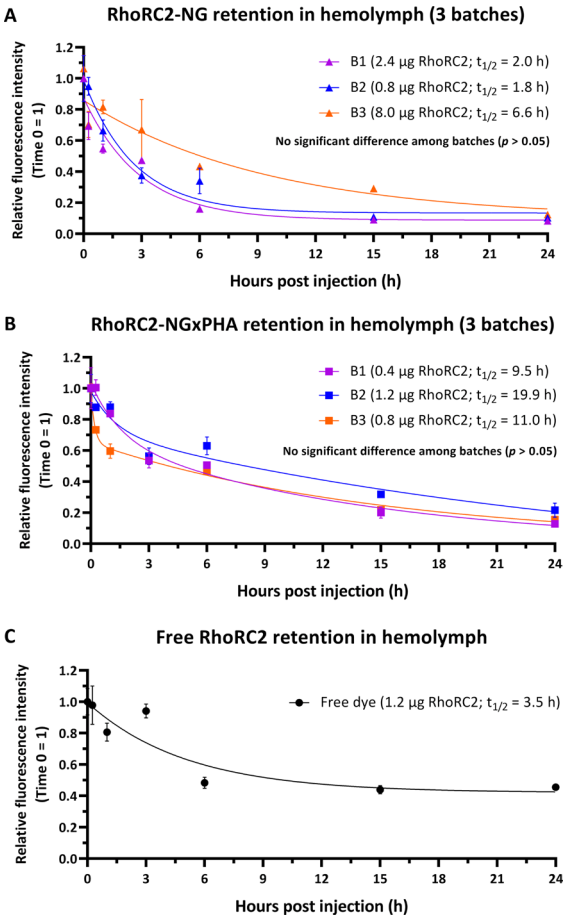

Figure 3. Retention of two distinct NG types in silkworm hemolymph post systemic administration. Three batches (B1, B2, B3) of RhoRC2-NG (**A**) and RhoRC2-NG×PHA (**B**) as well as the free dye RhoRC2 (**C**) were used. A total of 8×10^9 particles of each NG batch were injected into individual silkworms, followed by collection of hemolymph at indicated time points. Given the slight variations in estimated RhoRC2 loading among the NG batches, the amount of RhoRC2 injected into each silkworm is indicated in the parentheses in the legend. Fluorescence intensities were normalized to the initial time point (0 h) to adjust for loading variability, allowing comparison of relative retention profiles. Terminal half-lives ($t_{1/2}$) in hemolymph (containing hemocytes) were estimated using a one-phase decay model for RhoRC2-NG (**A**) and free RhoRC2 (**C**), while a two-phase decay model was used for RhoRC2-NG×PHA (**B**); these values are shown in parentheses in the legend. Notably, based on the observed batch variations, the half-life of NGs appears to be positively related to the injected amount of RhoRC2. An extra sum-of-squares F test revealed no significant retention differences among batches within each NG type ($p > 0.05$). Measurements were performed in biological duplicates (pooled hemolymph from 3–5 silkworms per sample), with each sample measured in technical triplicates. Data represent the mean ± SEM for each time point, based on all six replicates.

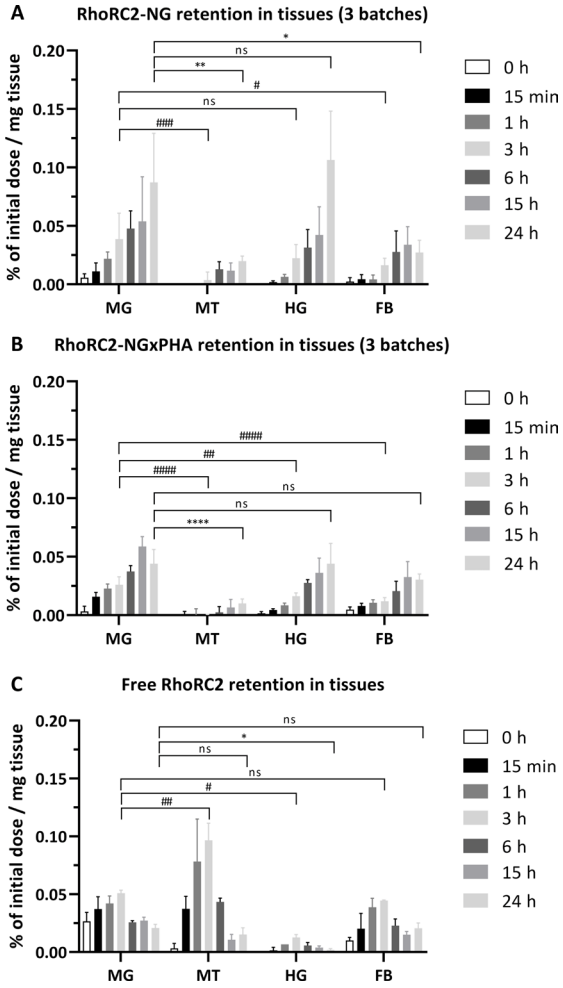

Figure 4. Tissue retention of two distinct NG types in silkworms following systemic administration. Three batches of RhoRC2-NG (**A**) and RhoRC2-NG×PHA (**B**) were injected, along with a free dye control, RhoRC2 (**C**). Each silkworm received 8×10^9 particles for NG or 1.2 µg of free dye, and tissues were collected at the specified time points. Data represent mean ± SD from biological duplicates (pooled tissues from 3–5 silkworms per sample) across all three batches (except for the free dye control), with each sample measured in technical triplicates. Abbreviations: MG (midgut), MT (Malpighian tubules), HG (hindgut), FB (fat body). Statistical comparisons were conducted at two key time points (3 h and 24 h post injection) using one-way ANOVA followed by Dunnett's multiple comparisons test, comparing MT, HG, and FB to MG at each respective time point. Significance indicators: $^{*/\#}p < 0.05$; $^{**/\#\#}p < 0.01$; $^{***/\#\#\#}p < 0.001$; $^{****/\#\#\#\#}p < 0.0001$; ns (not significant).

the free dye showed stronger retention in the Malpighian tubules.

3.5. Distinct protein corona profiles of phosphate-functionalized and unmodified NGs

To investigate the prolonged retention of RhoRC2-NG×PHA in hemolymph compared to RhoRC2-NG, likely due to enhanced granulocyte uptake, we incubated unlabeled NGs and NG×PHA in hemolymph for 24 h. After incubation, both types displayed similar particle sizes and zeta potentials after incubation (Table S2, Appendix A. Supplementary information, *https://www.ddtjournal.com/action/getSupplementalData.php?ID=257*).

Next, we explored NG interactions with hemolymph proteins by analyzing the protein corona composition after a 24 h incubation of unlabeled NGs or NG×PHA. Liquid chromatography coupled with mass spectrometry (LC-MS/MS) identified proteins < 200 kDa, constituting 96% of the corona for both NG types (Figure S5A, Appendix A. Supplementary information, *https://*

www.ddtjournal.com/action/getSupplementalData.php?ID=257); Appendix D (*https://www.ddtjournal.com/action/getSupplementalData.php?ID=260*). Full list of hard corona proteins on NGs). As shown in Figure S5B (*https://www.ddtjournal.com/action/getSupplementalData.php?ID=257*), differences in the most abundant proteins included higher proportions of C-type lectin domain proteins on NGs, critical for innate immunity (*35*) (48.3% of total identified proteins on NGs *vs.* 26.3% on NG×PHA). Conversely, there were lower proportions of nutrient storage proteins on NGs, which are abundant in hemolymph (*36*) (24.8% on NGs and 41.4% on NG×PHA). Among them, lipid-binding proteins, particularly apolipophorins and low molecular weight lipoproteins (*36*), accounted for 8.61% on NGs and 24.41% on NG×PHA (Table S3, Appendix A. Supplementary information, *https://www.ddtjournal.com/action/getSupplementalData.php?ID=257*). Other proteins comprised 26.9% and 32.3% of total quantities, respectively.

We identified two low molecular weight lipoproteins (LPs), 30KP2 (BmLP7) and PBMHP-6 (BmLP1), among the lipid-binding proteins that might affect NG×PHA's interaction with granulocytes. BmLP7, which appeared only on NG×PHA (1.04%), can penetrate hemocytes, while BmLP1, more abundant on NG×PHA than NGs (13.62% *vs.* 5.52%), can recruit hemocytes to BmLP1-coated substances (*37*). These differences likely facilitate NG×PHA's interaction with hemocytes *in vivo*.

3.6. Phosphate-functionalized NGs as reliable antifungal carriers with reduced batch variability and improved efficacy

In our initial study, itraconazole-loaded NGs (NG-ITZ) exhibited a lower minimal inhibitory concentration (MIC) against *A. fumigatus* in a protein-free medium compared to free itraconazole (ITZ) (*6*). Since NGs do not interact with the fungus in protein-rich conditions (Figure S1A, *https://www.ddtjournal.com/action/getSupplementalData.php?ID=257*) (*7*), we did not expect any antifungal effects of NG-ITZ under such conditions. However, after observing similar biodistribution patterns between empty NGs and NG×PHA, we decided to reassess NG-ITZ.

We determined the MIC and median effective dose (ED_{50}) of NG-ITZ against *A. fumigatus*, comparing these results with previous data on NG×PHA-ITZ and free ITZ (*6, 7*). NG-ITZ (two batches tested) exhibited ED_{50} values of 1.9 and 2.1 mg/kg larva, slightly higher than those of NG×PHA-ITZ (two batches, both 1.3 mg/kg larva), and consistent with the corresponding MIC values in silkworm hemolymph (2-4 μg/mL for NG-ITZ *vs.* 1 μg/mL for NG×PHA-ITZ (Table S4, Appendix A. Supplementary information, *https://www.ddtjournal.com/action/getSupplementalData.php?ID=257*). The MIC values in RPMI was also in line with these trends (1 μg/mL for NG-ITZ *vs.* 0.5 μg/mL for NG×PHA-ITZ). Importantly, NG-ITZ demonstrated better *in vivo* antifungal effect than free ITZ (ED_{50} > 4.7 mg/kg larva), though not as effective as NG×PHA-ITZ. Moreover, NG-ITZ exhibited greater batch variability in antifungal effects compared to NG×PHA-ITZ, underscoring NG×PHA's potential as a more consistent and reliable antifungal drug carrier, with enhanced fungal interaction and improved biodistribution.

4. Discussion

Phosphate functionalization of NGs enhances their interactions with fungi and promotes faster internalization by silkworm granulocytes, which are similar to mammalian neutrophils and play a key role in the initial recognition of foreign materials (*38,39*). This dual effect strikes a balance between improved antifungal activity and increased immune cell uptake, illustrating the trade-off in systemic antifungal delivery strategies. Notably, both unmodified and phosphate-functionalized NGs selectively interact with granulocytes, rather than the plasmatocytes, emphasizing their potential for immune-specific targeting. The accelerated internalization of phosphate-functionalized NGs further underscores their enhanced functionality, suggesting broad applications, including optimizing drug delivery to specific immune cell populations.

While the biodistribution patterns of PG-SH-based NGs in animal models remain limited, our findings (Figures 4A-4B) align with previous data on Cy7-labeled PG-SH-based NGs in mice (Cy7-NG×HEA quenched with 2-hydroxyethyl acrylate) (*12*). *In vivo* imaging in mice, particularly at 3 h post injection, revealed that Cy7-NG×HEA was primarily cleared *via* hepato-biliary excretion (liver and intestine) rather than renal clearance (kidneys and bladder), likely due to the NG's particle size (*12*). The similarity in biodistribution patterns between silkworms and mice reinforces the silkworms as a reliable and cost-effective tool for initial nanocarrier biodistribution studies.

Our findings further demonstrate that NG×PHA-ITZ delivers superior *in vivo* antifungal effects with less variability compared to NG-ITZ (Table S4, *https://www.ddtjournal.com/action/getSupplementalData.php?ID=257*), highlighting NG×PHA as a promising nanocarrier. However, additional optimization is necessary to achieve fungal-specific drug delivery, as phosphorylation alone may not suffice. Future research will focus on quantifying the degree of phosphorylation in NG×PHA, exploring its tunability, and examining its impact on biodistribution. This could offer valuable insights into how surface functionalization influences nanocarrier behaviour. While potential heterogeneity introduced by PHA byproducts with multiple acrylate groups is expected to be minimal based on the synthesis process (*40*), their role in structural homogeneity and

biodistribution remains an important consideration. Future studies will aim to characterize these byproducts in greater detail to better understand their impact on the system's overall performance.

Finally, the similar biodistribution patterns of NGs in silkworms and mammals further validate the silkworm model as an effective, cost-efficient platform for early *in vivo* evaluation of antimicrobial nanocarriers. This model provides critical insights into cellular interactions and biodistribution, informing the development of future antimicrobial therapies.

Acknowledgements

We thank Sina Hirsch (Würzburg University Hospital) for organizing the international sample shipment and Stephanie Lamer (University of Würzburg) for the LC-MS/MS analysis.

Funding: This work was supported by the German Research Foundation (DFG)-TRR 225 "Biofabrication" (project number 326998133, subprojects A06, B07, B08), DFG-GRK/RTG 2157 "3DInfect" (270563345, subproject P01) and DFG-TRR124 "FungiNet" (210879364, subproject A03). Y. Y. received the Postdoctoral Fellowship for Research in Japan from the Japan Society for the Promotion of Science (JSPS). A. M. received Research Grant by Life Science Foundation of Japan, Research Incentive Grant by The Uehara Memorial Foundation, Team Research Grant by Teikyo University, and JSPS Kakenhi (Grant#22K15461).

Conflict of Interest: Kazuhisa Sekimizu is a consultant for Genome Pharmaceutical Institute, Co., Ltd. The other authors have no conflicts to declare.

References

1. Denning DW. Global incidence and mortality of severe fungal disease. Lancet Infect Dis. 2024; 24:428-438.
2. Bongomin F, Gago S, Oladele RO, Denning DW. Global and multi-national prevalence of fungal diseases-estimate precision. J Fungi. 2017; 3:57.
3. Hossain CM, Ryan LK, Gera M, Choudhuri S, Lyle N, Ali KA, Diamond G. Antifungals and Drug Resistance. Encyclopedia. 2022; 2:1722-1737.
4. Garg A, Sharma GS, Goyal AK, Ghosh G, Si SC, Rath G. Recent advances in topical carriers of anti-fungal agents. Heliyon. 2020; 6:e04663.
5. Zhang X, Malhotra S, Molina M, Haag R. Micro- and nanogels with labile crosslinks – from synthesis to biomedical applications. Chem Soc Rev. 2015; 44:1948-1973.
6. Horvat S, Yu Y, Manz H, Keller T, Beilhack A, Groll J, Albrecht K. Nanogels as antifungal-drug delivery system against *Aspergillus fumigatus*. Adv Nanobiomed Res. 2021; 1:2000060.
7. Vogel T, Kohlmann S, Abboud Z, Thusek S, Fella F, Teßmar J, Sekimizu K, Miyashita A, Beilhack A, Groll J, Yu Y, Albrecht K. Beyond the charge: interplay of nanogels' functional group and zeta-potential for antifungal drug delivery to human pathogenic fungus *Aspergillus fumigatus*. Macromol Biosci. 2024;e2400082.
8. Mouyna I, Dellière S, Beauvais A, Gravelat F, Snarr B, Lehoux M, Zacharias C, Sun Y, de Jesus Carrion S, Pearlman E, Sheppard DC, Latgé JP. What are the functions of chitin deacetylases in *Aspergillus fumigatus*? Front Cell Infect Microbiol. 2020; 10:28.
9. Zamani A, Edebo L, Sjöström B, Taherzadeh MJ. Extraction and precipitation of chitosan from cell wall of zygomycetes fungi by dilute sulfuric acid. Biomacromolecules. 2007; 8:3786-3790.
10. Mitchell MJ, Billingsley MM, Haley RM, Wechsler ME, Peppas NA, Langer R. Engineering precision nanoparticles for drug delivery. Nat Rev Drug Discov. 2021; 20:101-124.
11. Li SD, Huang L. Pharmacokinetics and biodistribution of nanoparticles. Mol Pharmaceutics. 2008; 5:496-504.
12. Zilkowski I, Theodorou I, Albrecht K, Ducongé F, Groll J. Subtle changes in network composition impact the biodistribution and tumor accumulation of nanogels. Chem Commun. 2018; 54:11777-11780.
13. Gracheva I, Konovalova M, Aronov D, Moiseeva E, Fedorov A, Svirshchevskaya E. Size-dependent biodistribution of fluorescent furano-allocolchicinoid-chitosan formulations in mice. Polymers. 2021; 13:2045.
14. Khan M, Yamasta A, Parvin M, Ferdaus J, Ahmed H, Arbab AS. Experimental study of processing of PCL (polycaprolactone)-peptides nanoparticles and its biodistribution analysis for drug delivery system. Micro and Nano Syst Lett. 2024; 12:18.
15. Panthee S, Paudel A, Hamamoto H, Sekimizu K. Advantages of the silkworm as an animal model for developing novel antimicrobial agents. Front Microbiol. 2017; 8:373.
16. Hamamoto H, Urai M, Ishii K, *et al*. Lysocin E is a new antibiotic that targets menaquinone in the bacterial membrane. Nat Chem Biol. 2015; 11:127-133.
17. Nakamura I, Kanasaki R, Yoshikawa K, Furukawa S, Fujie A, Hamamoto H, Sekimizu K. Discovery of a new antifungal agent ASP2397 using a silkworm model of *Aspergillus fumigatus* infection. J Antibiot. 2017; 70:41-44.
18. Lutz J, Yu Y, Wolf AK, Beilhack A, Groll J, Albrecht K. Impact of surface functionality on biodistribution of gold nanoparticles in silkworms. Adv Nanobiomed Res. 2024; 4:2200146.
19. Stichler S, Jungst T, Schamel M, Zilkowski I, Kuhlmann M, Böck T, Blunk T, Teßmar J, Groll J. Thiol-ene clickable poly(glycidol) hydrogels for biofabrication. Ann Biomed Eng. 2017; 45:273-285.
20. Singh S, Zilkowski I, Ewald A, Maurell-Lopez T, Albrecht K, Möller M, Groll J. Mild oxidation of thiofunctional polymers to cytocompatible and stimuli-sensitive hydrogels and nanogels. Macromol Biosci. 2013; 13:470-482.
21. Groll J, Singh S, Albrecht K, Moeller M. Biocompatible and degradable nanogels *via* oxidation reactions of synthetic thiomers in inverse miniemulsion. J Polym Sci Part A Polym Chem. 2009; 47:5543-5549.
22. Zilkowski I, Ziouti F, Schulze A, Hauck S, Schmidt S, Mainz L, Sauer M, Albrecht K, Jundt F, Groll J. Nanogels enable efficient miRNA delivery and target gene downregulation in transfection-resistant multiple myeloma cells. Biomacromolecules. 2019; 20:916-926.

23. Clark KD, Strand MR. Hemolymph melanization in the silkmoth *Bombyx mori* involves formation of a high molecular mass complex that metabolizes tyrosine. J Biol Chem. 2013; 288:14476-14487.
24. Shimabukuro M, Xu J, Sugiyama M, Taniai K, Kadono-Okuda K, Kato Y, Yamamoto M, Chowdhury S, Choi KS, Choi KH, Miyanoshita A, Debnath CN, Yamakawa M. Signal transudation for cecropin B gene expression in adherent hemocytes of the silkworm, *Bombyx mori* (Lepidoptera: Bombycidae). Appl Entomol Zool. 1996; 31:135-143.
25. Matsumoto Y, Sekimizu K. Silkworm as an experimental animal for research on fungal infections. Microbiol Immunol. 2019; 63:41-50.
26. Tansil NC, Li Y, Koh LD, Peng TC, Win KY, Liu XY, Han MY. The use of molecular fluorescent markers to monitor absorption and distribution of xenobiotics in a silkworm model. Biomaterials. 2011; 32:9576-9583.
27. Lavine MD, Strand MR. Insect hemocytes and their role in immunity. Insect Biochem Mol Biol. 2002; 32:1295-1309.
28. Wago H. Humoral factors promoting the adhesive properties of the granular cells and plasmatocytes of the silkworm, *Bombyx mori*, and their possible role in the initial cellular reactions to foreignness. Cell Immunol. 1980; 54:155-169.
29. Longmire MR, Ogawa M, Hama Y, Kosaka N, Regino CA, Choyke PL, Kobayashi H. Determination of optimal rhodamine fluorophore for *in vivo* optical imaging. Bioconjug Chem. 2008; 19:1735-1742.
30. Wyatt GR, Loughheed TC, Wyatt SS. The chemistry of insect hemolymph; organic components of the hemolymph of the silkworm, *Bombyx mori*, and two other species. J Gen Physiol. 1956; 39:853-868.
31. Toutain PL, Bousquet-mélou A. Plasma terminal half-life. J Vet Pharmacol Therap 2004; 27:427-439.
32. Awais MM, Fei S, Xia J, Feng M, Sun J. Insights into midgut cell types and their crucial role in antiviral immunity in the lepidopteran model *Bombyx mori*. Front Immunol. 2024; 15:1349428.
33. Hamamoto H, Horie R, Sekimizu K. Pharmacokinetics of anti-infectious reagents in silkworms. Sci Rep. 2019; 9:9451.
34. Casali A, Batlle E. Intestinal stem cells in mammals and *Drosophila*. Cell Stem Cell. 2009; 4:124-127.
35. Xia X, You M, Rao XJ, Yu XQ. Insect C-type lectins in innate immunity. Dev Comp Immunol. 2018; 83:70-79.
36. Zhang Y, Dong Z, Wang D, Wu Y, Song Q, Gu P, Zhao P, Xia Q. Proteomics of larval hemolymph in *Bombyx mori* reveals various nutrient-storage and immunity-related proteins. Amino Acids. 2014; 46:1021-1031.
37. Ye L, Zhang Y, Dong Z, Guo P, Zhao D, Li H, Hu H, Zhou X, Chen H, Zhao P. Five silkworm 30K proteins are involved in the cellular immunity against fungi. Insects. 2021; 12:107.
38. Fingerhut L, Dolz G, de Buhr N. What is the evolutionary fingerprint in neutrophil granulocytes? Int J Mol Sci. 2020; 21:4523.
39. Eleftherianos I, Heryanto C, Bassal T, Zhang W, Tettamanti G, Mohamed A. Haemocyte-mediated immunity in insects: cells, processes and associated components in the fight against pathogens and parasites. Immunology. 2021; 164:401-432.
40. Steckler R. Phosphate esters of hydroxyalkyl acrylates and hydroxy alkyl methacrylates. Alcolac Inc., U.S., 1974.

Received April 30, 2025; Revised June 10, 2025; Accepted June 21, 2025.

[§]These authors contributed equally to this work.

**Address correspondence to:*
Kazuhisa Sekimizu, Endowed Course "Drug Discoveries by Silkworm Models", Faculty of Pharmaceutical Sciences, Teikyo University, 359 Otsuka, Hachioji, 192-0395 Tokyo, Japan.
E-mail: sekimizu@main.teikyo-u.ac.jp

Krystyna Albrecht, Department for Functional Materials in Medicine and Dentistry, Institute of Functional Materials and Biofabrication, University of Würzburg, 97070 Würzburg, Germany.
E-mail: Krystyna.albrecht@uni-wuerzburg.de

Released online in J-STAGE as advance publication June 27, 2025.

Original Article

DOI: 10.5582/ddt.2025.01035

Opsin 3-mediated regulation of blue light-induced β-hexosaminidase release from mast cells

Hiroyuki Yamamoto[1,2,*], Miki Kiryu[2], Yoshikazu Sawaguchi[3], Toshiyuki Yamada[2]

[1] Department of Health and Nutritional Sciences, Faculty of Food and Health Sciences, Aichi Shukutoku University, Aichi, Japan;
[2] Department of Microbiology and Molecular Cell Biology, Nihon Pharmaceutical University, Saitama, Japan;
[3] Faculty of Biomedical Engineering, Toin University of Yokohama, Yokohama, Japan.

SUMMARY: The human body is constantly exposed to light from the environment, and intense light is a source of skin inflammation. Although cellular responses to high-energy ultraviolet light have long been reported, the photoresponsive mechanism occurring after skin exposure to visible light remains unclear. This study focused on mast cells involved in inflammation and examined the expression of photoreceptors and their effects on degranulation in mast cells. Photoreceptors expressed in two mast cell cultures (P-815 and RBL-2H3) were examined by RT-PCR and western blotting to demonstrate that OPN3 was expressed in RBL-2H3 cells. Next, the effect of visible light exposure on degranulation was evaluated by measuring β-hexosaminidase activity in the culture medium. The results show that β-hexosaminidase release was most strongly induced at wavelengths of ~460 nm, which corresponds to the absorption peak of OPN3. In addition, suppression of OPN3 expression by siRNA reduced β-hexosaminidase release at 460 nm. These results suggest that OPN3 expressed in mast cells mediates degranulation in skin inflammation that occurs upon exposure to intense light.

Keywords: blue light, opsin 3, mast cell, degranulation, photoresponse

1. Introduction

Photosensitivity is a condition that causes itching, redness, and rashes on the skin under exposure to sunlight, which may be manifested by ultraviolet (*1*) or visible light (*2,3*). Although cellular responses to high-energy ultraviolet light have long been reported, the photoresponsive mechanism occurring after skin exposure to visible light remains unclear.

The induction of inflammation in the skin following exposure to visible light occurs through the secretion of inflammatory cytokines. In keratinocytes, the activation of opsins promotes the secretion of inflammatory cytokines such as IL-3 and IL-6 (*4,5*), which is known to induce inflammation. Additionally, blue light is absorbed by intracellular chromophores, such as those found in mitochondria, leading to the generation of reactive oxygen species (ROS) (*6*). The ROS produced then induce the secretion of inflammatory cytokines (TNF-α, IL-1β, *etc.* (*5-7*)), thereby promoting inflammatory responses. These mechanisms are considered to be one of the causes of skin inflammation induced by visible light.

Mast cells are distributed in many tissues, and together with basophils constitute the main source of histamine (*8*). The mast cell surface expresses FcεRI, a receptor for IgE antibodies, which causes increased intracellular calcium ion concentrations, then degranulation and the release of histamine and other chemical transmitters from the granules to the extracellular environment (*9*). Histamine causes vasodilation, increased vascular permeability, and contraction of smooth muscle, leading to a variety of immediate allergic symptoms (*10*).

In recent years, the expression of photoreceptors in skin has been clarified and reported to show various responses to exposure to visible light and ultraviolet radiation (*11-14*). However, the effects of visible light on mast cells have not been reported so far. In this study, we therefore focused on opsin as a photoreceptor and explored its expression in mast cells. We also examined the effects of light exposure on degranulation, focusing on the induction of allergies, in which mast cells play a major role.

2. Materials and Methods

2.1. Cell culture

Cells of the mouse mast cell line P-815 (*15*) and rat basophilic leukemia and mast cell line RBL-2H3

(*16,17*), which are widely employed as models for immunologically induced mast cell degranulation, were supplied by Health Science Research Resources Bank (Osaka, Japan). Cells were cultured in DMEM (Nissui Pharmaceutical, Tokyo, Japan) supplemented with 10% (v/v) fetal bovine serum (FBS, Moretate Biotech, Bulimba, Australia) in a humidified atmosphere of 5% CO_2 and 95% air at 37°C.

2.2. Expression of opsins in mast cell lines

The expression of opsins was assessed using reverse transcription-polymerase chain reaction (RT-PCR). Total RNA was extracted from the P-815 cells and RBL-2H3 cells using TriPure Isolation Reagent (Roche Life Science, Indianapolis, IN, USA), and genomic DNA was removed with DNase I. cDNA was synthesized using ReverTra Ace (Toyobo, Osaka, Japan) according to manufacturer instructions. The primers used are listed in Table 1. PCR amplification was performed using Quick Taq® HS DyeMix (Toyobo) following the manufacturer's instructions. The following PCR cycles were employed: initial denaturation at 95°C for 5 min, followed by 30 to 40 cycles (depending on the primer) at 94°C for 1 min, 60°C for 1 min, and 72°C for 1 min. PCR products were electrophoresed on ethidium bromide-containing 2% agarose gels and visualized under UV illumination.

For quantification of OPN3 expression, quantitative PCR was performed using a StepOne system (Applied Biosystems, Foster City, CA, USA) with THUNDERBIRD® Next SYBR™ qPCR Mix (Toyobo). The primers used are listed in Table 1. Specificity of PCR products was verified by melt curve. The Ct values for the samples were normalized to that of β-actin, and the relative expression was calculated using the comparative Ct method.

2.3. β-Hexosaminidase assay

Cells were prepared in DMEM with 10% FBS at 5 × 10^5 cells/mL and cultured in 96-well microplates at 200 μL per well. After 24 h incubation, DMEM with 10% FBS was removed, 100 μL of DMEM with 1% FBS was added to each well, and the cells were irradiated with light for 15 min. The irradiation was performed using the Okazaki Large Spectrograph with wavelengths of 350 nm, 450 nm, 550 nm, 650 nm and 750 nm. Each wavelength was regulated at 1.7-2.2 W/m^2. After irradiation, the supernatants were collected for measuring β-hexosaminidase activity. The supernatant of cells not exposed to light was used as a negative control, while total β-hexosaminidase extracted using 100 μL of Triton X-100 was used as a positive control. A moiety of 10 μL per prepared sample was transferred to a 96-well microplate, and 100 μL of 2 mM p–nitrophenyl–*N*–acetyl–β–*D*–glucosaminide solution was added and then incubated at 37°C for 30 min. After incubation, the amount of paranitrophenol produced by the reaction was determined based on absorbance at a wavelength of 410 nm.

2.4. Western blotting analysis

Samples (20 μg) of the cell lysates were separated on a 12% (w/v) polyacrylamide gel (*18*). Proteins were blotted onto nitrocellulose membranes (Protran BA85; GE Healthcare, Chicago, IL, USA) in a semi-dry blotting system (NA-1513; Nihon Eidoh Co., Tokyo, Japan) (*19*). Nitrocellulose membranes were blocked with 2% (w/v) skim milk in Tris-buffered saline. Blocked membranes were incubated with rabbit anti-opsin 3 antibody (1:3,000; Genetex, Irvine, CA, USA), mouse anti-GAPDH antibody (1:10,000; Fujifilm Wako Pure Chemical, Osaka, Japan). This was followed by incubation with horseradish peroxidase-conjugated goat anti-rabbit immunoglobulin G (IgG) antibody (1:10,000; Seracare, Camarillo, CA, USA) or horseradish peroxidase-conjugated goat anti-mouse IgG antibody (1:3,000; Seracare). The blots were subsequently developed using the ImmunoStar LD chemiluminescent reagent

Table 1. Primers for RT-PCR

Target	Sense primer	Antisense primer
rat OPN1-SW	TCTTCACAGTCTTCATCGCCAG	CCAGGTATAGTGCTCGCTTC
rat OPN1-MW/LW	AGCAGAGACCATTATTGCCAGC	GTCCATACAGCAGCCCAGAC
rat OPN2	CACCTCACTGCATGGCTACTT	ATGGGGATGGTGAAGTGGAC
rat OPN3	GTCTGGGCGATCTGCTGGTA	ATGCCAAAGAGTAGAGCCAGAT
rat OPN4	TGGAACAGCACTCAGAACATC	AAAGACAGCCCCACAGAAGG
rat OPN5	AAGCCTGATTACCATGACTGC	TGGCAATGATCTTCGCGTATG
rat β-actin	AACCCTAAGGCCAACCGTGAAAAG	CGACCAGAGGCATACAGGGACAAC
mouse OPN1-SW	TGGGCTCTGTAGCAGGTCTA	CAGGACCACCATCAGTGCAT
mouse OPN1-MW/LW	AACTTGGCAGTTGCTGACCT	AGGCCTGTGATTCCACACAAT
mouse OPN2	GGGCCCCAATTTTTATGTGCC	ACAGGGCGATTTCACCTCCAA
mouse OPN3	CATTACCACCCTCACTGTGCT	GATCTTCAACACAGCGAAGCATT
mouse OPN4	GTTCTGAGAGTGAAGTGGGCT	AAGCTTCCAGGCTTGTGACAT
mouse OPN5	AACCACACTGCCCTACCTCA	TCTCTTCAGCCAGACCCCATA
mouse β-actin	TGACAGGATGCAGAAGGAGA	CATCTGCTGGAAGGTGGACA

(Fujifilm Wako Pure Chemical) and a LuminoGraph chemiluminescent imaging system (Atto Corporation, Tokyo, Japan).

2.5. RNAi-induced opsin 3 knockdown assay

INTERFERin (Polyplus-transfection, Illkirch, France) was used to transfect rat opsin 3 siRNA (AGCAAUGGGCUAUGACACC(dTdT); Bioneer Corporation, Daejeon, Republic of Korea) into RBL-2H3 cells. At 48 h after transfection, opsin 3 expression was measured through quantitative RT-PCR analysis.

2.6. Statistical analysis

Statistical analyses were performed using Student's *t*-tests implemented in SPSS Statistics (version 29.0.2.0; IBM, Chicago, Il, USA). A p-value < 0.05 was considered indicative of statistical significance.

3. Results

3.1. Expression of opsins in mast cells

We analyzed the expression of opsin in the mouse mast cell line P-815 and rat basophilic leukemia cell line RBL-2H3 using RT-PCR (Figure 1A). OPN2, OPN3 and OPN4 mRNA were expressed in P-815 cells. Expression of OPN1-MW/LW, OPN2 and OPN3 was observed in RBL-2H3 cells. OPN1-MW/LW and OPN2 in RBL-2H3 cells demonstrated two different PCR products. The expression of OPN3 mRNA in RBL-2H3 cells was confirmed by Western blotting (Figure 1B). A band of approximately 40 kDa was detected in RBL-2H3 cells.

3.2. Effect of light exposure on β-hexosaminidase release

We evaluated whether light exposure induces degranulation from mast cells, using β-hexosaminidase release as an indicator (Figure 2A). The results show that exposure to wavelengths between 350 and 550 nm increased β-hexosaminidase release. In contrast, no change in β-hexosaminidase release was observed with exposure to wavelengths longer than 650 nm. Next, to examine in more detail the wavelengths to which RBL-2H3 cells respond, we measured β-hexosaminidase released from RBL-2H3 cells when exposed to various wavelengths at 20 nm intervals (Figure 2B). The results show that wavelengths in the ultraviolet region at 340 nm and around 460 nm induced the release of β-hexosaminidase.

3.3. Downregulation of OPN3 expression by siRNA and its effect on β-hexosaminidase release

We examined the release of β-hexosaminidase after light exposure in RBL-2H3 cells in which OPN3 expression was suppressed by siRNA. siRNA knockdown of OPN3 in RBL-2H3 cells reduced OPN3 expression to approximately 28% of the control level (Figure 3A). Western blotting further revealed that OPN3 expression

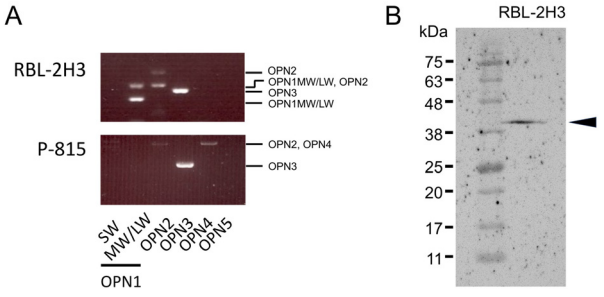

Figure 1. Expression of opsins in murine mast cell line P-815 and rat mast cell line RBL-2H3. RT-PCR analysis of opsin mRNA expression in RBL-2H3 cells and P-815 cells (**A**). Western blotting for OPN3 using RBL-2H3 cells (**B**).

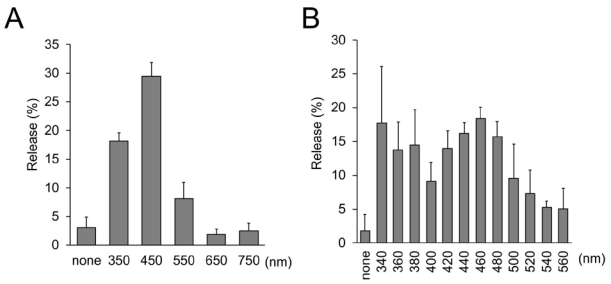

Figure 2. Wavelength dependency of degranulation in RBL-2H3. The degranulation from mast cells was evaluated with β-hexosaminidase release as an indicator. Monochromatic light was separated using the Okazaki Large Spectrograph, and cellular responses were evaluated at intervals of 100 nm (**A**) or 20 nm (**B**).

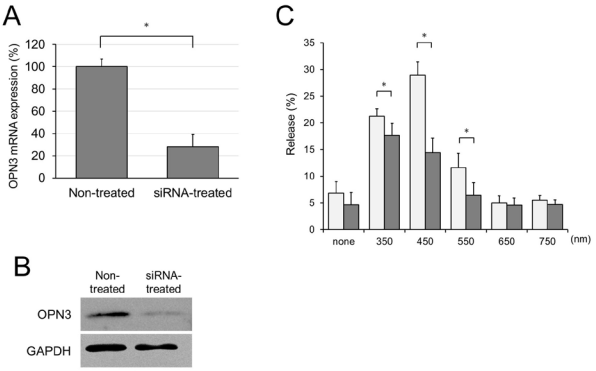

Figure 3. Effect of blue light on degranulation in mast cells with OPN3 knockdown. Evaluation of the OPN3 knockdown efficiency in RBL-2H3 cells following siRNA treatment by quantitative RT-PCR (**A**) and western blotting (**B**). Quantitative RT-PCR results are presented as mean ± SD (n = 3). Statistical significance was determined by Student's *t*-tests compared to non-treated control cells (p < 0.05). Comparison of degranulation in response to blue light exposure between non-treated control cells and OPN3 knockdown (OPN3-KD) cells (**C**). Open bars represent the non-treated control cells, while filled bars indicate OPN3-KD cells. Data are shown as mean ± SD (n = 8). *p < 0.05, determined by Student's *t*-tests compared to non-treated control cells.

was reduced in cells treated with OPN3 siRNA (Figure 3B). Next, the light response of RBL-2H3 cells with OPN3 expression reduced by siRNA was examined based on β-hexosaminidase release. As shown in Figure 3C, β-hexosaminidase release was significantly suppressed upon stimulation with light at wavelengths of 350 nm, 450 nm and 550 nm. Among these, the most pronounced suppression (approximately 49.8%) was observed at 450 nm, which is close to the peak response wavelength of OPN3, while the release observed at 350 nm was less pronounced.

4. Discussion

In this study, we explored opsin expressed in non-visual cells using RBL-2H3 cells and P-815 cells as mast cell models and found that OPN3 is commonly expressed. Several groups have previously reported that opsin receptors are expressed in multiple cells in skin, a non-visual tissue (*11,12,20*). It has been shown that 11-*cis*-retinal is produced by all-*trans*-retinal in response to light and metabolism of retinal, which is required for opsin activity, and it has been reported that OPN expressed in skin is functional (*21*). The presence of a photoreceptor cycle in skin has suggests that opsins expressed on mast cells would also be functional.

To determine the wavelengths to which mast cells respond, spectrograms were used to evaluate β-hexosaminidase release as an indicator of spectral light response. β-hexosaminidase release was maximal at ~460 nm (*22*). Since the strongest response of the photoreceptor OPN3 was observed at this wavelength, the release of β-hexosaminidase is considered to be mediated by OPN3.

OPN3 has been reported to increase intracellular calcium ion concentrations. Increased intracellular calcium ion concentrations have been shown to trigger the release of intracellular secretory granules in various cells (*23,24*). Based on this observation, it was assumed that the activation of OPN3 is responsible for the elevated β-hexosaminidase release recorded at the 460 nm wavelength. Accordingly, when OPN3 expression was suppressed with siRNA, the release of β-hexosaminidase at ~450 nm was reduced. These findings indicate that exposure of mast cells to blue light increases the release of β-hexosaminidase *via* expressed OPN3.

Short wavelengths of light penetrate less deeply into the tissues of biological organisms than do long wavelengths. With a transmittance of ~30%, only a small proportion of blue light is able to reach the dermal layer, where mast cells are located (*25*). The observed phenomena may therefore constitute the response mechanism of the organism when blue light reaches the dermal layer due to exposure to intense light or damage to the epidermal layer. In general, the response to blue light varies between different skin cells. In keratinocytes, exposure to blue light decreases their migration ability (*21*). In melanocytes, melanin production is increased (*26*). In fibroblasts, the expression of matrix metalloproteinase, a collagen-degrading enzyme, is increased resulting in decreased skin elasticity (*27*).

Our results demonstrate that OPN3 is expressed in mast cells and that blue light induces mast cell degranulation *via* OPN3. The enhancement of degranulation by blue light may be considered to be one of the defensive mechanisms involved in skin homeostasis.

Acknowledgements

This work was supported by funding from the KOSÉ Cosmetology Research Foundation to HY and by JSPS KAKENHI (grant numbers: JP23K05029 and JP20K05829) to HY. This work was also supported by the NIBB Collaborative Research Experiment for the Okazaki Large Spectrograph (21-502, 22NIBB603, and 23NIBB601) to HY.

Funding: None.

Conflict of Interest: The authors have no conflicts of interest to disclose.

References

1. Cavinato M, Jansen-Dürr P. Molecular mechanisms of UVB-induced senescence of dermal fibroblasts and its relevance for photoaging of the human skin. Exp Gerontol. 2017; 94:78-82.
2. Sklar LR, Almutawa F, Lim HW, Hamzavi I. Effects of ultraviolet radiation, visible light, and infrared radiation on erythema and pigmentation: A review. Photochem Photobiol Sci. 2013; 12:54-64.
3. Ezekwe N, Maghfour J, Kohli I. Visible Light and the Skin. Photochem Photobiol. 2022; 98:1264-1269.
4. Lago JC, Ganzerla MD, Dias ALA, Savietto JP. The influence of blue light exposure on reconstructed 3-dimensional skin model: Molecular changes and gene expression profile. JID Innov. 2024; 4:100252.
5. Liu L, Ma J, Chen W, Zhang J, Zuo W, Wang M, Li J. UVB-induced HaCat cell damage and Myricaria Paniculata's molecular effects. Sci Rep. 2025; 15:10909.
6. Nakashima Y, Ohta S, Wolf AM. Blue light-induced oxidative stress in live skin. Free Radic Biol Med. 2017; 108:300-310.
7. Kumar D, Ahmed M, Andrabi NI, Singh CP, Saroch D, Bharitkar YP, Kour G, Madishetti S, Bhagat A, Shukla SK, Ahmed Z. Anti-inflammatory and anti-oxidant potential of Dispiro-indanedione hybrid of parthenin *via* regulating Nrf2 and NF-κB/MAPK pathways. Eur J Pharmacol. 2025; 177547.
8. Dileepan KN, Raveendran VV, Sharma R, Abraham H, Barua R, Singh V, Sharma R, Sharma M. Mast cell-mediated immune regulation in health and disease. Front Med (Lausanne). 2023; 10:1213320.
9. Macglashan D, Jr. IgE and Fc{epsilon}RI regulation. Ann N Y Acad Sci. 2005; 1050:73-88.
10. Church MK. Allergy, histamine and antihistamines. Handb

Exp Pharmacol. 2017; 241:321-331.
11. Tsutsumi M, Ikeyama K, Denda S, Nakanishi J, Fuziwara S, Aoki H, Denda M. Expressions of rod and cone photoreceptor-like proteins in human epidermis. Exp Dermatol. 2009; 18:567-570.
12. Haltaufderhyde K, Ozdeslik RN, Wicks NL, Najera JA, Oancea E. Opsin expression in human epidermal skin. Photochem Photobiol. 2015; 91:117-123.
13. Castellano-Pellicena I, Uzunbajakava NE, Mignon C, Raafs B, Botchkarev VA, Thornton MJ. Does blue light restore human epidermal barrier function *via* activation of Opsin during cutaneous wound healing? Lasers Surg Med. 2019; 51:370-382.
14. Wicks NL, Chan JW, Najera JA, Ciriello JM, Oancea E. UVA phototransduction drives early melanin synthesis in human melanocytes. Curr Biol. 2011; 21:1906-1911.
15. Schellenberg H, Domen Joz R. P-815 mast cell tumor in suspension as a substrate for the testing of carcinostatic substances. Med Exp Int J Exp Med. 1962; 7:137-143.
16. Morita Y, Siraganian RP. Inhibition of IgE-mediated histamine release from rat basophilic leukemia cells and rat mast cells by inhibitors of transmethylation. J Immunol. 1981; 127:1339-1344.
17. Hemmerich S, Pecht I. Isolation and purification of an Fc epsilon receptor activated ion channel from the rat mast cell line RBL-2H3. Biochemistry. 1988; 27:7488-7498.
18. Laemmli UK. Cleavage of structural proteins during the assembly of the head of bacteriophage T4. Nature. 1970; 227:680-685.
19. Burnette WN. "Western blotting": electrophoretic transfer of proteins from sodium dodecyl sulfate--polyacrylamide gels to unmodified nitrocellulose and radiographic detection with antibody and radioiodinated protein A. Anal Biochem. 1981; 112:195-203.
20. Suh S, Choi EH, Atanaskova Mesinkovska N. The expression of opsins in the human skin and its implications for photobiomodulation: A Systematic Review. Photodermatol Photoimmunol Photomed. 2020; 36:329-338.
21. Yamamoto H, Okada M, Sawaguchi Y, Yamada T. Expression of opsin and visual cycle-related enzymes in fetal rat skin keratinocytes and cellular response to blue light. Biochem Biophys Rep. 2024; 39:101789.
22. Sugihara T, Nagata T, Mason B, Koyanagi M, Terakita A. Absorption characteristics of vertebrate non-visual Opsin, Opn3. PLoS One. 2016; 11:e0161215.
23. Bertram R, Sherman A, Satin LS. Metabolic and electrical oscillations: partners in controlling pulsatile insulin secretion. Am J Physiol Endocrinol Metab. 2007; 293:E890-900.
24. Stojilkovic SS. Ca^{2+}-regulated exocytosis and SNARE function. Trends Endocrinol Metab. 2005; 16:81-83.
25. Akihiro K, Eisaku K, Tomohisa Y, Shunki Y, Shuichi K, Shuichi M. Ultra long-range visible light propagation of human skin. Nihon Gazo Gakkaishi. 2017; 56:466-472.
26. Regazzetti C, Sormani L, Debayle D, Bernerd F, Tulic MK, De Donatis GM, Chignon-Sicard B, Rocchi S, Passeron T. Melanocytes sense blue light and regulate pigmentation through Opsin-3. J Invest Dermatol. 2018; 138:171-178.
27. Moriwaki S. Light-emitting diodes as a new medical tool in aesthetic dermatology. Photomed Photobiol. 2018; 39:1-5.

Received April 16, 2025; Revised June 10, 2025; Accepted June 19, 2025.

**Address correspondence to:*
Hiroyuki Yamamoto, Department of Health and Nutritional Sciences, Faculty of Food and Health Sciences, Aichi Shukutoku University, Nagakute City, Aichi, 480-1197, Japan.
E-mail: yamahiro@asu.aasa.ac.jp

Released online in J-STAGE as advance publication June 25, 2025.

Original Article

DOI: 10.5582/ddt.2025.01034

Discovery of SARS-CoV-2 papain-like protease inhibitors through machine learning and molecular simulation approaches

Li Li[1], Jinyang Li[1], Quanling Zhang[1], Yifei Huang[2], Yongxin Bao[1,3,*], Xiaowen Tang[1,4,*]

[1] School of Pharmacy, Qingdao University, Qingdao, Shandong, China;
[2] College of Life Sciences, Qingdao University, Qingdao, Shandong, China;
[3] Qingdao Women and Children's Hospital Affiliated to Qingdao University, Qingdao, Shandong, China;
[4] Shandong Provincial Key Laboratory of Pathogenesis and Prevention of Brain Diseases, Qingdao University, Qingdao, Shandong, China.

SUMMARY: The papain-like protease (PLpro), a cysteine protease found in severe acute respiratory syndrome coronavirus 2 (SARS-CoV-2), plays a crucial role in viral replication by cleaving the viral polyproteins and interfering with the host's innate immune response through deubiquitination and deISGylation activities. Consequently, targeting PLpro has emerged as an appealing therapeutic strategy against SARS-CoV-2 infection. Despite considerable efforts in the development of PLpro inhibitors, there is currently no drug available on the market that specifically targets PLpro. Improving drug screening strategies and identifying additional candidate compounds could significantly contribute to the advancement of antiviral agents targeting PLpro. To address this pressing issue, our present study has developed a highly efficient compound screening strategy based on a supervised machine learning approach. Integrated with further molecular simulation approaches such as molecular docking, molecular dynamics simulations, and quantum chemical calculations, we have identified seven compounds with potent inhibitory activity against PLpro. Notably, two of these compounds exhibited superior activity compared to Jun12682, which is currently considered the best-performing inhibitor against PLpro. Furthermore, some crucial residues in SARS-CoV-2 PLpro were recognized as favorable contributors to the binding with inhibitor, which would provide valuable insights for the development of more potent and highly selective SARS-CoV-2 PLpro inhibitors. The compound screening strategy and potential PLpro inhibitor candidates revealed in the present study would hold promise for advancing the development of antiviral drugs targeting SARS-CoV-2 and its variants.

Keywords: SARS-CoV-2, papain-like protease inhibitor, machine learning, virtual screening, molecular simulation

1. Introduction

The global Coronavirus Disease 2019 (COVID-19) pandemic, caused by severe acute respiratory syndrome coronavirus 2 (SARS-CoV-2), has posed a serious threat to public health security worldwide. Although various approved COVID-19 vaccines have played a critical role in controlling the pandemic (*1*), the continuous emergence of SARS-CoV-2 variants, such as the recently identified JN.1 (BA.2.86.1.1) and KP.2 (JN.1.11.1.2), threatens the efficacy of current vaccines (*2*). Moreover, vaccines are primarily used to prevent COVID-19, but for patients already infected with the virus, effective treatment options are still necessary. Therefore, the development of specific antiviral drugs targeting SARS-CoV-2 remains an essential measure in addressing this ongoing threat.

Papain-like protease (PLpro), a viral cysteine protease essential for SARS-CoV-2 replication, cleaves polyproteins pp1a and pp1ab to generate non-structural proteins (nsp). In addition to processing viral proteins, PLpro also targets host proteins such as ubiquitin and interferon-stimulated gene 15 (ISG15), performing deubiquitinating and deISGylating activities that suppress the host's innate immune response (*3*). Consequently, PLpro inhibition holds promise for suppressing viral propagation and restoring host's immune function (*4*), making it a key target for antiviral drug development.

Since the outbreak of the COVID-19 pandemic, numerous inhibitors targeting PLpro have been discovered through structure-based drug design, virtual screening, and high-throughput screening methods (*5*). These inhibitors can be categorized into non-covalent and covalent inhibitors based on their binding modes as summarized in Figure 1. GRL0617, the first non-covalent PLpro inhibitor (*6*), exhibited relatively low activity against SARS-CoV-2 in cell-based assays, despite the moderate enzymatic activity (IC_{50}~1.39

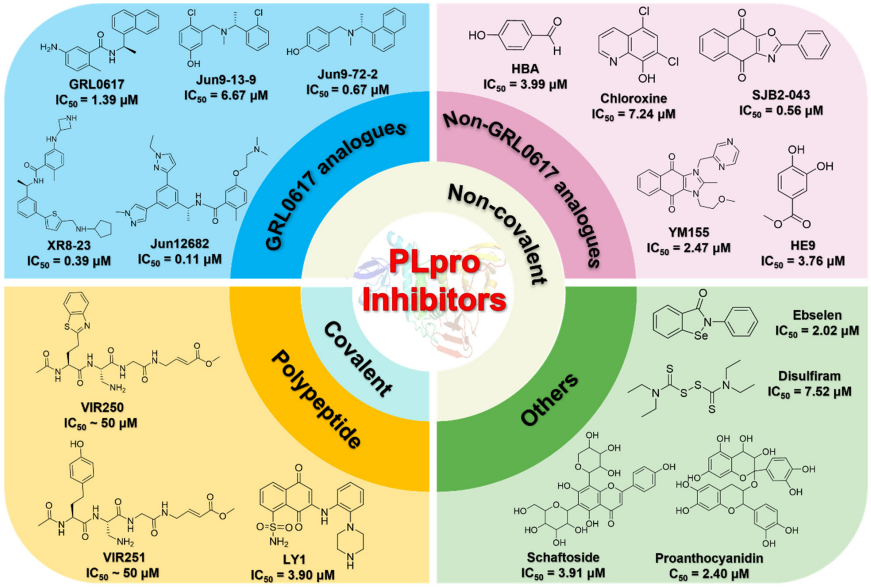

Figure 1. Representation and classification of SARS-CoV-2 PLpro inhibitors.

μM). Subsequently, Structural optimization led to more potent analogs such as XR8-23 (IC_{50}~0.39 μM) (*7*) and Jun12682 (IC_{50}~106.8 ± 5.0 nM) (*8*), the latter showing strong activity against multiple variants. In addition, some non-GRL0617 analogs (such as chloroxine (*9*), SJB2-043 (*10*), HE9 (*11*), HBA (*11*) and YM155 (*12*)) and several non-specific inhibitors, (including ebselen (*13*), disulfiram (*14*), schaftoside (*15*) and proanthocyanidi (*16*)) also exhibit promising antiviral activity. By contrast, covalent inhibitors targeting PLpro like LY1 (*17*) and peptide-based VIR250 and VIR251 (*18*) have also been reported. However, most candidates face limitations such as insufficient antiviral activity, poor pharmacokinetics, or inadequate target selectivity, preventing clinical translation. So far, only HL-21 has entered Phase I trials, and there are currently no FDA-approved drugs targeting PLpro. These challenges underscore the need for improved screening strategies and novel chemical scaffolds to accelerate PLpro-targeted drug discovery.

In recent years, artificial intelligence (AI) has become an increasingly powerful tool in drug discovery (*19*). Notably, the 2024 Nobel Prizes in Physics and Chemistry has underscored the pivotal role of AI in advancing scientific research. Recently, some potent SARS-CoV-2 Mpro inhibitors with strong cellular activity were discovered by a using machine learning approach (*20*), shortly thereafter, a lead compound (PF-07957472) targeting SARS-CoV-2 PLpro that showed high efficacy in mouse models was also identified by using AI technique (*21*). For the purpose of improving the drug screening efficiency and providing more candidate compounds to assist the development of anti-COVID-19 drugs, an integrated screening strategy that combined machine learning and molecular simulation approaches (*22,23*) was developed and further utilized to perform the screening of SARS-CoV-2 PLpro inhibitor. As a result, the current study identified seven compounds (Cpd-1~4, Cpd-6, Cpd-8, and Cpd-14) that exhibited higher binding affinity on PLpro compared to GRL0617. Among them, two compounds, Cpd-1 and Cpd-3, showed more potent inhibitory activity than the currently best-performing compound, Jun12682. These compounds hold promise for advancing the development of a new generation of inhibitors targeting SARS-CoV-2 and its variants.

2. Methods

The screening strategy of SARS-CoV-2 papain-like protease inhibitors in the current study refers to machine learning-based classification, molecular simulation (molecular docking, molecular dynamics simulation, and quantum chemical calculation) based screening and verification. The workflow of the screening strategy is exhibited in Figure 2.

2.1. Data preparation

The initial database was constructed based on the inhibitory activity data for 3,935 FDA-approved drugs and clinical trial candidate compounds against SARS-CoV-2 PLpro (*24*). To ensure data quality, the following preprocessing steps were performed before training the machine learning models: (1) Eliminating the compounds with invalid information, such as lacking structural information, containing ambiguous or even non-numeric data. Only compounds with structural information (in SMILES format) and inhibition rates against SARS-CoV-2 PLpro were retained. (2) Establishing an activity threshold of 60%, wherein

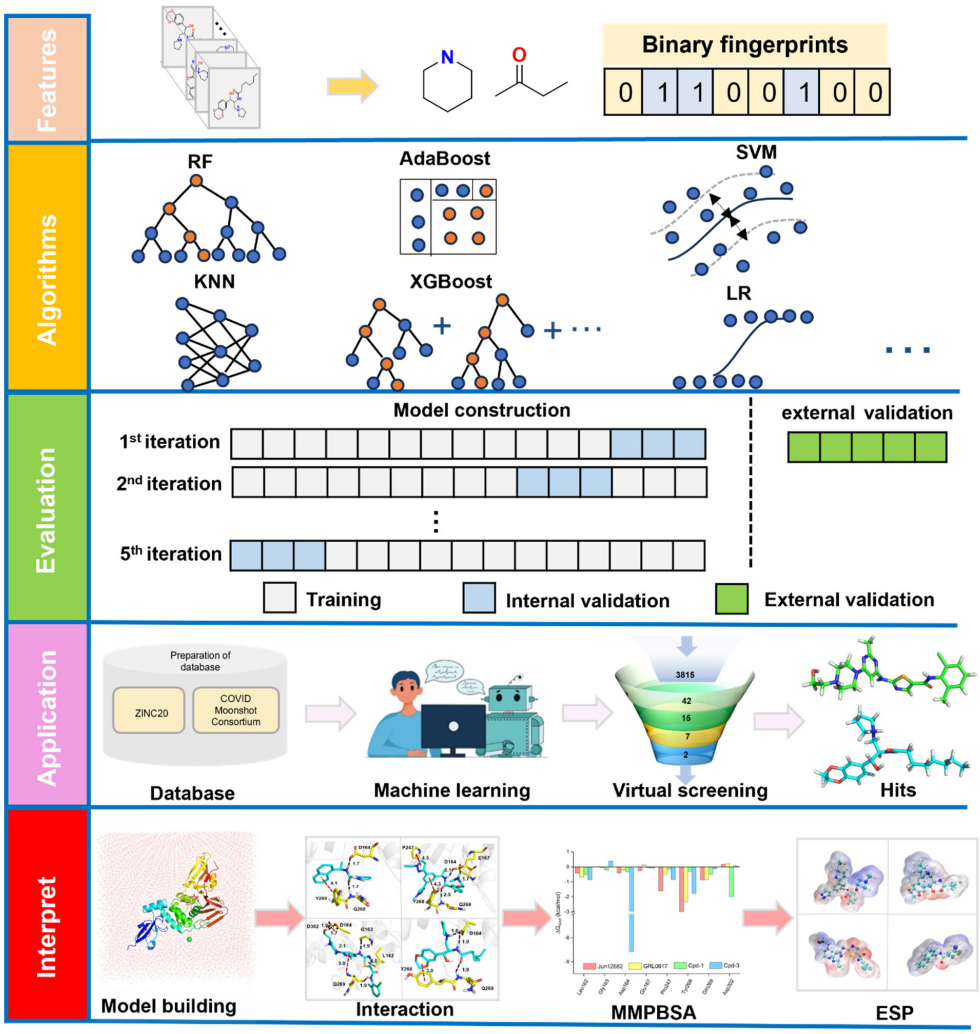

Figure 2. Workflow of the screening strategy in the present study.

compounds with an inhibition rate of 60% or higher were defined as active, while those lower than 60% were labeled as inactive. As a result, a binary dataset of 3,428 compounds consisting of 249 active and 3,179 inactive data was obtained (Supplementary Materials 1). (3) In view of the imbalance between active and inactive data, 1,000 compounds randomly selected from the inactive data, together with all the active data, were collected to construct a combined dataset of 1,249 compounds with a 4:1 ratio of inactive to active data (Supplementary Materials 2). (4) Further splitting the combined dataset into an 8:2 ratio for machine learning model training and internal validation. To achieve more realistic model performance, a 5-fold cross-validation strategy was applied. Additionally, 79 active compounds obtained from SARS-CoV-2 PLpro patent literature and 341 compounds randomly selected from the inactive data were collected for external validation (Supplementary Materials 3).

FDA-approved drugs (*https://www.fda.gov/*) are increasingly favored for new drug development because their well-documented toxicity profiles and human pharmacokinetics significantly reduce both the development time and costs. Moreover, surveys by the National Cancer Institute have shown that three-quarters of all drugs used globally over the past half-century to treat various human diseases are derived from natural resources. Therefore, for the final screening of potential SARS-CoV-2 PLpro inhibitors, 3,815 compounds from FDA-approved drugs (previously unevaluated) and natural products curated from the ZINC database, as well as the COVID Moonshot platform were compiled as prediction dataset (Supplementary Materials 4).

2.2. Machine learning

Six molecular descriptors and fingerprints, including Morgan fingerprint (MorganFP), MACCS fingerprint (MACCSFP), E-state fingerprint (E-stateFP), Avalon fingerprint (AvalonFP), Atom-pairs fingerprint (Atom-PairFP) and RDKit descriptors (RDKit-Des), were employed to describe the molecular structures when performing the machine learning. Further details regarding the molecular fingerprints and descriptors

can be found in Table S1 (*https://www.ddtjournal.com/action/getSupplementalData.php?ID=261*). Meanwhile, 14 algorithms, including decision trees, random forests, extreme gradient boosting (XGBoost), support vector machines (SVM), gradient boosting decision trees, gradient boosting machines (GBM), logistic regression, K-nearest neighbors (KNN), linear discriminant analysis (LDA), stochastic gradient descent, adaptive boosting, bootstrap aggregating, voting classifier, and multilayer perceptron classifier were adopted for machine learning model construction. Eventually, a total of 84 machine learning models were generated and further evaluated to establish the SARS-CoV-2 PLpro inhibitors screening models. In addition, RDKit was employed for the generation of all molecular features and fingerprints, and scikit-learn was employed to implement the model construction.

To evaluate the predictive ability and robustness of the constructed machine learning models, the following evaluation metrics were used in this study: area under the receiver operating characteristic curve (AUC), F1 score (F1), precision (Pre), sensitivity (Se), and specificity (Sp). The calculation methods of them are listed as follows:

$$Pre = TP / (TP + FP)$$
$$Se = TP / (TP + FN)$$
$$Sp = TN / (TN + FP)$$
$$F1 = 2 \times (Pre \times Se) / (Sp + Se)$$

Where, true positive (TP) refers to instances correctly classified as positive, while true negative (TN) denotes those correctly classified as negative. False positive (FP) represents instances incorrectly classified as positive, and false negative (FN) denotes those incorrectly classified as negative. The F1 score is a metric that provides a comprehensive evaluation of the model by considering both precision (Pre) and sensitivity (Se). A higher F1 score (closer to 1) indicates a stronger generalization ability of the mode. AUC is a key indicator for evaluating the performance of classification models. The model performance will be better if the AUC value is closer to 1 (*25*).

2.3. Molecular docking

The initial receptor model was constructed based on the crystal structure of the SARS-CoV-2 PLpro in complex with GRL0617 (PDB ID: 7CJM). Protein and ligand parts were extracted and processed for subsequent molecular docking experiments. Compounds screened by the machine learning model underwent further optimization using the OPLS4 force field. Protonated states of ionizable groups were defined at pH 7.0 ± 0.2, which simulated the slightly fluctuating pH conditions in the physiological environment. The protonated states of titratable residues in receptor structure were also calculated at the same pH for ligand preparation. Molecular docking analysis utilized AutoDock Vina (*26*), where the centroid of the ligand (GRL0617) was defined as the center of the docking grid, and the size of the grid was set to 25 × 25 × 25 $Å^3$. Finally, flexible molecular docking based on induced fit theory was executed, and results (binding mode and docking score) with the best docking score were recorded.

2.4 Classical molecular dynamics simulation

The ligand-receptor complex models were obtained from molecular docking. All molecular dynamics (MD) simulations were performed using the *pmemd* module in the AMBER18 molecular simulation package. The Amber ff14SB force field (*27*) was employed for the protein, and the TIP3P model (*28*) was used for the solvent water molecules. The force field parameter of the ligand was generated from the general AMBER force field (GAFF), and the partial atomic charge was defined by the restrained electrostatic potential (RESP) (*29*) charge based on HF/6-31G* calculation with the Gaussian09 package.

The initial coordinates and topology files were generated by the *tleap* program with neutralization and solvation. The subsequent classical MD simulations were carried out by using the periodic boundary condition with the cubic model. After a series of energy minimization, programmed heating (0 to 300 K, NVT, 100 ps), density equilibrium (300 K, 1.0 atm, NPT, 100 ps), and preequilibrium (300 K, 1.0 atm, NPT, 100 ps), a final 100 ns MD simulation with a 2 fs time step was performed under the NVT ensemble to generate trajectories. During the MD simulation, the high-frequency stretching vibration of all hydrogen-containing bonds was constrained by using the SHAKE algorithm (*30*), and a 12 Å cutoff was applied to van der Waals (LJ-12 potential) and electrostatic interactions (PME strategy). Finally, *cpptraj* was used for trajectories analysis and PyMOL was used for visualization.

The binding free energy was calculated using the MM/GBSA method (*31*) *via* the *MMPBSA.py* module, based on 100 snapshots extracted from the stable phase of the MD trajectory. All energies were expressed in kcal/mol. The calculation method for binding free energy is listed as follows:

$$\Delta G_{bind} = G_{complex} - G_{receptor} + G_{ligand}$$

Where, ΔG_{bind} represents the total binding free energy between PLpro and its inhibitor. $G_{complex}$ denotes the energy of the protein-inhibitor complex, while $G_{receptor}$ and G_{ligand} refer to the individual energies of the PLpro and the inhibitor, respectively. The free energy components in the MM/GBSA approach were determined as follows:

$$\Delta G_{bind} = \Delta G_{gas} + \Delta G_{solv} - T\Delta S$$
$$= \Delta E_{vdw} + \Delta E_{ele} + \Delta G_{polar} + \Delta G_{nonpola} - T\Delta S$$
$$= \Delta E_{vdw} + \Delta E_{ele} + \Delta E_{GB} + \Delta E_{SA} - T\Delta S$$

Herein, ΔG_{gas} and ΔG_{solv} denote the gas-phase and solvation energy components of the total free energy (ΔG_{bind}), respectively. ΔG_{gas} consists of van der Waals (ΔE_{vdw}) and electrostatic (ΔE_{ele}) contributions. ΔG_{polar} and $\Delta G_{nonpolar}$ refer to the polar and nonpolar components of the solvation free energy, respectively. The terms ΔE_{GB} and ΔE_{SA} represent the polar and nonpolar contributions, respectively. The absolute temperature of the system is denoted by T, and the entropy related to the system is denoted as ΔS. The term $T\Delta S$ represents the entropy contribution.

2.5 Electrostatic potential calculation

The Gaussian09 program (Revision D.01) was utilized to calculate the electrostatic potential surface of the screened molecules. The calculation was performed based on density functional theory (DFT) at the B3LYP/6-311+G(2d,p) level. The restrained electrostatic potential (RESP) charges were computed using Multiwfn. Finally, Visual Molecular Dynamics (VMD, version 1.9.4a53) was used to visualize the molecular surface electrostatic potential maps, providing a clear graphical representation of the charge distribution across the molecules.

3. Results

3.1. Reliability analysis of datasets

Reliable datasets that refer to the training and validating set are an important guarantee for the accurate construction of the machine learning models. Herein, we applied t-distributed stochastic neighbor embedding (t-SNE) analysis by using a Euclidean distance metric to evaluate the reliability of the datasets for machine learning. Figure 3 illustrates the chemical space distributions of the collected compounds in training, validation, and prediction datasets, as visualized by t-SNE. Results showed that the distribution of training and validating datasets overlapped sufficiently, indicating that the construction and evaluation of the machine learning models are reliable. Furthermore, the distribution of datasets for model application (prediction dataset) and model construction (training and validation datasets) also presented a rough overlap, demonstrating the reliability of the subsequent machine learning-based SARS-CoV-2 PLpro inhibitor screening.

3.2. Machine learning-based model construction and application

To construct an accurate SARS-CoV-2 PLpro inhibitor prediction strategy, we developed 84 classification models based on 14 machine learning algorithms combined with 6 molecular fingerprints. Figure 4 shows the performance of the constructed classification models, which were evaluated through AUC and F1 score.

The performance of these models exhibited significant variations. For the machine learning algorithms, the average AUC values for the Random Forest, XGBoost, SVM, and GBDT models were dramatically higher than those of other models, as summarized on the right sidebar of Figure 4A, demonstrating the excellent performance of these four algorithms. Among them, models constructed with the Random Forest algorithm exhibited the best performance (with most models' AUC values closer to 1). For molecular fingerprints and

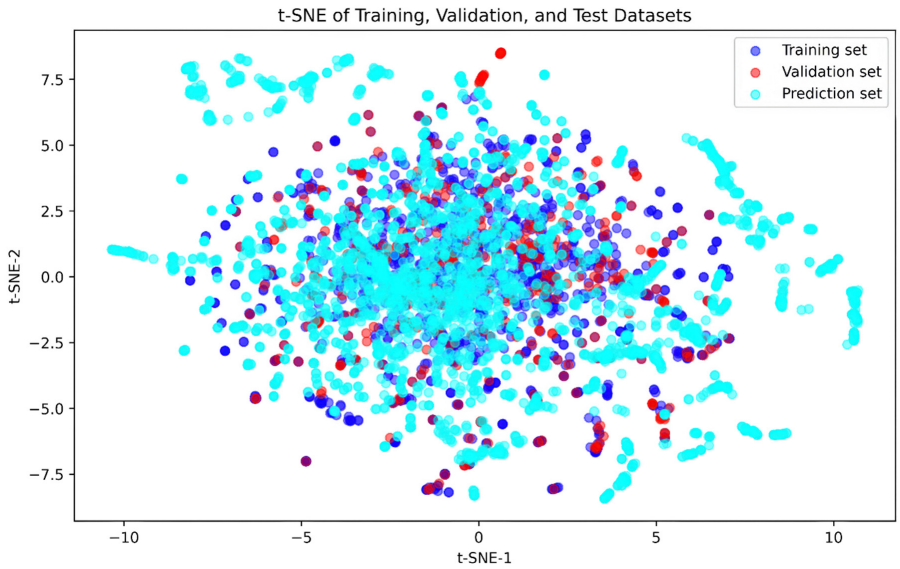

Figure 3. t-SNE of training, validation, and prediction datasets.

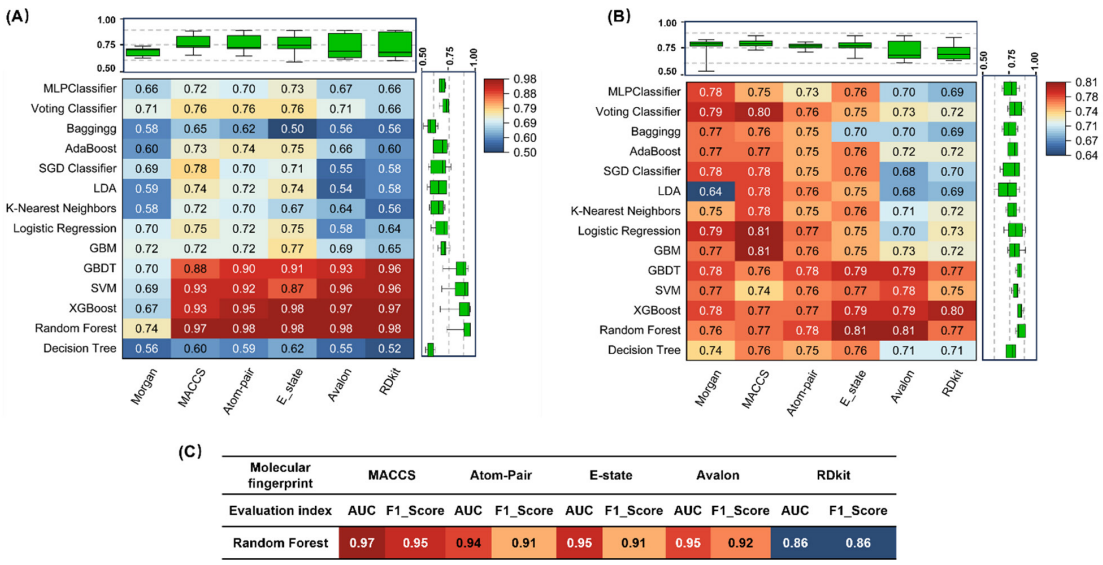

Figure 4. Performance evaluation of the constructed machine learning models. Heatmap of AUC **(A)** and F1 score **(B)** in internal validation. **(C)** The AUC values and F1 scores in external validation of models constructed by Random Forest algorithm with MACCSFP, E-stateFP, AtomPairFP, AvalonFP, and RDKit-Des.

descriptors, models employing MACCSFP, E-stateFP, AvalonFP, Atom-PairFP, and RDKit-Des achieved higher AUC values, especially for models with the four superior algorithms (Random Forest, XGBoost, SVM, and GBDT, where the AUC values exceeded 0.90 for most models). In contrast, models using MorganFP showed a lower performance (below 0.75). Additional assessment criteria (F1 score listed in Figure 4B) also highlighted the superior performance of models with the algorithms and descriptors aforementioned. Overall, models constructed by Random Forest algorithm with the five descriptors (MACCSFP, E-stateFP, AvalonFP, Atom-PairFP, and RDKit-Des) were level pegging in the internal validation (Figure 4A~B and Table S2, *https://www.ddtjournal.com/action/getSupplementalData.php?ID=261*). Furthermore, an external validation dataset containing 79 active compounds and 341 inactive compounds was introduced to evaluate the generalization ability of the five models as shown in Figure 4C and Table S3 (*https://www.ddtjournal.com/action/getSupplementalData.php?ID=261*). Apparently, four models presented superior performance with AUC and F1 score about 0.90, whereas the Random Forest-RDKit model was slightly inferior compared with other models, with both assessment criteria being lower than 0.90. Consequently, models based on Random Forest models with four molecular fingerprints (MACCSFP, E-stateFP, Atom-PairFP, and AvalonFP) were selected for the subsequent screening of compounds with potential SARS-CoV-2 PLpro inhibition activity.

In order to obtain the SARS-CoV-2 PLpro inhibitor more efficiently, we adopted a strategy of using multiple models to present the intersection of results to perform the machine learning-based compound screening. Herein, the Venn diagram obtained from the online data visualization tool Venn (*http://www.ehbio.com/test/venn*) was employed. As shown in Figure 5, each of the four machine learning models was able to screen out approximately 100 compounds from the prediction database, among which 42 compounds listed in Table S4 (*https://www.ddtjournal.com/action/getSupplementalData.php?ID=261*) were obtained as the intersection of the four models eventually. In general, the 42 compounds that have been identified simultaneously by the four different classification models tend to have a higher probability of being active against SARS-CoV-2 PLpro. The current strategy that taking the intersection of multiple model predictions can reduce the probability of false positives, and further improve the efficiency of drug discovery.

3.3. Molecular simulation-based compound assessment

After screening out the compounds with potential inhibitory activity, molecular docking-based binding affinity evaluation was employed to obtain the compounds with high inhibitory activity targeting SARS-CoV-2 PLpro. Reliability evaluation of the molecular docking protocol used in the present study was performed in the first instance. As displayed in Figure S1 (*https://www.ddtjournal.com/action/getSupplementalData.php?ID=261*), the redocked binding conformations of the two ligands (GRL0617 and Jun12682) were consistent with their original conformations in the co-crystal structures, namely, the molecular docking protocol adopted in the present study can describe the ligand-protein interactions precisely. Subsequently, binding affinities of the 42 compounds screened from

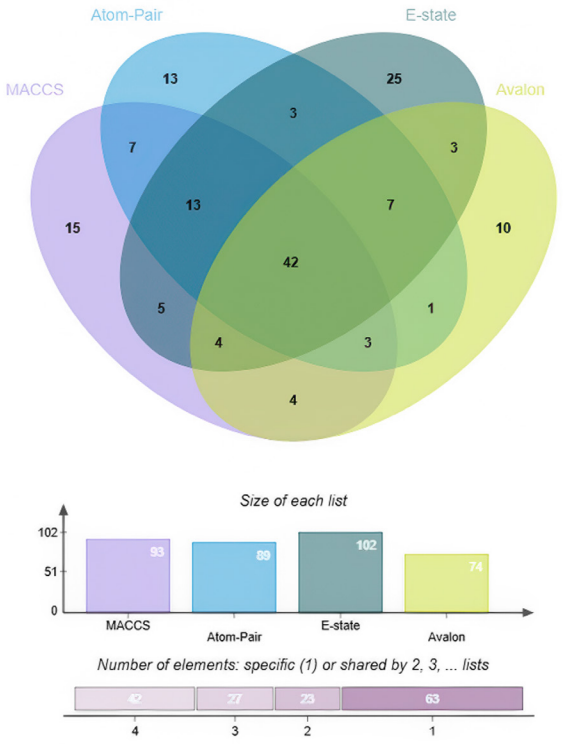

Figure 5. Interactive Venn diagrams for the intersection of multiple model predictions.

the machined learning-based classification models were calculated through molecular docking. Fifteen compounds were identified with high inhibitory activity compared with GRL0617, however, no compound was found to be more potent than Jun12682 (binding affinity data were listed in Table S4 (*https://www.ddtjournal.com/action/getSupplementalData.php?ID=261*), and the fifteen compounds were renamed as Cpd-1~15 for convenience in Figure S1 (*https://www.ddtjournal.com/action/getSupplementalData.php?ID=261*).

Considering that the target binding affinity of some compounds (such as Cpd-1, -9.38 kcal/mol) was very close to that of Jun12682 (-9.57 kcal/mol), we further employed a dynamic evaluation method based on molecular dynamics (MD) simulation to provide more accurate assessments on the potential inhibitory activity of the fifteen compounds. A total of 18 systems that contained Cpd-1~15, the two positive compounds GRL0617 and Jun12682, as well as the apo form of the target protein, were simulated through the MD simulation. Confirmed by the root mean square deviation (RMSD), all systems reached the equilibrium state within 100 ns MD simulation (Figure S2, *https://www.ddtjournal.com/action/getSupplementalData.php?ID=261*). The target binding free energies of Cpd-1~15, GRL0617, and Jun12682 were calculated based on the MM/GBSA method and demonstrated in Figure S3 (*https://www.ddtjournal.com/action/getSupplementalData.php?ID=261*). Under the more accurate evaluation method, only 7 compounds (Cpd-1~4, Cpd-6, Cpd-8, Cpd-14) revealed superior target binding ability than GRL0617, which was significantly different from the result with a molecular docking-based evaluation approach. Surprisingly, Cpd-1 and Cpd-3 exhibited dramatically high target binding ability, suggesting their potential as more potent inhibitors than the current best-performing SARS-CoV-2 PLpro inhibitor Jun12682.

3.4. Analysis of ligand-receptor interactions

Figure 6A displays the decomposition of the binding free energy of the seven highly active compounds and the two positive compounds to the target. Apparently, the gas-phase energy component (ΔG_{gas}) is the prime contributor to binding free energy (ΔG_{bind}). Compounds with more tight binding to the target (Cpd-1~3 and Jun12682 with lower ΔG_{bind}) possess significantly low ΔG_{gas} (about -150 kcal/mol for Cpd-1~3 *vs.* about -70 kcal/mol for others). According to the computational principle, ΔG_{gas} consists of van der Waals (ΔE_{vdw}) and electrostatic (ΔE_{ele}) terms. Values of the two terms for these compounds are both correlated with the trend of final ΔG_{bind}. Nevertheless, the differences of ΔE_{ele} term for all the 9 compounds are apparently higher than those of ΔE_{vdw} (-16.66~-117.34 kcal/mol for ΔE_{ele} and -31.84~-54.60 kcal/mol for ΔE_{vdw}), indicating that the electrostatic interactions are critical for the ligand binding to the target.

Further ligand-protein interaction analysis was performed to present more detailed descriptions of the binding pattern of the screened compounds with SARS-CoV-2 PLpro. As shown in Figure 6B, all the nine compounds bind to the binding site through some polar interactions such as hydrogen bonds and π–π interactions. Especially, these interactions are extremely abundant in the binding pattern of highly active compounds to the target, which could be a reasonable explanation on the critical role of electrostatic interactions to the ligand binding. For the binding site in target protein, the aromatic side chain of Tyr268 provides CH–π or π–π interactions with most compounds, and Asp164 and Gln269 are conserved in the hydrogen bond interactions of almost all compounds. Additional hydrogen bond occupancy analysis also suggested the pivotal role of these polar residues in ligand binding (Table S5, *https://www.ddtjournal.com/action/getSupplementalData.php?ID=261*). In particular, Asp302 shows the same binding area as Asp164 as revealed in Figure 6B, contributes a hydrogen bond occupancy of 104.98% in the binding pattern of Cpd-1, and Asp164 donates as high as 179.52% in the binding pattern of Cpd-3. The total hydrogen bond occupancy related to Cpd-1 and Cpd-3 was significantly higher than that of Jun12682 and GRL0617, demonstrating again the superior target binding ability of Cpd-1 and Cpd-3.

3.5 Identification of key residues on ligand binding

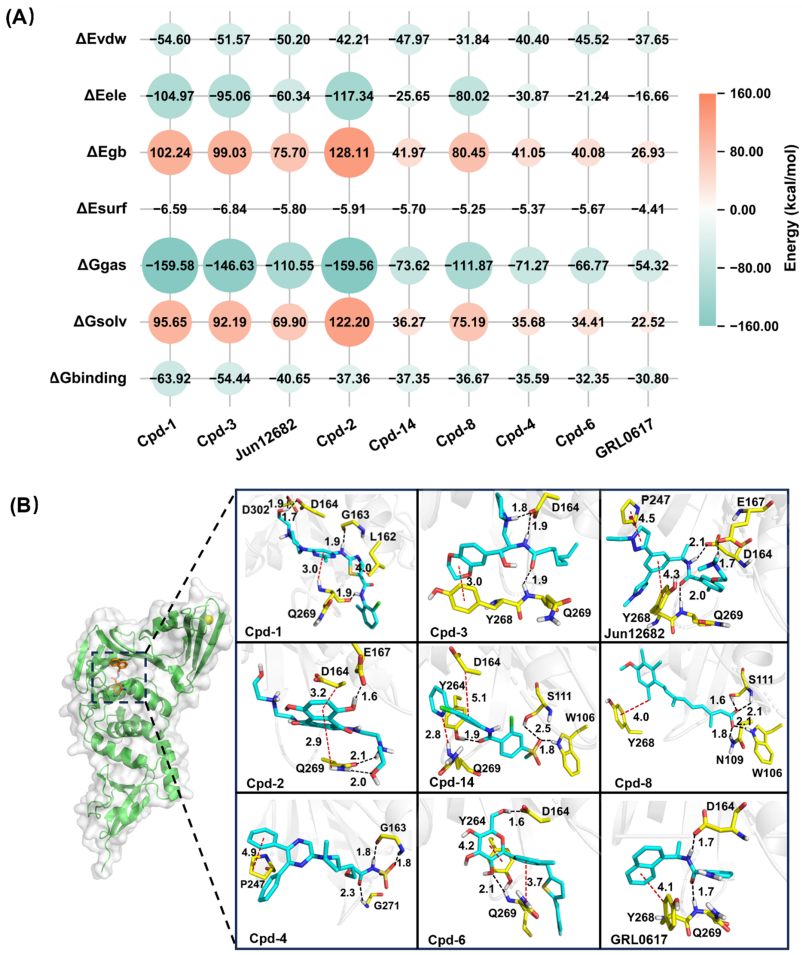

Figure 6. (A) Decomposition of binding free energy (kcal/mol) for the nine compounds. **(B)** Binding modes of the nine compounds in the binding site of SARS-CoV-2 PLpro. Ligands and key residues are shown with cyan and yellow stick models, respectively. Hydrogen bonds are represented by black dashed lines, π–π and CH–π interactions are represented by red dashed lines.

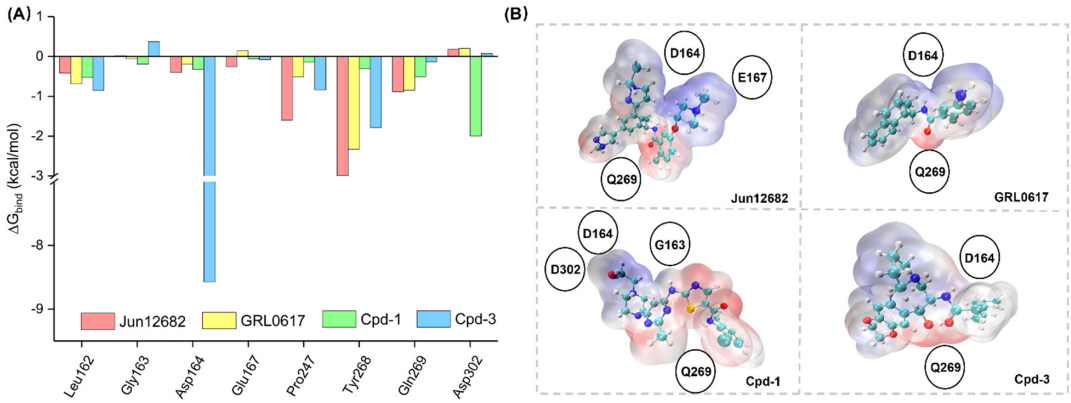

Figure 7. (A) Binding free energy contributions of some key residues in the four ligand-receptor binding systems. **(B)** Surface electrostatic potential maps of the four compounds in binding conformations. Electron-deficient and electron-rich regions are colored in blue and red, respectively. Some key residues around them are highlighted in circles.

For a more detailed presentation, binding free energy contributions of some crucial residues in the four ligand-receptor binding systems were calculated and displayed in Figure 7A. Results indicate that most of these residues make favorable contributions to the ligand binding, among which Tyr268 makes significant and conserved contributions to the four compounds. Notably, the contribution of Asp164 on the binding of Cpd-3 is dramatically high among all residues, and Asp302 provides a remarkable contribution to the binding of Cpd-1. The residue binding free energy contributions are consistent with the distributions of hydrogen bond

occupancy aforementioned, which highlights the significance of these polar residues in ligand binding, and also provides reasonable explanations for the high target binding free energy of Cpd-1 and Cpd-3.

Figure 7B illustrates the surface electrostatic potentials of the four compounds in the specific conformation when binding to SARS-CoV-2 PLpro. Apparently, some electronegative residues, like Asp164, Glu167, and Asp302, are situated around the electron-deficient region of the ligand, and Gln269 is close to the electron-rich region. Such an electrical matching mode can disperse the charge and provide a favorable ligand-protein binding pattern. In summary, the favorable electrostatic potential contributions of the key residues would provide valuable insights for the development of more potent and highly selective SARS-CoV-2 PLpro inhibitors.

4. Discussion

The current study highlights the significance of targeting the protease PLpro in the development of COVID-19 therapeutics, given the rapid mutation and widespread transmission of SARS-CoV-2. While some candidates, such as GRL0617 and its analogs, have shown weak to moderate *in vitro* potency, they often suffer from limitations that hinder clinical translation, such as insufficient antiviral activity and metabolic stability *in vitro* and *in vivo* (*32*), poor pharmacokinetic performance (*33*), limited selectivity (*34*), or toxicity concerns (*35*). To overcome these limitations, we employed an integrated screening strategy combining machine learning and molecular simulation approaches, which led to the identification of seven promising PLpro inhibitors (Cpd-1~4, Cpd-6, Cpd-8, and Cpd-14). Among them, Cpd-1 and Cpd-3 exhibited the strongest binding affinities and inhibitory potential against PLpro, making them prime candidates for further experimental validation. In addition, we identified several key residues critical for ligand binding, which may inform future optimization efforts aimed at enhancing potency and selectivity.

Although the present findings are promising, they merely represent initial steps towards drug development. To verify the reliability and therapeutic potential of the identified compounds, extensive experimental validation is still required. In this study, we employed a series of molecular simulation techniques—including molecular docking and molecular dynamics simulations—to assess the binding stability of candidate inhibitors with SARS-CoV-2 PLpro. While such computational strategies are highly valuable for identifying promising drug candidates (*36*), their outcomes must be substantiated by experimental data. Therefore, future research will focus on enzymatic assays and cell-based antiviral evaluations to confirm the inhibitory activity and antiviral efficacy of the screened compounds, thereby facilitating their further advancement toward clinical application.

In conclusion, our study contributes to overcoming the limitations that hinder clinical translation in two key ways. First, the integration of machine learning and molecular simulations offers an efficient framework for identifying structurally novel and potentially more drug-like inhibitors. Second, our residue-level interaction analysis provides mechanistic insights that may guide further lead optimization to improve target specificity and binding stability. While experimental validation is still required, our findings offer a solid foundation for the rational development of next-generation PLpro inhibitors. The candidate compounds and structural insights reported here may help accelerate the development of effective antivirals targeting SARS-CoV-2 and its evolving variants.

Supporting Information

Detailed information on molecular fingerprints (Table S1), performance of classification models in internal validation (Table S2) and external validation (Table S3). Molecular docking scores of the 42 compounds from intersection of the four optimal machine learning models (Table S4), hydrogen bond occupancy analysis of the polar residues involved in ligand binding (Table S5). Redock analysis and docking scores of the screened compounds (Figure S1), RMSD of the 18 MD simulated systems (Figure S2), and binding free energy of the top 15 compounds (Figure S3). (*https://www.ddtjournal.com/action/getSupplementalData.php?ID=261*)

Lists of the initial database (Supplementary Materials 1), training set (Supplementary Materials 2), external validation set (Supplementary Materials 3), and prediction dataset (Supplementary Materials 4) used in the machine learning models. (*https://www.ddtjournal.com/action/getSupplementalData.php?ID=262*)

Funding: This work was supported by research grants of Natural Science Foundation of Shandong Province (ZR2024QH448), the Key Program of Brain Science and Technology (STI2030-Major Projects 2021ZD0202900) and Key Project by Qingdao Bureau of Sciences and Technology (22-3-3-HYGG-25-HY).

Conflict of Interest: The authors have no conflicts of interest to disclose.

References

1. Zhu C, Pang S, Liu J, Duan Q. Current Progress, Challenges and prospects in the development of COVID-19 vaccines. Drugs. 2024; 84:403-423.
2. Kaku Y, Uriu K, Kosugi Y, Okumura K, Yamasoba D, Uwamino Y, Kuramochi J, Sadamasu K, Yoshimura K, Asakura H, Nagashima M, Ito J, Sato K. Virological characteristics of the SARS-CoV-2 KP.2 variant. Lancet Infect Dis. 2024; 24:e416.

3. Yang H, Rao Z. Structural biology of SARS-CoV-2 and implications for therapeutic development. Nat Rev Microbiol. 2021; 19:685-700.
4. Shin D, Mukherjee R, Grewe D, *et al*. Papain-like protease regulates SARS-CoV-2 viral spread and innate immunity. Nature. 2020; 587:657-662.
5. Protić S, Crnoglavac Popović M, Kaličanin N, Prodanović O, Senćanski M, Milićević J, Stevanović K, Perović V, Paessler S, Prodanović R, Glišić S. SARS-CoV-2 PLpro inhibition: evaluating *in silico* repurposed fidaxomicin's antiviral activity through *in vitro* assessment. ChemistryOpen. 2024; 13:e202400091.
6. Freitas BT, Durie IA, Murray J, Longo JE, Miller HC, Crich D, Hogan RJ, Tripp RA, Pegan SD. Characterization and noncovalent inhibition of the deubiquitinase and deISGylase activity of SARS-CoV-2 papain-like protease. ACS Infect Dis. 2020; 6:2099-2109.
7. Shen Z, Ratia K, Cooper L, Kong D, Lee H, Kwon Y, Li Y, Alqarni S, Huang F, Dubrovskyi O, Rong L, Thatcher G, Xiong R. Design of SARS-CoV-2 PLpro Inhibitors for COVID-19 Antiviral Therapy Leveraging Binding Cooperativity. J Med Chem. 2022; 65:2940-2955.
8. Tan B, Zhang X, Ansari A, Jadhav P, Tan H, Li K, Chopra A, Ford A, Chi X, Ruiz FX, Arnold E, Deng X, Wang J. Design of a SARS-CoV-2 papain-like protease inhibitor with antiviral efficacy in a mouse model. Science. 2024; 383:1434-1440.
9. Xu Y, Chen K, Pan J, Lei Y, Zhang D, Fang L, Tang J, Chen X, Ma Y, Zheng Y, Zhang B, Zhou Y, Zhan J, Xu W. Repurposing clinically approved drugs for COVID-19 treatment targeting SARS-CoV-2 papain-like protease. Int J Biol Macromol. 2021; 188:137-146.
10. Cho CC, Li SG, Lalonde TJ, Yang KS, Yu G, Qiao Y, Xu S, Ray Liu W. Drug repurposing for the SARS-CoV-2 papain-like protease. ChemMedChem. 2022; 17:e202100455.
11. Srinivasan V, Brognaro H, Prabhu PR, *et al*. Antiviral activity of natural phenolic compounds in complex at an allosteric site of SARS-CoV-2 papain-like protease. Commun Biol. 2022; 5:805.
12. Zhao Y, Du X, Duan Y, *et al.* High-throughput screening identifies established drugs as SARS-CoV-2 PLpro inhibitors. Protein Cell. 2021; 12:877-888.
13. Weglarz-Tomczak E, Tomczak JM, Talma M, Burda-Grabowska M, Giurg M, Brul S. Identification of ebselen and its analogues as potent covalent inhibitors of papain-like protease from SARS-CoV-2. Sci Rep. 2021; 11:3640.
14. Sargsyan K, Lin CC, Chen T, Grauffel C, Chen YP, Yang WZ, Yuan HS, Lim C. Multi-targeting of functional cysteines in multiple conserved SARS-CoV-2 domains by clinically safe Zn-ejectors. Chem Sci. 2020; 11:9904-9909.
15. Yi Y, Zhang M, Xue H, *et al.* Schaftoside inhibits 3CLpro and PLpro of SARS-CoV-2 virus and regulates immune response and inflammation of host cells for the treatment of COVID-19. Acta Pharm Sin B. 2022; 12:4154-4164.
16. Kuo CJ, Chao TL, Kao HC, Tsai YM, Liu YK, Wang LH, Hsieh MC, Chang SY, Liang PH. Kinetic characterization and inhibitor screening for the proteases leading to identification of drugs against SARS-CoV-2. Antimicrob Agents Chemother. 2021; 65:e02577-20.
17. Yu W, Zhao Y, Ye H, Wu N, Liao Y, Chen N, Li Z, Wan N, Hao H, Yan H, Xiao Y, Lai M. Structure-Based Design of a Dual-Targeted Covalent Inhibitor Against Papain-like and Main Proteases of SARS-CoV-2. J Med Chem. 2022; 65:16252-16267.
18. Rut W, Lv Z, Zmudzinski M, Patchett S, Nayak D, Snipas SJ, El Oualid F, Huang TT, Bekes M, Drag M, Olsen SK. Activity profiling and crystal structures of inhibitor-bound SARS-CoV-2 papain-like protease: a framework for anti-COVID-19 drug design. Sci Adv. 2020; 6:eabd4596.
19. Li Y, Li L, Wang S, Tang X. EQUIBIND: A geometric deep learning-based protein-ligand binding prediction method. Drug Discov Ther. 2023; 17:363-364.
20. Boby ML, Fearon D, Ferla M, *et al*. Open science discovery of potent noncovalent SARS-CoV-2 main protease inhibitors. Science. 2023; 382:eabo7201.
21. Garnsey MR, Robinson MC, Nguyen LT, *et al.* Discovery of SARS-CoV-2 papain-like protease (PLpro) inhibitors with efficacy in a murine infection model. Sci Adv. 2024; 10:eado4288.
22. Zhao J, Shi X, Wang Z, Xiong S, Lin Y, Wei X, Li Y, Tang X. Hepatotoxicity assessment investigations on PFASs targeting L-FABP using binding affinity data and machine learning-based QSAR model. Ecotoxicol Environ Saf. 2023; 262:115310.
23. Wei X, Liu N, Feng Y, Wang H, Han W, Zhuang M, Zhang H, Gao W, Lin Y, Tang X, Zheng Y. Competitive-like binding between carbon black and CTNNB1 to ΔNp63 interpreting the abnormal respiratory epithelial repair after injury. Sci Total Environ. 2024; 929:172652.
24. Hu H, Wang Q, Su H, Shao Q, Zhao W, Chen G, Li M, Xu Y. Identification of cysteine 270 as a novel site for allosteric modulators of SARS-CoV-2 papain-like protease. Angew Chem. 2022; 61:e202212378.
25. Li Y, Wang Z, Ma S, Tang X, Zhang H. Chemical space exploration and machine learning-based screening of PDE7A inhibitors. Pharmaceuticals. 2025; 18:444
26. Trott O, Olson AJ. AutoDock Vina: improving the speed and accuracy of docking with a new scoring function, efficient optimization, and multithreading. J Comput Chem. 2010; 31:455-461.
27. Duan Y, Wu C, Chowdhury S, Lee MC, Xiong G, Zhang W, Yang R, Cieplak P, Luo R, Lee T, Caldwell J, Wang J, Kollman P. A point-charge force field for molecular mechanics simulations of proteins based on condensed-phase quantum mechanical calculations. J Comput Chem. 2003; 24:1999-2012.
28. Jorgensen WL, Chandrasekhar J, Madura JD, Impey RW, Klein ML. Comparison of simple potential functions for simulating liquid water. J Chem Phys. 1983; 79:926-935.
29. Bayly CI, Cieplak P, Cornell W, Kollman PA. A well-behaved electrostatic potential based method using charge restraints for deriving atomic charges: the RESP model. J Phys Chem. 1993; 97:10269-10280.
30. Ryckaert J-P, Ciccotti G, Berendsen HJC. Numerical integration of the cartesian equations of motion of a system with constraints: molecular dynamics of n-alkanes. J Comput Phys. 1977; 23:327-341.
31. Genheden S, Ryde U. The MM/PBSA and MM/GBSA methods to estimate ligand-binding affinities. Expert Opin Drug Discov. 2015; 10:449-461.
32. Velma GR, Shen Z, Holberg C, *et al.* Non-covalent inhibitors of SARS-CoV-2 papain-like protease (PLpro): *in vitro* and *in vivo* antiviral activity. J Med Chem. 2024; 67:13681-13702.
33. Garnsey MR, Robinson MC, Nguyen LT, *et al.* Discovery of SARS-CoV-2 papain-like protease (PLpro) inhibitors with efficacy in a murine infection model. Sci Adv. 2024; 10:eado4288.

34. Zmudzinski M, Rut W, Olech K, *et al.* Ebselen derivatives inhibit SARS-CoV-2 replication by inhibition of its essential proteins: PLpro and Mpro proteases, and nsp14 guanine N7-methyltransferase. Sci Rep. 2023; 13:9161.
35. Hu H, Wang Q, Su H, Shao Q, Zhao W, Chen G, Li M, Xu Y. Identification of cysteine 270 as a novel site for allosteric modulators of SARS-CoV-2 papain-like protease. Angew Chem Int Ed Engl. 2022; 61:e202212378.
36. Li Z, Li X, Huang YY, *et al.* Identify potent SARS-CoV-2 main protease inhibitors *via* accelerated free energy perturbation-based virtual screening of existing drugs. Proc Natl Acad Sci U S A. 2020; 17:27381-27387.

Received April 16, 2025; Revised May 21, 2025; Accepted June 22, 2025.

**Address correspondence to:*
Yongxin Bao, Qingdao Women and Children's Hospital Affiliated to Qingdao University, Qingdao 266034, China.
E-mail: byx285788575@163.com

Xiaowen Tang, School of Pharmacy, and Shandong Provincial Key Laboratory of Pathogenesis and Prevention of Brain Diseases, Qingdao University, Qingdao 266071, China.
E-mail: xwtang1219@qdu.edu.cn

Released online in J-STAGE as advance publication June 27, 2025.

Original Article

DOI: 10.5582/ddt.2025.01022

Trpa1 knockout favors colon tumorigenesis in dextran sulfate sodium (DSS)-induced colitis mice

Fangzhou Dou[1], Shasha Hu[2], Daoran Lu[1], Jianjun Gao[1,*]

[1] Department of Pharmacology, School of Pharmacy, Qingdao University, Qingdao, Shandong, China;
[2] Department of Pathology, The affiliated Hospital of Qingdao University, Qingdao, Shandong, China.

SUMMARY: Chronic inflammation in the colon has been recognized as a key pathogenic mechanism driving colorectal cancer development. TRPA1 (transient receptor potential ankyrin 1), a key member of the TRP cation channel superfamily, is closely implicated in inflammatory processes and has emerged as a promising therapeutic target for anti-inflammatory drug development. However, the precise role of TRPA1 in colorectal carcinogenesis and its potential as a therapeutic target for colorectal cancer (CRC) remain incompletely understood. In this study, we demonstrate that *Trpa1* knockout significantly exacerbates DSS-induced colitis-associated tumorigenesis in murine models, a phenomenon mechanistically linked to *Trpa1* deficiency-mediated aggravation of inflammatory bowel pathology. RNAseq and gene knockout effect analysis revealed a consistently low expression pattern of *TRPA1* across colorectal cancer cell lines (n = 58, median log2(TPM+1) = 0.025), with limited impact on cell viability upon *TRPA1* knockout. Notably, analysis of human clinical specimens revealed substantial downregulation of TRPA1 expression in CRC compared to adjacent normal tissues. Kaplan-Meier survival analysis further indicated that patients with TRPA1-low tumors exhibited significantly poorer overall survival outcomes. These collective data suggest a tumor-suppressive role for TRPA1 in colorectal carcinogenesis, potentially through its immunomodulatory functions within the colitis-cancer transformation axis.

Keywords: TRPA1, colitis, colon cancer, CRC, carcinogenesis, DSS

1. Introduction

Colorectal cancer (CRC), a gastrointestinal malignant tumor, poses a severe threat to global human health. Epidemiological studies reveal CRC currently ranks as the third most commonly diagnosed cancer and the second leading cause of cancer-related mortality worldwide (*1,2*). According to the 2020 Global Cancer Statistics report, approximately 1.93 million new CRC cases and 0.94 million related deaths were recorded globally, accounting for nearly 10% and 9.4% of total cancer incidence and fatalities respectively (*3,4*). These epidemiological patterns underscore the critical need for elucidating the underlying pathogenesis of CRC, which holds paramount importance for developing effective prevention strategies and therapeutic interventions.

The pathogenesis of CRC stems from a complex interplay between genetic susceptibility, modifiable lifestyle factors (particularly alcohol use, red meat consumption, and obesity), and comorbidities including inflammatory bowel disease (IBD) and diabetes mellitus (*3,5,6*). Compelling epidemiological evidence indicates a particularly strong association between IBD and CRC susceptibility, with IBD patients (encompassing both ulcerative colitis and Crohn's disease) exhibiting 2-3-fold elevated CRC risk compared to the general population (*7-9*). Emerging evidence reveals that the persistent inflammatory milieu facilitates carcinogenesis through dysregulated activation of cytokine/chemokine networks and immune cell populations, collectively orchestrating tumor initiation, progression, and metastasis – a pathological continuum formally designated as the "inflammation-cancer transformation" (*10*). Systematic investigation into the molecular mechanisms underlying chronic inflammation-driven malignant transformation of colonic epithelial cells is imperative for advancing our understanding of CRC tumorigenesis and progression.

TRPA1 (transient receptor potential ankyrin 1), a pivotal member of the TRP cation channel superfamily, exhibits distinctive homotetrameric architecture with six transmembrane domains, enabling its remarkable capacity to integrate multimodal exogenous stimuli ranging from thermal fluctuations to chemical irritants and mechanical stress (*11,12*). This polymodal

receptor demonstrates endogenous activation through inflammatory mediators such as bradykinin and trypsin (*13*). Mechanistically, TRPA1 drives calcium influx to potentiate the release of neuropeptides (*e.g.*, substance P) and pro-inflammatory cytokines (*e.g.*, IL-6, TNF-α), thereby enhancing nociceptor sensitization through autocrine/paracrine signaling pathways (*14*). These pathophysiological insights not only underscore the central regulatory role of TRPA1 in inflammatory pain transduction but also identify it as a promising therapeutic target for the development of analgesic and anti-inflammatory drugs (*15-17*). However, the precise role of TRPA1 in colorectal carcinogenesis remains incompletely understood, and its potential as a therapeutic target for colon cancer requires further validation.

In this study, we utilized *Trpa1* knockout ($Trpa1^{-/-}$) mice to investigate the role of this molecule in inflammation-driven colorectal carcinogenesis and assessed the impact of *TRPA1* genetic ablation on colorectal cancer cell survival. Additionally, by analyzing TRPA1 expression in human CRC tissues and its correlation with patient prognosis, we comprehensively analyzed the role of this molecule in the pathology of CRC.

2. Materials and Methods

2.1. Agents and animals

DSS (molecular weight: 40,000) and azoxymethane (AOM) were purchased from Shanghai Aladdin Biochemical Technology Co., Ltd. (Shanghai, China). $Trpa1^{+/-}$ C57BL/6N mice were purchased from Cyagen Biosciences Co., Ltd. (Jiangsu, China). The $Trpa1^{-/-}$ and wild type C57BL/6N mice used in the experiment were bred from the above-mentioned heterozygous mice. All experimental animals were housed in a specific pathogen-free environment, and the mice had free access to water and food. All experimental procedures strictly adhered to international guidelines for the care and use of laboratory animals.

2.2. The model of inflammation-tumor transformation

Female wild-type and $Trpa1^{-/-}$ C57BL/6N mice (7-8-week-old) were utilized in this study. Animals were divided into three groups based on genotype and treatment protocols: (1) wild-type control group (NC group, n = 5), receiving intraperitoneal injection of an equivalent volume of saline; (2) wild-type DSS-treated group (WT+DSS group, n = 11); and (3) $Trpa1^{-/-}$ DSS-treated group ($Trpa1^{-/-}$+DSS group, n = 9). The latter two groups were intraperitoneally injected with 10 mg/kg body weight of azoxymethane (AOM) for chemical induction on day 0 of the experiment. Starting from day 5, the WT+DSS and $Trpa1^{-/-}$+DSS groups were subjected to cyclic intervention with 1% DSS solution and sterile drinking water (Figure 1A), establishing a chronic colitis model through intermittent DSS exposure. The NC group received sterile drinking water throughout the experimental period. Body weight was monitored every 3 days, and the characteristics of the feces and the presence of blood in the stool were recorded regularly.

At the experimental endpoint, mice were sacrificed, and colonic tissues were fully dissected. The length from the anorectal junction to the cecal base was measured, and macroscopic tumor nodules were counted under a dissecting microscope. Colon tissue samples were fixed in 4% paraformaldehyde, followed by paraffin embedding, sectioning, and hematoxylin-eosin (HE) staining for histopathological analysis.

2.3. The model of subacute colitis

This study utilized 7-8-week-old female C57BL/6N mice, including wild-type and $Trpa1^{-/-}$ strains. Animals were divided into three groups based on genotype and treatment protocols: wild-type control group (NC group, n = 8), wild-type DSS-treated group (WT+DSS group, n = 8), and $Trpa1^{-/-}$ DSS-treated group ($Trpa1^{-/-}$+DSS group, n = 8). The experimental protocol comprised two phases: 1% DSS solution was administered *via* free drinking water from days 0-30, followed by 1.5% DSS solution from days 31-42. Control animals received sterile drinking water throughout the 42-day period.

Systematic monitoring was conducted every three days, encompassing body weight measurement and fecal consistency assessment, with disease severity quantified using the Disease Activity Index (DAI). Post-sacrificed, colonic specimens were collected. Colon length was measured from the anorectal junction to the cecal base, and histopathological analyses were performed on colonic tissues, including HE staining, Alcian blue (AB) staining, and periodic acid-Schiff (PAS) staining.

2.4. Histopathological analyses

Histochemical staining of murine colonic tissues, including HE, AB, and PAS, was performed using Solarbio (Beijing, China) kits. Tissue sections were dewaxed in xylene and rehydrated through a graded ethanol series (100%, 95%, 80%, 70%) prior to staining. For HE, sections were stained with Mayer's hematoxylin for 5 min, differentiated in 0.5% acid-alcohol for 2-5 sec, rinsed in running water for 20 min for nuclear bluing, and counterstained with 1% aqueous eosin Y for 1 min. AB staining involved 3% acetic acid pretreatment (3 min), incubation with 1% Alcian blue 8GX (in 3% acetic acid) in a humid chamber (30 min, RT), followed by three 1-min distilled water rinses and Nuclear Fast Red counterstaining (5 min). PAS staining protocol comprised

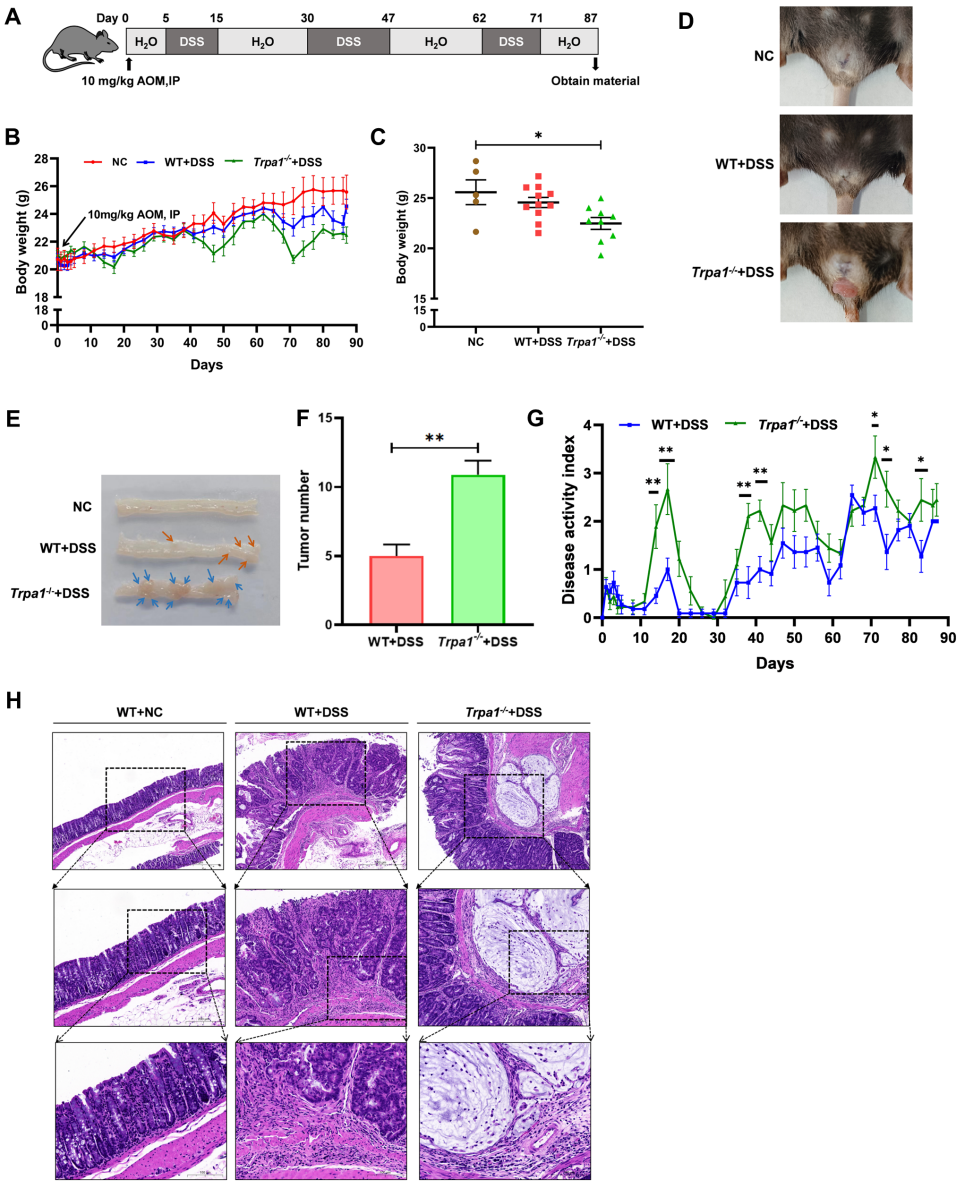

Figure 1. ***Trpa1*** **deficiency promotes colitis-associated tumorigenesis in mice.** Colitis-associated tumorigenesis model was established by intraperitoneal injection of 10 mg/kg AOM followed by DSS induction. The NC group received saline injection and drank sterile drinking water, while the WT+DSS and *Trpa1*$^{-/-}$+DSS groups were injected with AOM and alternately administered 1% DSS and drinking water. (**A**) Schematic diagram for the establishment of the AOM/DSS-induced colitis-associated tumorigenesis model. (**B**) Body weight changes of mice in each group during the experiment. (**C**) Comparison of body weight differences among groups before sacrifice. (**D**) Representative images of anal changes in mice from each group. (**E** and **F**) The number of colonic tumors in each group. (**G**) DAI scores of model mice. (**H**) HE staining of colonic tissues from the AOM/DSS-induced tumorigenesis model, with magnifications of 100×, 200×, and 400× from top to bottom. *$p < 0.05$, **$p < 0.01$.

oxidation with 1% periodic acid (5-8 min), Schiff reagent incubation (15 min, dark), and Gill's hematoxylin nuclear staining (1-2 min) with acid-alcohol differentiation. All sections were dehydrated through an ethanol-xylene gradient, mounted with neutral resin, air-dried, and digitally imaged using a 3DHISTECH (Hungary) panoramic scanner at 20× magnification.

2.5. Analysis of TRPA1 expression and gene knockout effects in CRC cells

This study leveraged the DepMap Public 24Q2 dataset to analyze RNA-seq profiles and CRISPR-Cas9 knockout screening data targeting TRPA1, with cell viability metrics quantified from CRC cell lines (*18*). Utilizing Python (v3.12.2), data preprocessing and integration were performed with pandas, followed by matrix operations executed *via* numpy. Pearson correlation coefficients and their statistical significance between TRPA1 expression levels and post-knockout cell viability scores were calculated using scipy.stats. Data visualization was implemented through matplotlib.pyplot to generate scatter plots illustrating gene expression-phenotypic effect correlations.

2.6. Analysis of TRPA1 expression in CRC tissues and prognosis of patients

TCGA database was utilized for RNA sequencing data and clinical information about CRC. R-4.4.3-win were employed for the following data analysis. Analysis was performed using the limma package to identify differential expression of TRPA1 between cancer tissues and matched adjacent normal tissues. Visualization of TRPA1 expression patterns was achieved through ggplot2 and ggpubr packages, generating scatter plots and paired boxplots comparing tumor-normal pairs. The CRC cohort was stratified into high- and low-expression subgroups based on median TRPA1 expression levels. Kaplan-Meier survival analysis with log-rank testing (implemented *via* survival and survvminer packages) evaluated the correlation between TRPA1 expression and overall survival (OS).

2.7. Statistical analyses

The animal experimental data were visualized using GraphPad Prism 8.0. Pathological section images were captured and exported *via* SlideViewer software after scanning with a panoramic tissue cell scanner, and colonic goblet cells were counted using ImageJ. Statistical differences were analyzed *via* One-way ANOVA or *t*-test in SPSS. Data are shown as the mean ± standard error of the mean (Mean ± SEM). Statistical significance was defined as $p < 0.05$.

3. Results

3.1. *Trpa1* knockout favors colorectal tumorigenesis in mice with colitis

As outlined in Figure 1A, we successfully established an AOM/DSS-induced mouse model of colitis-associated tumorigenesis. During the experimental period, both WT+DSS and *Trpa1*$^{-/-}$+DSS groups exhibited body weight reduction compared to the control group, with *Trpa1*-knockout mice demonstrating a more pronounced weight loss trend (Figure 1B). Pre-sacrificed body weight measurements revealed that *Trpa1*$^{-/-}$+DSS mice showed 12.1±2.3% reduction compared to the NC group ($p < 0.05$) and 8.5 ± 2.4% reduction relative to the WT+DSS group (Figures 1C). Notably, severe diarrhea was observed in the *Trpa1*$^{-/-}$+DSS group as early as day 9 of the experiment, while only occasional soft stools were detected in WT+DSS group counterparts during the same period. Prolonged DSS intervention led to gradual manifestation of intestinal hemorrhage symptoms in both groups. By the experimental endpoint, rectal prolapse was observed in 22% of *Trpa1*$^{-/-}$+DSS mice, a pathological phenotype completely absent in the WT+DSS group (Figure 1D). Anatomical analysis demonstrated a significantly increased tumor burden in *Trpa1*-deficient mice, with the mean tumor count (10.9 ± 1.0 *vs* 5.0 ± 0.8) being markedly higher than that in the wild-type model group ($p < 0.01$) (Figures 1E-1F). Additionally, these animals exhibited colonic dilation and cecal atrophy. Quantitative DAI assessment indicated significantly elevated scores in *Trpa1*$^{-/-}$+DSS group throughout the induction period, suggesting intensified colonic inflammatory responses compared to WT+DSS group (Figure 1G).

Pathological evaluation through HE staining of colonic tissues from three experimental groups further validated differential progression in inflammation-tumor transformation. NC group maintained intact mucosal architecture with orderly arranged crypts and no pathological alterations (Figure 1H). AOM/DSS model groups universally exhibited tumor characteristics, including crypt structural destruction, glandular structural disorganization, and substantial inflammatory cell infiltration. Notably, *Trpa1*-deficient mice displayed exacerbated pathological progression. Histological analysis revealed mucinous vacuole formation in 44.4% of *Trpa1*$^{-/-}$+DSS specimens, suggesting the potential formation of mucinous adenocarcinoma (Figure 1H). These pathological features indicate that *Trpa1* gene deletion accelerates malignant progression in inflammation-associated colorectal tumor.

3.2. *TRPA1* is a non-essential gene for CRC cell survival

The above findings suggest that TRPA1 plays a critical role in tumor initiation suppression. Based on this phenotypic characteristic, we further investigated its regulatory effects on cancer cell-autonomous proliferation. Utilizing the DepMap database (2024Q2 release), we identified 58 human colorectal cancer cell lines with both whole-transcriptome sequencing data and genome-wide CRISPR-Cas9 loss-of-function screening data. Results revealed a consistently low expression pattern of *TRPA1* across colorectal cancer cell lines (median log2(TPM+1) = 0.025), with limited impact on cell viability upon *TRPA1* knockout (CRISPR scores ranging from -0.3 to 0.3, Figure 2). Furthermore, no

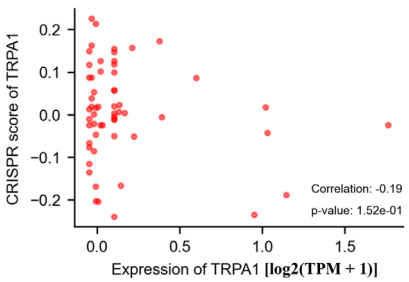

Figure 2. Correlation analysis between TRPA1 expression levels and CRISPR scores in colorectal cancer cells. Pearson correlation coefficients and their statistical significance between TRPA1 expression levels (log2(TPM+1)) and post-knockout cell viability scores were calculated.

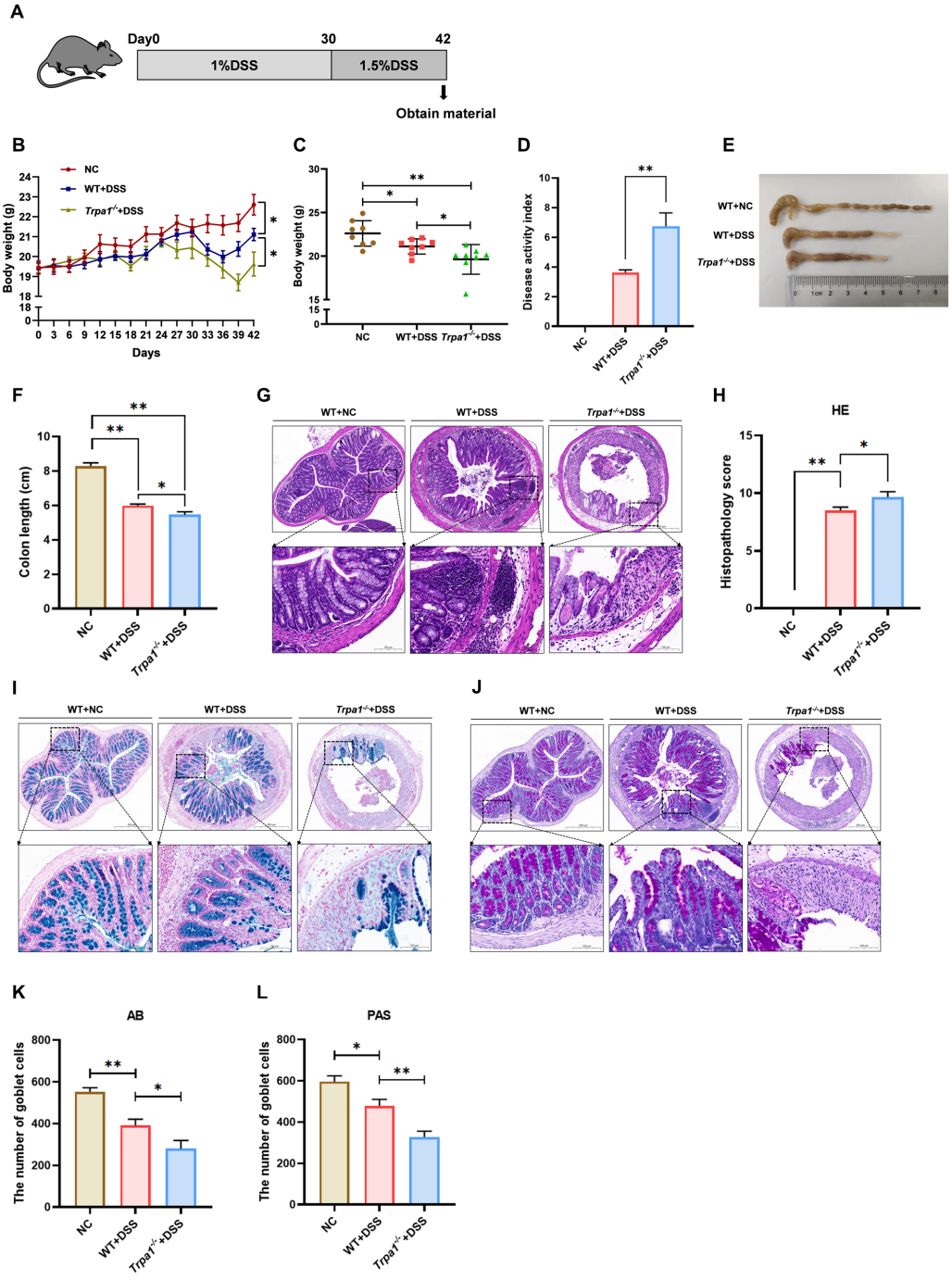

Figure 3. *Trpa1* deficiency exacerbates colitis in mice. Colitis was induced by 1%-1.5% DSS. The NC group was allowed free access to sterile drinking water, while the WT+DSS and *Trpa1*$^{-/-}$+DSS groups were given free access to 1%-1.5% DSS to induce colitis. (**A**) Schematic diagram of the DSS-induced subacute colitis model in mice. (**B**) Changes in body weight of mice in each group over time. (**C**) Comparison of body weight differences among groups before sacrifice. (**D**) Comparison of DAI scores among groups before sacrifice. (**E** and **F**) Representative images of colons in each group, as well as colon length measurement and comparison. (**G**) HE staining of colonic cross-sections from each group, with images shown at 100× and 400× magnification. (**H**) Histopathological scoring of HE-stained colonic tissues in each group. (**I and J**) Representative images of AB (I) and PAS (J) staining of colonic cross-sections from each group (100× and 400× magnification). (**K** and **L**) Quantification of goblet cells in colonic cross-sections stained with AB (K) and PAS (L) in each group. *$p < 0.05$, **$p < 0.01$.

significant correlation was observed between TRPA1 expression levels and knockout-mediated viability changes ($r = 0.19$, $p = 0.15$, Figure 2). These data indicate that *TRPA1* is unlikely to function as a core essential gene for colorectal cancer cell survival, and its tumor-suppressing effects may arise through non-cell-autonomous mechanisms, potentially involving the regulation of immune-epithelial interactions within the tumor microenvironment.

3.3. TRPA1 deficiency exacerbates DSS-induced colitis in mice

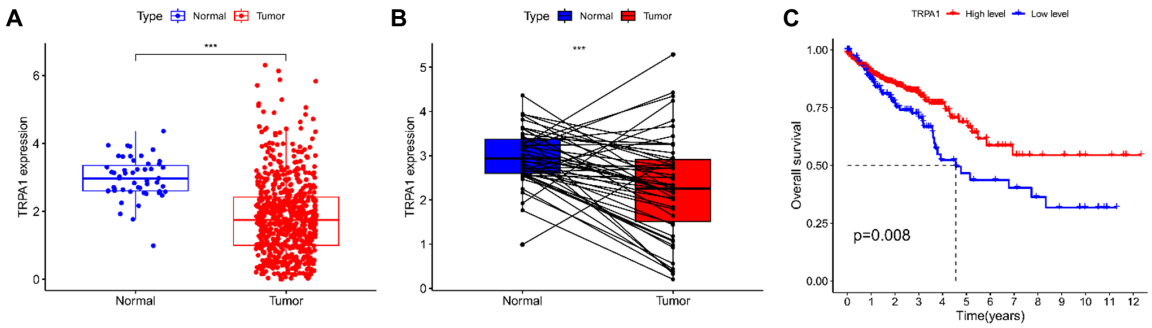

Figure 4. Clinical relevance of TRPA1 expression in CRC patients Differential expression analysis of TRPA1 in unpaired (**A**) and paired (**B**) samples from the TCGA-COAD/READ cohort. (C) Overall survival analysis between high- and low-TRPA1 expression groups. ***$p < 0.001$.

Our previous findings suggested a potential suppressive role of TRPA1 in colitis-associated tumorigenesis, while its lack of direct impact on CRC cell proliferation implies that its anti-tumorigenic effects may be mediated through inflammatory regulation. To elucidate the role of TRPA1 in colitis, we established a subacute colitis model using 1.0%-1.5% DSS-induced ulcerative colitis, following the protocol outlined by Li *et al.* (*19*) (Figure 3A). During the experimental period, NC group mice exhibited steady weight gain, normal feeding/drinking behaviors, and maintained fecal consistency. In contrast, both WT+DSS and *Trpa1*$^{-/-}$+DSS groups developed diarrhea by day 15, with *Trpa1*-deficient mice displaying earlier onset of hematochezia, reduced locomotor activity, and accelerated weight loss (Figure 3B). Terminal measurements revealed significantly lower body weight ($p < 0.05$) and elevated DAI scores ($p < 0.01$) in *Trpa1*$^{-/-}$+DSS mice compared to WT+DSS controls (Figures 3C-3D). Colonic length analysis demonstrated significant colon shortening in DSS-treated groups (Figure 3E), with *Trpa1*$^{-/-}$+DSS mice exhibiting a 8.3% greater reduction in colon length than WT+DSS counterparts (5.5±0.2 cm *vs.* 6.0±0.1 cm, $p < 0.05$; Figure 3F).

Histopathological evaluation *via* HE staining (Figure 3G) revealed distinct mucosal stratification and intact crypt architecture in NC mice. DSS-challenged groups exhibited severe epithelial damage, including crypt distortion, marked goblet cell depletion, and dense submucosal lymphocytic infiltration. Notably, *Trpa1*$^{-/-}$+DSS mice displayed exacerbated pathology characterized by near-complete epithelial denudation, lymphoid follicle formation, and a 1.2-fold increase in histological severity scores ($p < 0.05$; Figure 3H). AB/PAS staining (Figures 3I-3J) confirmed goblet cell loss across experimental groups, with *Trpa1* deficiency amplifying DSS-induced depletion (Figures 3K-3L).

These collective findings demonstrate that *Trpa1* ablation significantly aggravates DSS-driven ulcerative colitis. The amplified inflammatory milieu in *Trpa1*-deficient mice provides a mechanistic link between enhanced colitis severity and accelerated neoplastic transformation observed in prior experiments.

3.4. Clinical relevance of TRPA1 expression in CRC patients

To establish the clinical significance of TRPA1 in human colorectal carcinogenesis, we systematically analyzed its expression patterns and prognostic value using the TCGA-COAD/READ cohort ($n = 647$ tumor tissues *vs.* $n = 51$ matched adjacent normal tissues). RNA sequencing data revealed significant downregulation of TRPA1 in malignant tissues compared to non-tumor counterparts ($p < 0.001$; Figures 4A-4B). Stratification of patients by median TRPA1 expression demonstrated striking survival disparities. Kaplan-Meier analysis showed that the high-TRPA1 subgroup ($n = 324$) had significantly prolonged overall survival compared to the low-expression cohort ($n = 323$) ($p = 0.008$; Figure 4C).

These findings align with our preclinical models, collectively indicating that TRPA1 functions as a tumor suppressor in colorectal cancer pathogenesis, with its loss correlating with aggressive disease progression and poor clinical outcomes.

4. Discussion

The role of TRPA1 in CRC remains controversial. Some studies propose that TRPA1 promotes colon cancer cell proliferation by coupling with the Na^+/Ca^{2+} exchanger 1 (NCX1) to maintain calcium homeostasis (*20*). However, other research suggests that TRPA1 activation-induced Ca^{2+} influx may trigger apoptosis under specific conditions. For instance, in metastatic colorectal cancer cells, oxidative stress-activated TRPA1 mediates mitochondrial dysfunction and apoptosis (*21*). Our study investigated the role of TRPA1 in tumor initiation and progression from the perspective of inflammation-cancer transformation. Our findings demonstrated that *Trpa1* knockout exacerbated colon tumor development, with both tumor number and size increased compared to wild-type mice. Despite the limited impact of TRPA1 deletion on colorectal cancer survival, we hypothesize

that TRPA1 may indirectly suppress tumorigenesis by mitigating inflammatory responses.

The role of TRPA1 in inflammatory processes is complex. While TRPA1 is generally considered pro-inflammatory in acute settings—where its knockout or inhibition attenuates inflammation—our observations in a three-month chronic inflammation-tumor transformation model indicated more severe colonic inflammation in *Trpa1*-knockout mice compared to wild-type counterparts. This suggests a potential dichotomy in TRPA1 functionality between acute and chronic inflammatory contexts. To further clarify, we established a subacute colitis model and confirmed that TRPA1 retains its anti-inflammatory role in this system. Our previous data indicated that *Trpa1* knockout increased the proportion of Th1 cells in subacute colitis mice, thereby exacerbating inflammatory progression (data not shown). Consistent with our findings, Samuel Bertin *et al*. demonstrated that dual knockout of *IL-10* and *Trpa1* in mice resulted in significantly aggravated spontaneous colitis compared to single *IL-10* knockout controls, a phenomenon mechanistically linked to *Trpa1* deletion-driven enhancement of Th1 cell differentiation (*22*). Thus, TRPA1 may exert opposing roles in acute versus chronic colitis pathology. The tumor-promoting effects of TRPA1 deficiency likely operate indirectly by amplifying pro-inflammatory pathways that facilitate inflammation-tumor transformation in colonic epithelium.

Previous studies suggest that TRPA1 exerts a direct tumor-suppressive role in colon cancer cells, wherein its activation promotes Ca^{2+} influx, leading to tumor cell death *via* mitochondrial dysfunction and apoptosis (*21*). Thus, an alternative explanation proposes that *Trpa1* knockout exacerbates inflammatory responses (which drive inflammation-to-tumor transformation) while simultaneously eliminating TRPA1-mediated tumor cell cytotoxicity, collectively promoting colorectal tumorigenesis. However, our study revealed notably low TRPA1 expression in CRC cells, implying that its direct tumor-suppressive effects may be minimal. Instead, TRPA1 likely suppresses tumorigenesis primarily through attenuating chronic colonic inflammation.

These collective data suggest a tumor-suppressive role for TRPA1 in colorectal tumorigenesis, potentially through its immunomodulatory functions within the colitis-tumor transformation axis. The inverse relationship between TRPA1 expression and malignant features across experimental systems underscores its potential as both a prognostic biomarker and a therapeutic target for inflammation-associated colorectal malignancies.

Funding: None.

Conflict of Interest: The authors have no conflicts of interest to disclose.

References

1. Yang Y, Gao Z, Huang A, Shi J, Sun Z, Hong H, Gu J. Epidemiology and early screening strategies for colorectal cancer in China. Chin J Cancer Res. 2023; 35:606-617.
2. Huang R, Jin X, Liu Q, Bai X, Karako K, Tang W, Wang L, Zhu W. Artificial intelligence in colorectal cancer liver metastases: From classification to precision medicine. Biosci Trends. 2025; 19:150-164.
3. Sawicki T, Ruszkowska M, Danielewicz A, Niedźwiedzka E, Arłukowicz T, Przybyłowicz KE. A review of colorectal cancer in terms of epidemiology, risk factors, development, symptoms and diagnosis. Cancers. 2021; 13:1011.
4. Xi Y, Xu P. Global colorectal cancer burden in 2020 and projections to 2040. Transl Oncol. 2021; 14:101174.
5. Sandler RS. Epidemiology and risk factors for colorectal cancer. Gastroenterol Clin North Am. 1996; 25:717-735.
6. Keum N, Giovannucci E. Global burden of colorectal cancer: emerging trends, risk factors and prevention strategies. Nat Rev Gastroenterol Hepatol. 2019; 16:713-732.
7. Johnson CM, Wei C, Ensor JE, Smolenski DJ, Amos CI, Levin B, Berry DA. Meta-analyses of colorectal cancer risk factors. Cancer Causes Control. 2013; 24:1207-1222.
8. Shahgoli VK, Noorolyai S, Ahmadpour Youshanlui M, Saeidi H, Nasiri H, Mansoori B, Holmskov U, Baradaran B. Inflammatory bowel disease, colitis, and cancer: unmasking the chronic inflammation link. Int J Colorectal Dis. 2024; 39:173.
9. Sato Y, Tsujinaka S, Miura T, Kitamura Y, Suzuki H, Shibata C. Inflammatory bowel disease and colorectal cancer: Epidemiology, etiology, surveillance, and management. Cancers (Basel). 2023; 15:2634.
10. Lv J, Liu J, Chao G, Zhang S. PARs in the inflammation-cancer transformation of CRC. Clin Transl Oncol. 2023; 25:1242-1251.
11. Gustafsson AB, Dorn GW 2nd. Evolving and expanding the roles of mitophagy as a homeostatic and pathogenic process. Physiol Rev. 2019; 99:853-892.
12. Zhang M, Ma Y, Ye X, Zhang N, Pan L, Wang B. TRP (transient receptor potential) ion channel family: structures, biological functions and therapeutic interventions for diseases. Signal Transduct Target Ther. 2023; 8:261.
13. Ye W, Tu YH, Cooper AJ, Zhang Z, Katritch V, Liman ER. Activation stoichiometry and pore architecture of TRPA1 probed with channel concatemers. Sci Rep. 2018; 8:17104.
14. Talavera K, Startek JB, Alvarez-Collazo J, Boonen B, Alpizar YA, Sanchez A, Naert R, Nilius B. Mammalian transient receptor potential TRPA1 channels: From structure to disease. Physiol Rev. 2020; 100:725-803.
15. Woo J, Jang MW, Lee J, Koh W, Mikoshiba K, Lee CJ. The molecular mechanism of synaptic activity-induced astrocytic volume transient. J Physiol. 2020; 598:4555-4572.
16. Bautista DM, Pellegrino M, Tsunozaki M. TRPA1: A gatekeeper for inflammation. Annu Rev Physiol. 2013; 75:181-200.
17. Iannone LF, Nassini R, Patacchini R, Geppetti P, De Logu F. Neuronal and non-neuronal TRPA1 as therapeutic targets for pain and headache relief. Temperature (Austin). 2023; 10:50-66.

18. Current DepMap Release data, including CRISPR Screens, PRISM Drug Screens, Copy Number, Mutation, Expression, and Fusions. DepMap, Broad (2024). DepMap 24Q2 Public. Figshare+. Dataset. *https://doi.org/10.25452/figshare.plus.25880521.v1*.
19. Li J, Dou F, Hu S, Gao J. Involvement of adaptive immune responses in a model of subacute colitis induced with dextran sulfate sodium in C57BL/6 mice. Drug Discov Ther. 2023; 17:294-298.
20. Zhou L, Zhou G, Li J, Guo R, Dong H. NCX1 interacts with TRPA1 to promote cell proliferation and tumor growth of colon cancer *via* disruption of calcium homeostasis. J Adv Res. 2025; S2090-1232(25)00129-8.
21. Faris P, Rumolo A, Pellavio G, Tanzi M, Vismara M, Berra-Romani R, Gerbino A, Corallo S, Pedrazzoli P, Laforenza U, Montagna D, Moccia F. Transient receptor potential ankyrin 1 (TRPA1) mediates reactive oxygen species-induced Ca(2+) entry, mitochondrial dysfunction, and caspase-3/7 activation in primary cultures of metastatic colorectal carcinoma cells. Cell Death Discov. 2023; 9:213.
22. Bertin S, Aoki-Nonaka Y, Lee J, *et al.* The TRPA1 ion channel is expressed in CD4+ T cells and restrains T-cell-mediated colitis through inhibition of TRPV1. Gut. 2017; 66:1584-1596.

Received March 11, 2025; Revised May 19, 2025; Accepted May 27, 2025.

**Address correspondence to:*
Jianjun Gao, Department of Pharmacology, School of Pharmacy, Qingdao University, Qingdao, Shandong, China.
E-mail: gaojj@qdu.edu.cn

Released online in J-STAGE as advance publication June 20, 2025.

Correspondence

DOI: 10.5582/ddt.2025.01055

The pTau217/Aβ_{1-42} plasma ratio: The first FDA-cleared blood biomarker test for diagnosis of Alzheimer's disease

Shasha Hu[1], Haizhou Yu[2], Jianjun Gao[3,*]

[1] Department of Pathology, The Affiliated Hospital of Qingdao University, Qingdao, Shandong, China;
[2] Department of Anesthesiology, Weihai Central Hospital Affiliated to Qingdao University, Weihai, Shandong, China;
[3] Department of Pharmacology, School of Pharmacy, Qingdao University, Qingdao, Shandong, China.

SUMMARY: As the most prevalent form of dementia, Alzheimer's disease (AD) represents a major public health challenge. Early diagnosis is crucial to delaying disease progression, and yet the gold standard for detection of biomarkers — cerebral positron emission tomography (PET) imaging and cerebrospinal fluid biomarker analysis — is constrained by invasiveness, high costs, and limited accessibility. On May 16, 2025, the FDA granted its first clearance to the Lumipulse G blood test, which utilizes the plasma pTau217/Aβ_{1-42} ratio, for the diagnosis of amyloid plaques in symptomatic patients age 55 or older. In clinical validation, concordance rates with amyloid PET brain scans/the results of cerebrospinal fluid biomarker detection were 91.7% (positive) and 97.3% (negative). Similar blood-based assays have previously been approved in Japan (HISCL™ A$\beta_{42/40}$), the United Kingdom (PrecivityAD2™), and China. While concerns regarding false-positive/false-negative rates necessitate continued attention and their role as adjunctive diagnostic tools requires integration with comprehensive clinical assessment and other tests, the rapid development and regulatory clearance of these blood-based biomarker assays undeniably offer promising prospects for transforming the diagnostic and therapeutic paradigm for AD.

Keywords: β Amyloid 1-42, Lumipulse G, Alzheimer's disease, PrecivityAD2, A$\beta_{42/40}$

Alzheimer's disease (AD) is a central nervous system degenerative disease that typically manifests with an insidious onset and is characterized by a slow progression, representing the most common dementia subtype (*1*). Clinically, the disease presents with memory impairment and cognitive decline, accompanied by behavioral and psychiatric alterations. These symptoms progressively compromise patients' ability to perform everyday activities and ultimately severely impact their quality of life and impose a substantial caregiving burden on their families. According to statistics from the World Health Organization, the global population living with dementia is projected to increase from 55 million in 2019 to 139 million by 2050, with AD accounting for approximately 60-70% of these cases (*2*). Currently, the treatment options for AD are limited, and their efficacy is not satisfactory (*3-5*). As the population continues age, the number of AD cases will continue to increase, creating one of the most serious global health crises.

AD exhibits a continuum of pathogenesis, with pathological alterations potentially occurring decades prior to the manifestation of clinical symptoms. Early diagnosis and timely intervention are therefore critical to delaying or even halting disease progression (*3,6*). The current gold standard for AD biomarker diagnosis relies on positron emission tomography (PET) brain scans demonstrating β-amyloid or Tau positivity, coupled with cerebrospinal fluid (CSF) analysis revealing decreased Aβ_{1-42} levels alongside elevated levels of total Tau and phosphorylated Tau (pTau) protein. These diagnostic modalities have demonstrated substantial reliability, but they also have significant limitations: CSF biomarker collection involves considerable invasiveness and patient discomfort, while PET imaging remains prohibitively expensive. These constraints restrict their widespread clinical implementation, thereby impeding early screening and diagnosis of AD. Blood-based biomarker detection has emerged as a promising focus of research to overcome these limitations. Nevertheless, challenges in analytical sensitivity and specificity have historically prevented blood tests from replacing cerebral PET imaging and CSF biomarker analysis as the clinical diagnostic standard for AD.

On May 16, 2025, the US Food and Drug Administration (FDA) granted its first clearance for an *in vitro* blood-based diagnostic test for AD (*7*). This test aids in AD diagnosis by detecting the plasma ratio of pTau217 to Aβ_{1-42} and is intended for early

identification of amyloid plaques associated with AD in the brains of adult patients age 55 and older who exhibit AD-related symptoms. Unlike invasive lumbar puncture for CSF collection, this technique requires only peripheral blood sampling, offering a less invasive and more patient-friendly approach. The blood test is considered substantially equivalent to the previously approved Lumipulse G assay for the $A\beta_{1-42}/A\beta_{1-40}$ ratio in CSF samples. The clearance was based on a prior clinical study involving 499 plasma samples from adults with cognitive impairment (*7*). The study utilized the Lumipulse G assay to measure the plasma pTau217/$A\beta_{1-42}$ ratio and compared results with amyloid PET scans or CSF testing. Clinical data showed that 91.7% of individuals with positive Lumipulse G results were confirmed to be amyloid-positive by PET or CSF testing, while 97.3% of those with negative Lumipulse G results had negative amyloid PET or CSF outcomes (*7*). Fewer than 20% of the 499 tested patients had indeterminate Lumipulse G results. The primary risks of the Lumipulse G pTau217/$A\beta_{1-42}$ plasma ratio test include the potential for false-positive and false-negative results. A critical point worth mentioning is that this test is not intended for screening purposes and should not serve as the sole diagnostic criterion. Treatment decisions must incorporate comprehensive clinical evaluation and/or supplementary test results for integrated assessment.

Blood biomarker diagnostic tests for AD have previously been cleared in other countries. HISCL™ β Amyloid 1-42 and HISCL™ β Amyloid 1-40 assay kits, which aid in identifying brain Aβ deposition by calculating the plasma $A\beta_{42}/A\beta_{40}$ ratio, have been cleared in Japan. Clinical studies demonstrate that this test has good sensitivity and specificity, with an area under the curve of 0.895, comparable to PET scans and CSF testing results (*8*). Another AD blood biomarker test, the PrecivityAD2™ test, received medical device certification from the Medicines and Healthcare products Regulatory Agency in the United Kingdom in February 2025 (*9*). Clinical research has shown that this test has a negative predictive value (NPV) of 92% and a positive predictive value (PPV) of 91%, positioning it as a potential alternative to CSF testing and PET scans (*10*). In addition, several blood biomarker-based AD diagnostic kits have also received marketing approval in China.

The recent FDA clearance of the Lumipulse G pTau217/$A\beta_{1-42}$ plasma ratio assay, alongside the progressive regulatory clearance of similar blood-based biomarker tests in countries including Japan, the United Kingdom, and China, represents a significant advancement in the area of non-invasive blood diagnostics for AD. While concerns regarding false-positive/false-negative rates necessitate continued attention and their established role as adjunctive diagnostic tools requires integration with comprehensive clinical assessment and other tests, the rapid development and regulatory clearance of these blood-based biomarker assays undeniably offer promising prospects for transforming the diagnostic and therapeutic paradigm for AD.

Funding: None.

Conflict of Interest: The authors have no conflicts of interest to disclose.

References

1. Scheltens P, De Strooper B, Kivipelto M, Holstege H, Chételat G, Teunissen CE, Cummings J, van der Flier WM. Alzheimer's disease. Lancet. 2021; 397:1577-1590.
2. World Health Organization. World failing to address dementia challenge. *https://www.who.int/news/item/02-09-2021-world-failing-to-address-dementia-challenge* (accessed June 1, 2025). .
3. Lu DR, Dou FZ, Gao JJ. Development of amyloid beta-directed antibodies against Alzheimer's disease: Twists and turns. Drug Discov Ther. 2023; 17:440-444.
4. Ma YN, Wang ZJ, Tang W. Deep cervical lymphaticovenous anastomosis in Alzheimer's disease: A promising frontier or premature enthusiasm? BioSci Trends. 2025; 19:144-149.
5. Gu XL, Qi L, Qi Q, Zhou J, Chen S, Wang L. Monoclonal antibody therapy for Alzheimer's disease focusing on intracerebral targets. BioSci Trends. 2024; 18:49-65.
6. Ma YN, Xia Y, Karako K, Song PP, Tang W, Hu XQ. Serum proteomics reveals early biomarkers of Alzheimer's disease: The dual role of APOE-ε4. BioSci Trends. 2025; 19:1-9.
7. US Food and Drug Administration. FDA Clears First Blood Test Used in Diagnosing Alzheimer's Disease. *https://www.fda.gov/news-events/press-announcements/fda-clears-first-blood-test-used-diagnosing-alzheimers-disease* (accessed June 5, 2025).
8. Sysmex. Early Detection of Alzheimer's Disease with a Simple Blood Test. *https://www.sysmex-europe.com/products/diagnostics/immunochemistry/alzheimer-disease/* (accessed June 7, 2025).
9. C2N Diagnostics. C2N Diagnostics' PrecivityAD2™ Blood Test Receives MHRA Medical Device Certification in the United Kingdom. *https://c2n.com/news-releases/c2n-diagnostics-precivityad2-blood-test-receives-mhra-medical-device-certification-in-the-united-kingdomnbsp* (accessed June 10, 2025).
10. Palmqvist S, Tideman P, Mattsson-Carlgren N, *et al*. Blood biomarkers to detect Alzheimer disease in primary care and secondary care. JAMA. 2024; 332:1245-1257.

Received May 25, 2025; Revised June 18, 2025; Accepted June 23, 2025.

**Address correspondence to:*
Jianjun Gao, Department of Pharmacology, School of Pharmacy, Qingdao University, Qingdao, Shandong, China.
E-mail: gaojj@qdu.edu.cn

Released online in J-STAGE as advance publication June 28, 2025.

Correspondence

DOI: 10.5582/ddt.2025.01048

Acoltremon: The first TRPM8 agonist approved for the treatment of dry eye disease

Yang Zhou, Wenzhu Zhang, Fusheng Sun*

Department of Pharmacy, Qingdao Municipal Hospital, University of Health and Rehabilitation Sciences, Qingdao, Shandong, China.

SUMMARY: Dry eye disease (DED) is a common ocular surface disorder that markedly affects the quality of life (QoL) of patients. Conventional treatments for DED were unable to meet current medical needs. Acoltremon, a transient receptor potential melastatin 8 (TRPM8) agonist, was first approved by the US Food and Drug Administration on May 28, 2025 for treatment of the signs and symptoms of DED. Acoltremon activates TRPM8 receptors, thereby increasing tear production and providing a cooling sensation for symptom relief. Results of clinical trials demonstrated that 0.003% acoltremon markedly alleviated signs and symptoms of DED. Adverse events associated with acoltremon were primarily instillation site pain, and no serious ocular adverse events were noted. Acoltremon has multiple advantages: rapid onset of action, significant alleviation of dry eye signs and symptoms, and favorable safety and tolerability. In summary, the approval of acoltremon represents a new therapeutic perspective on the management of DED.

Keywords: acoltremon, dry eye disease, TRPM8 agonist, cold thermoreceptor modulator, tear production

Dry eye disease (DED) is a multifactorial ocular surface disease that is marked by a loss of tear film homeostasis and that is accompanied by ocular symptoms. The etiologies of DED include tear film instability and hyperosmolarity, inflammation of and damage to the ocular surface, and neurosensory abnormalities (*1*). DED is characterized by insufficient tear production and/or excessive tear evaporation that leads to a series of symptoms including discomfort, in forms such as redness, burning, itching, or a gritty sensation, and impaired vision. This disease predominantly occurs in females and individuals over the age of 50 and it adversely affects a patient's quality of life (QoL) and daily activities (*2,3*). Conventional treatments for DED include lubricants (artificial tears, gels, ointments, and autologous serum), corticosteroids, immunosuppressants (cyclosporine, tacrolimus, and lifitegrast), and a cholinergic agonist (a nasal spray formulation of varenicline) (*4,5*). However, the problems with current conventional treatments mainly include their modest efficacy, unpleasant adverse reactions, and slow onset of action (*6-8*). Thus, development of innovative therapies for the treatment of DED is critical.

Acoltremon (brand name: Tryptyr) is a first-in-class transient receptor potential melastatin 8 (TRPM8) agonist developed by Alcon Laboratories. It was approved by the US Food and Drug Administration on May 28, 2025 for treatment of the signs and symptoms of DED (*9*). TRPM8, a polymodal, calcium-permeable nonselective cation channel, is recognized as a physiological sensor of environmental cold. It is expressed on neurons of the ophthalmic division of the trigeminal nerve in the cornea and eyelid (*10-12*). Studies have demonstrated that TRPM8 plays an important role in regulating tear production and blink rate (*12*). As a cold thermoreceptor modulator, acoltremon activates TRPM8 receptors, thereby increasing tear production and providing a cooling sensation for symptom relief (*10,11*). In addition, due to its cooling stimulation, acoltremon may also benefit patients suffering from neuropathic ocular pain, for which treatment options are currently scarce (*13,14*). Therefore, acoltremon as a TRMP8 agonist has a dual role of both increasing tear production and decreasing ocular discomfort in the treatment of DED (*15*).

Multiple clinical trials have revealed the efficacy and safety of acoltremon for the treatment of DED. A randomized, vehicle-controlled, phase 2b study (COMET-1) evaluated the efficacy of acoltremon (0.0014% and 0.003%, twice a day for 84 days) compared to a vehicle (*15*). Results indicated that 0.003% acoltremon significantly alleviated signs and multiple symptoms of dry eye versus the vehicle. In COMET-2 and COMET-3 (two pivotal phase 3 clinical trials), patients were randomly assigned in equal proportions to receive 0.003% acoltremon or a vehicle

administered twice a day as one drop per eye for 90 days. The primary endpoint of phase 3 clinical trials was the proportion of patients in which an increase in tear production ≥ 10 mm was achieved from pre-drop at the baseline to post-drop on Day 14 according to an unanesthetized Schirmer score. In COMET-2, an increase in tear production ≥ 10 mm from the baseline was achieved in 42.6% of patients treated with acoltremon by Day 14, compared to 8.2% in patients treated with the vehicle (*16*). In COMET-3, an increase in tear production ≥10 mm from the baseline was achieved in 53.2% of patients given acoltremon by Day 14, versus 14.4% in those treated with the vehicle (*16*). The results of clinical studies demonstrated that acoltremon significantly improved tear production in patients with DED ($p < 0.01$) (*16*). Additional data from secondary endpoints showed that acoltremon rapidly increased and consistently maintained tear production compared to the vehicle, beginning on Day 1 and persisting to Day 90 (*17*). In terms of safety, the most frequently noted ocular adverse event in clinical trials with acoltremon was instillation site pain (50%), and no serious adverse events were observed (*16,17*).

Acoltremon is the first TRPM8 agonist approved for the treatment of DED, and it offers clinical advantages because of its rapid onset of action, significant alleviation of dry eye signs and symptoms, and favorable safety and tolerability. Further clinical research needs to be conducted to confirm its real-world efficacy and safety, but the approval of acoltremon offers an innovative and effective approach for treating the signs and symptoms of DED. Overall, the successful development of acoltremon, with its novel mechanisms, is expected to lead to new perspectives on and advances in the management of DED.

Funding: This manuscript was supported by Qingdao Key Medical and Health Discipline Project.

Conflict of Interest: The authors have no conflicts of interest to disclose.

References

1. Craig JP, Nichols KK, Akpek EK, Caffery B, Dua HS, Joo C, Liu Z, Nelson JD, Nichols JJ, Tsubota K, Stapleton F. TFOS DEWS II Definition and Classification report. Ocul Surf. 2017; 15:276-283.
2. Hakim FE, Farooq AV. Dry eye disease: An update in 2022. JAMA. 2022; 327:478-479.
3. Wan KH, Chen LJ, Young AL. Depression and anxiety in dry eye disease: A systematic review and meta-analysis. Eye (Lond). 2016; 30:1558-1567.
4. Safir M, Twig G, Mimouni M. Dry eye disease management. BMJ. 2024; 384:e77344.
5. Zhuang-Yan A, Syed YY. Perfluorohexyloctane ophthalmic solution: A review in dry eye disease. Drugs. 2024; 84:441-448.
6. O'Neil EC, Henderson M, Massaro-Giordano M, Bunya VY. Advances in dry eye disease treatment. Curr Opin Ophthalmol. 2019; 30:166-178.
7. Jones L, Downie LE, Korb D, *et al*. TFOS DEWS II management and therapy report. Ocul Surf. 2017; 15:575-628.
8. Clayton JA. Dry eye. N Engl J Med. 2018; 378:2212-2223.
9. US FDA. FDA-approved Drugs. *https://www.accessdata.fda.gov/drugsatfda_docs/appletter/2025/217370Orig1s000ltr.pdf* (accessed June 1, 2025).
10. Yang JM, Li F, Liu Q, Ruedi M, Wei ET, Lentsman M, Lee HS, Choi W, Kim SJ, Yoon KC. A novel TRPM8 agonist relieves dry eye discomfort. BMC Ophthalmol. 2017; 17:101.
11. Yang JM, Wei ET, Kim SJ, Yoon KC. TRPM8 channels and dry eye. Pharmaceuticals (Basel). 2018; 11:125.
12. Parra A, Madrid R, Echevarria D, Del Olmo S, Morenilla-Palao C, Acosta MC, Gallar J, Dhaka A, Viana F, Belmonte C. Ocular surface wetness is regulated by TRPM8-dependent cold thermoreceptors of the cornea. Nat Med. 2010; 16:1396-1399.
13. Yoon HJ, Kim J, Yang JM, Wei ET, Kim SJ, Yoon KC. Topical TRPM8 agonist for relieving neuropathic ocular pain in patients with dry eye: A pilot study. J Clin Med. 2021; 10:250.
14. Valdes-Arias D, Locatelli EVT, Sepulveda-Beltran PA, Mangwani-Mordani S, Navia JC, Galor A. Recent United States developments in the pharmacological treatment of dry eye disease. Drugs. 2024; 84:549-563.
15. Wirta DL, Senchyna M, Lewis AE, Evans DG, McLaurin EB, Ousler GW, Hollander DA. A randomized, vehicle-controlled, Phase 2b study of two concentrations of the TRPM8 receptor agonist AR-15512 in the treatment of dry eye disease (COMET-1). Ocul Surf. 2022; 26:166-173.
16. TRYPTYR (acoltremon) ophthalmic solution. *https://www.accessdata.fda.gov/drugsatfda_docs/label/2025/217370s000lbl.pdf* (accessed June 16, 2025).
17. Alcon Inc. Alcon Announces Positive Topline Results From Phase 3 COMET Trials of AR-15512, a Novel Topical Drug Candidate for Dry Eye. *https://alcon.widen.net/s/gvp6nqtpql/ar-15512_global-press-release_final* (accessed June 1, 2025).

Received June 3, 2025; Revised June 20, 2025; Accepted June 22, 2025.

**Address correspondence to:*
Fusheng Sun, Department of Pharmacy, Qingdao Municipal Hospital, University of Health and Rehabilitation Sciences, Qingdao, Shandong, China.
E-mail: clinphar_slyy@163.com

Released online in J-STAGE as advance publication June 27, 2025.

Letter to the Editor

DOI: 10.5582/ddt.2025.01042

Primary cutaneous lymphoma is a microsatellite stable tumor: An analysis of microsatellite instability

Saki Maeda-Otsuka[§], Myangat Tselmeg Mijiddorj[§], Ikko Kajihara[*], Soichiro Sawamura, Katsunari Makino, Shinichi Masuguchi, and Satoshi Fukushima

Department of Dermatology and Plastic Surgery, Faculty of Life Sciences, Kumamoto University, Kumamoto, Japan.

SUMMARY: A deficiency in DNA mismatch repair (MMR) leads to microsatellite instability (MSI), which is associated with a favorable response to immune checkpoint inhibitors (ICIs), and the Promega MSI Analysis System is approved as a companion diagnostic tool for it. In this study, we investigated the MMR status in patients with primary cutaneous lymphoma (PCL) diagnosed at our hospital. MSI was found in 1 of the 29 patients (3.4%), an 87-year-old man diagnosed with subcutaneous panniculitis-like T-cell lymphoma. Only the NR-21 marker was present in both tumor and normal tissue, indicating that the MMR status was MSI-low, and he had a germline mutation of SLC7A8. Our study showed that most PCLs are microsatellite stable tumors. This study is a single-center small-sample investigation and requires validation in larger cohorts.

Keywords: DNA mismatch repair (MMR), Promega panel, mononucleotide markers

Letter to the Editor:

A deficiency in DNA mismatch repair (MMR) leads to microsatellite instability (MSI) and indicates a favorable therapeutic response to immune checkpoint inhibitors (ICIs). The Promega panel (Promega, Madison, WA, USA) is approved as a companion diagnostic tool to guide ICI administration. According to previous reports on malignant lymphoma, MSI has been detected in 27% of mycosis fungoides (*1*), 41% of adult T-cell leukemia/lymphoma (not only primary cutaneous lymphoma [PCL]) (*2*), and 13% of diffuse large B-cell lymphoma (*3*). However, there have been no reports of using the Promega panel for MSI analysis in PCL. Therefore, we investigated the MMR status in patients with PCLs diagnosed at our hospital.

A total of 29 paraffin-embedded sections were collected from patients diagnosed with PCLs at our hospital between 2016 and 2024. The age, sex, and pathological diagnoses are summarized in Table 1. Genomic DNA isolation, capillary electrophoresis, and MMR evaluation were conducted as previously described (*4*). Five mononucleotide markers (BAT-25, BAT-26, MONO-27, NR-21, and NR-24) were used to determine the MMR status of each sample. Institutional Review Board approval and written informed consent were obtained in accordance with the principles of the Declaration of Helsinki.

MSI was found in 1 of the 29 patients (3.4%) (Table 1, case 29), an 87-year-old man diagnosed with subcutaneous panniculitis-like T-cell lymphoma. Only the NR-21 marker was present in both tumor and normal tissue in Supplementary Figure S1 (*https://www.ddtjournal.com/action/getSupplementalData.php?ID=263*), indicating that the MMR status was MSI-low, and he had a germline mutation of SLC7A8.

Our study is the first, to our knowledge, to investigate the occurrence rate of MSI in patients with PCL, and we identified two findings. First, the occurrence rate of MSI is < 5% among skin tumors (*5*), and our results are similar to those of several previous studies. However, they differ in that our rate is lower than that reported for MSI in malignant lymphoma (*1-3*). These differences may be owing to our analysis of various types of PCLs and our method of analysis using the Promega panel. Second, no significant correlations were found between MSI and other clinical features, as demonstrated in Table 1. The absence of MSI in PCL suggests that the pathogenesis of PCL may not involve MSI.

However, our study has several limitations. This was a single-center study, and the evaluation was conducted using only one Promega Panel as our primary goal was to explore the potential therapeutic indications of ICIs based on MSI frequency. Additionally, the number of samples analyzed was small, as PCL is a rare malignant tumor.

Table 1. Representative results of capillary electrophoresis for microsatellite instability in primary cutaneous lymphoma

Patients	Age, year	Sex	Pathological diagnosis	MSI
1	64	Male	Adult T-cell leukemia/lymphoma	stable
2	87	Female	Primary cutaneous diffuse large B-cell lymphoma	stable
3	65	Male	Mycosis fungoides	stable
4	42	Male	Primary cutaneous anaplastic large cell lymphoma	stable
5	50	Male	Mycosis fungoides	stable
6	78	Female	Mycosis fungoides	stable
7	82	Female	Adult T-cell leukemia/lymphoma	stable
8	66	Male	Adult T-cell leukemia/lymphoma	stable
9	67	Male	Adult T-cell leukemia/lymphoma	stable
10	89	Male	Primary cutaneous diffuse large B-cell lymphoma	stable
11	86	Male	Adult T-cell leukemia/lymphoma	stable
12	62	Male	Mycosis fungoides	stable
13	72	Male	Mycosis fungoides	stable
14	83	Female	Primary cutaneous follicle center cell lymphoma	stable
15	85	Male	Primary cutaneous diffuse large B-cell lymphoma	stable
16	65	Female	Mycosis fungoides	stable
17	78	Male	Primary cutaneous CD4+ small/medium T-cell lymphoma	stable
18	34	Female	Mycosis fungoides	stable
19	66	Female	Mycosis fungoides	stable
20	61	Male	Adult T-cell leukemia/lymphoma	stable
21	60	Female	Primary cutaneous marginal zone lymphoma	stable
22	56	Female	Mycosis fungoides	stable
23	76	Male	Mycosis fungoides	stable
24	84	Male	Mycosis fungoides	stable
25	80	Male	Mycosis fungoides	stable
26	94	Female	Primary cutaneous diffuse large B-cell lymphoma	stable
27	70	Female	Primary cutaneous peripheral T-cell lymphoma, not otherwise specified	stable
28	67	Female	Mycosis fungoides	stable
29	87	Male	Subcutaneous panniculitis-like T-cell lymphoma	low

In conclusion, our study showed that most PCLs are microsatellite stable tumors, which warrants further validation in larger cohorts in the future.

Acknowledgements

We would like to express our gratitude to all the investigators and patients who participated in this study.

Funding: None.

Conflict of Interest: The authors have no conflicts of interest to disclose.

References

1. Scarisbrick JJ, Woolford AJ, Russell-Jones R, Whittaker SJ. Loss of heterozygosity on 10q and microsatellite instability in advanced stages of primary cutaneous T-cell lymphoma and possible association with homozygous deletion of PTEN. Blood. 2000; 95:2937-2942.
2. Hatta Y, Yamada Y, Tomonaga M, Miyoshi I, Said JW, Koeffler HP. Microsatellite instability in adult T-cell leukaemia. Br J Haematol. 1998; 101:341-344.
3. Tian T, Li J, Xue T, Yu B, Li X, Zhou X. Microsatellite instability and its associations with the clinicopathologic characteristics of diffuse large B-cell lymphoma. Cancer Med. 2020; 9:2330-2342.
4. Maeda-Otsuka S, Myangat TM, Kajihara I, Sakamoto R, Yamada-Kanazawa S, Sawamura S, Makino K, Masuguchi S, Fukushima S, Ihn H. Status of microsatellite stability in angiosarcoma: angiosarcoma is a microsatellite stable tumor. J Dermatol. 2021; 48:e368-369.
5. Quinn AG, Healy E, Rehman I, Sikkink S, Rees JL. Microsatellite instability in human non-melanoma and melanoma skin cancer. J Invest Dermatol. 1995; 104:309-312.

Received May 7, 2025; Revised June 11, 2025; Accepted June 22, 2025.

[§]These authors contributed equally to this work.
**Address correspondence to:*
Ikko Kajihara, Department of Dermatology and Plastic Surgery, Faculty of Life Sciences, Kumamoto University, 1-1-1 Honjo, Kumamoto 860-8556, Japan.
E-mail: kajiderma@gmail.com

Released online in J-STAGE as advance publication June 25, 2025.

DD&T
Drug Discoveries & Therapeutics

Guide for Authors

1. Scope of Articles

Drug Discoveries & Therapeutics (Print ISSN 1881-7831, Online ISSN 1881-784X) welcomes contributions in all fields of pharmaceutical and therapeutic research such as medicinal chemistry, pharmacology, pharmaceutical analysis, pharmaceutics, pharmaceutical administration, and experimental and clinical studies of effects, mechanisms, or uses of various treatments. Studies in drug-related fields such as biology, biochemistry, physiology, microbiology, and immunology are also within the scope of this journal.

2. Submission Types

Original Articles should be well-documented, novel, and significant to the field as a whole. An Original Article should be arranged into the following sections: Title page, Abstract, Introduction, Materials and Methods, Results, Discussion, Acknowledgments, and References. Original articles should not exceed 5,000 words in length (excluding references) and should be limited to a maximum of 50 references. Articles may contain a maximum of 10 figures and/or tables. Supplementary Data are permitted but should be limited to information that is not essential to the general understanding of the research presented in the main text, such as unaltered blots and source data as well as other file types.

Brief Reports definitively documenting either experimental results or informative clinical observations will be considered for publication in this category. Brief Reports are not intended for publication of incomplete or preliminary findings. Brief Reports should not exceed 3,000 words in length (excluding references) and should be limited to a maximum of 4 figures and/or tables and 30 references. A Brief Report contains the same sections as an Original Article, but the Results and Discussion sections should be combined.

Reviews should present a full and up-to-date account of recent developments within an area of research. Normally, reviews should not exceed 8,000 words in length (excluding references) and should be limited to a maximum of 10 figures and/or tables and 100 references. Mini reviews are also accepted, which should not exceed 4,000 words in length (excluding references) and should be limited to a maximum of 5 figures and/or tables and 50 references.

Policy Forum articles discuss research and policy issues in areas related to life science such as public health, the medical care system, and social science and may address governmental issues at district, national, and international levels of discourse. Policy Forum articles should not exceed 3,000 words in length (excluding references) and should be limited to a maximum of 5 figures and/or tables and 30 references.

Case Reports should be detailed reports of the symptoms, signs, diagnosis, treatment, and follow-up of an individual patient. Case reports may contain a demographic profile of the patient but usually describe an unusual or novel occurrence. Unreported or unusual side effects or adverse interactions involving medications will also be considered. Case Reports should not exceed 3,000 words in length (excluding references).

Communications are short, timely pieces that spotlight new research findings or policy issues of interest to the field of global health and medical practice that are of immediate importance. Depending on their content, Communications will be published as "Comments" or "Correspondence". Communications should not exceed 1,500 words in length (excluding references) and should be limited to a maximum of 2 figures and/or tables and 20 references.

Editorials are short, invited opinion pieces that discuss an issue of immediate importance to the fields of global health, medical practice, and basic science oriented for clinical application. Editorials should not exceed 1,000 words in length (excluding references) and should be limited to a maximum of 10 references. Editorials may contain one figure or table.

News articles should report the latest events in health sciences and medical research from around the world. News should not exceed 500 words in length.

Letters should present considered opinions in response to articles published in *Drug Discoveries & Therapeutics* in the last 6 months or issues of general interest. Letters should not exceed 800 words in length and may contain a maximum of 10 references. Letters may contain one figure or table.

3. Editorial Policies

For publishing and ethical standards, *Drug Discoveries & Therapeutics* follows the Recommendations for the Conduct, Reporting, Editing, and Publication of Scholarly Work in Medical Journals issued by the International Committee of Medical Journal Editors (ICMJE, *https://icmje.org/recommendations*), and the Principles of Transparency and Best Practice in Scholarly Publishing jointly issued by the Committee on Publication Ethics (COPE, *https://publicationethics.org/resources/guidelines-new/principles-transparency-and-best-practice-scholarly-publishing*), the Directory of Open Access Journals (DOAJ, *https://doaj.org/apply/transparency*), the Open Access Scholarly Publishers Association (OASPA, *https://oaspa.org/principles-of-transparency-and-best-practice-in-scholarly-publishing-4*), and the World Association of Medical Editors (WAME, *https://wame.org/principles-of-transparency-and-best-practice-in-scholarly-publishing*).

Drug Discoveries & Therapeutics will perform an especially prompt review to encourage innovative work. All original research will be subjected to a rigorous standard of peer review and will be edited by experienced copy editors to the highest standards.

Ethical Approval of Studies and Informed Consent: For all manuscripts reporting data from studies involving human participants or animals, formal review and approval, or formal review and waiver, by an appropriate institutional review board or ethics committee is required and should be described in the Methods section. When your manuscript contains any case details, personal information and/or images of patients or other individuals, authors must obtain appropriate written consent, permission and release in order to comply with all applicable laws and regulations concerning privacy and/or security of personal information. The consent form needs to comply with the relevant legal requirements of your particular jurisdiction, and please do not send signed consent form to *Drug Discoveries & Therapeutics* to respect your patient's and any other individual's privacy. Please instead describe the information clearly in the Methods (patient consent) section of your manuscript while retaining copies of the signed forms in the event they should be needed. Authors should also state that the study conformed to the provisions of the Declaration of Helsinki (as revised in 2013, *https://wma.net/what-we-do/medical-ethics/declaration-of-helsinki*). When reporting experiments on animals, authors should indicate whether the institutional and national guide for the care and use of laboratory animals was followed.

Reporting Clinical Trials: The ICMJE (*https:// icmje.org/recommendations/browse/publishing-and-editorial-issues/clinical-trial-registration.html*) defines a clinical trial as any research project that prospectively assigns people or a group of people to an intervention, with or without concurrent comparison or control groups, to study the relationship between a health-related intervention and a health outcome. Registration of clinical trials in a public trial registry

at or before the time of first patient enrollment is a condition of consideration for publication in *Drug Discoveries & Therapeutics*, and the trial registration number will be published at the end of the Abstract. The registry must be independent of for-profit interest and publicly accessible. Reports of trials must conform to CONSORT 2010 guidelines (*https://consort-statement.org/consort-2010*). Articles reporting the results of randomized trials must include the CONSORT flow diagram showing the progress of patients throughout the trial.

Conflict of Interest: All authors are required to disclose any actual or potential conflict of interest including financial interests or relationships with other people or organizations that might raise questions of bias in the work reported. If no conflict of interest exists for each author, please state "There is no conflict of interest to disclose".

Submission Declaration: When a manuscript is considered for submission to *Drug Discoveries & Therapeutics*, the authors should confirm that 1) no part of this manuscript is currently under consideration for publication elsewhere; 2) this manuscript does not contain the same information in whole or in part as manuscripts that have been published, accepted, or are under review elsewhere, except in the form of an abstract, a letter to the editor, or part of a published lecture or academic thesis; 3) authorization for publication has been obtained from the authors' employer or institution; and 4) all contributing authors have agreed to submit this manuscript.

Initial Editorial Check: Immediately after submission, the journal's managing editor will perform an initial check of the manuscript. A suitable academic editor will be notified of the submission and invited to check the manuscript and recommend reviewers. Academic editors will check for plagiarism and duplicate publication at this stage. The journal has a formal recusal process in place to help manage potential conflicts of interest of editors. In the event that an editor has a conflict of interest with a submitted manuscript or with the authors, the manuscript, review, and editorial decisions are managed by another designated editor without a conflict of interest related to the manuscript.

Peer Review: *Drug Discoveries & Therapeutics* operates a single-anonymized review process, which means that reviewers know the names of the authors, but the authors do not know who reviewed their manuscript. All articles are evaluated objectively based on academic content. External peer review of research articles is performed by at least two reviewers, and sometimes the opinions of more reviewers are sought. Peer reviewers are selected based on their expertise and ability to provide quality, constructive, and fair reviews. For research manuscripts, the editors may, in addition, seek the opinion of a statistical reviewer. Every reviewer is expected to evaluate the manuscript in a timely, transparent, and ethical manner, following the COPE guidelines (*https://publicationethics.org/files/cope-ethical-guidelines-peer-reviewers-v2_0.pdf*). We ask authors for sufficient revisions (with a second round of peer review, when necessary) before a final decision is made. Consideration for publication is based on the article's originality, novelty, and scientific soundness, and the appropriateness of its analysis.

Suggested Reviewers: A list of up to 3 reviewers who are qualified to assess the scientific merit of the study is welcomed. Reviewer information including names, affiliations, addresses, and e-mail should be provided at the same time the manuscript is submitted online. Please do not suggest reviewers with known conflicts of interest, including participants or anyone with a stake in the proposed research; anyone from the same institution; former students, advisors, or research collaborators (within the last three years); or close personal contacts. Please note that the Editor-in-Chief may accept one or more of the proposed reviewers or may request a review by other qualified persons.

Language Editing: Manuscripts prepared by authors whose native language is not English should have their work proofread by a native English speaker before submission. If not, this might delay the publication of your manuscript in *Drug Discoveries & Therapeutics*.

The Editing Support Organization can provide English proofreading, Japanese-English translation, and Chinese-English translation services to authors who want to publish in *Drug Discoveries & Therapeutics* and need assistance before submitting a manuscript. Authors can visit this organization directly at *https://www.iacmhr.com/iac-eso/support.php?lang=en. IAC-ESO* was established to facilitate manuscript preparation by researchers whose native language is not English and to help edit works intended for international academic journals.

Copyright and Reuse: Before a manuscript is accepted for publication in *Drug Discoveries & Therapeutics*, authors will be asked to sign a transfer of copyright agreement, which recognizes the common interest that both the journal and author(s) have in the protection of copyright. We accept that some authors (*e.g.*, government employees in some countries) are unable to transfer copyright. A JOURNAL PUBLISHING AGREEMENT (JPA) form will be e-mailed to the authors by the Editorial Office and must be returned by the authors by mail, fax, or as a scan. Only forms with a hand-written signature from the corresponding author are accepted. This copyright will ensure the widest possible dissemination of information. Please note that the manuscript will not proceed to the next step in publication until the JPA Form is received. In addition, if excerpts from other copyrighted works are included, the author(s) must obtain written permission from the copyright owners and credit the source(s) in the article.

4. Cover Letter

The manuscript must be accompanied by a cover letter prepared by the corresponding author on behalf of all authors. The letter should indicate the basic findings of the work and their significance. The letter should also include a statement affirming that all authors concur with the submission and that the material submitted for publication has not been published previously or is not under consideration for publication elsewhere. The cover letter should be submitted in PDF format. For an example of Cover Letter, please visit: Download Centre (*https://www.ddtjournal.com/downcentre)*.

5. Submission Checklist

The Submission Checklist should be submitted when submitting a manuscript through the Online Submission System. Please visit Download Centre (*https://www.ddtjournal.com/downcentre)* and download the Submission Checklist file. We recommend that authors use this checklist when preparing your manuscript to check that all the necessary information is included in your article (if applicable), especially with regard to Ethics Statements.

6. Manuscript Preparation

Manuscripts are suggested to be prepared in accordance with the "Recommendations for the Conduct, Reporting, Editing, and Publication of Scholarly Work in Medical Journals", as presented at *http://www.ICMJE.org*.

Manuscripts should be written in clear, grammatically correct English and submitted as a Microsoft Word file in a single-column format. Manuscripts must be paginated and typed in 12-point Times New Roman font with 24-point line spacing. Please do not embed figures in the text. Abbreviations should be used as little as possible and should be explained at first mention unless the term is a well-known abbreviation (*e.g.* DNA). Single words should not be abbreviated.

Title page: The title page must include 1) the title of the paper (Please note the title should be short, informative, and contain the major key words); 2) full name(s) and affiliation(s) of the author(s), 3) abbreviated names of the author(s), 4) full name, mailing address, telephone/fax numbers, and e-mail address of the corresponding author; 5) author contribution statements to specify the individual contributions of all authors to this manuscript, and 6) conflicts of interest (if you have an actual or potential conflict of interest to disclose, it must be included as a footnote on the title page of the manuscript; if no conflict of interest

exists for each author, please state "There is no conflict of interest to disclose").

Abstract: The abstract should briefly state the purpose of the study, methods, main findings, and conclusions. For article types including Original Article, Brief Report, Review, Policy Forum, and Case Report, a one-paragraph abstract consisting of no more than 250 words must be included in the manuscript. For Communications, Editorials, News, or Letters, a brief summary of main content in 150 words or fewer should be included in the manuscript. For articles reporting clinical trials, the trial registration number should be stated at the end of the Abstract. Abbreviations must be kept to a minimum and non-standard abbreviations explained in brackets at first mention. References should be avoided in the abstract. Three to six key words or phrases that do not occur in the title should be included in the Abstract page.

Introduction: The introduction should provide sufficient background information to make the article intelligible to readers in other disciplines and sufficient context clarifying the significance of the experimental findings.

Materials/Patients and Methods: The description should be brief but with sufficient detail to enable others to reproduce the experiments. Procedures that have been published previously should not be described in detail but appropriate references should simply be cited. Only new and significant modifications of previously published procedures require complete description. Names of products and manufacturers with their locations (city and state/country) should be given and sources of animals and cell lines should always be indicated. All clinical investigations must have been conducted in accordance with the Declaration of Helsinki (as revised in 2013, *https://wma.net/what-we-do/medical-ethics/declaration-of-helsinki*). All human and animal studies must have been approved by the appropriate institutional review board(s) and a specific declaration of approval must be made within this section.

Results: The description of the experimental results should be succinct but in sufficient detail to allow the experiments to be analyzed and interpreted by an independent reader. If necessary, subheadings may be used for an orderly presentation. All Figures and Tables should be referred to in the text in order, including those in the Supplementary Data.

Discussion: The data should be interpreted concisely without repeating material already presented in the Results section. Speculation is permissible, but it must be well-founded, and discussion of the wider implications of the findings is encouraged. Conclusions derived from the study should be included in this section.

Acknowledgments: All funding sources (including grant identification) should be credited in the Acknowledgments section. Authors should also describe the role of the study sponsor(s), if any, in study design; in the collection, analysis, and interpretation of data; in the writing of the report; and in the decision to submit the paper for publication. If the funding source had no such involvement, the authors should so state.

In addition, people who contributed to the work but who do not meet the criteria for authors should be listed along with their contributions.

References: References should be numbered in the order in which they appear in the text. Citing of unpublished results, personal communications, conference abstracts, and theses in the reference list is not recommended but these sources may be mentioned in the text. In the reference list, cite the names of all authors when there are fifteen or fewer authors; if there are sixteen or more authors, list the first three followed by *et al*. Names of journals should be abbreviated in the style used in PubMed. Authors are responsible for the accuracy of the references. The EndNote Style of *Drug Discoveries & Therapeutics* could be downloaded at **EndNote** (*https://www.ddtjournal.com/examples/Drug_Discoveries_Therapeutics.ens*).

Examples are given below:

Example 1 (Sample journal reference):

Nakata M, Tang W. Japan-China Joint Medical Workshop on Drug Discoveries and Therapeutics 2008: The need of Asian pharmaceutical researchers' cooperation. Drug Discov Ther. 2008; 2:262-263.

Example 2 (Sample journal reference with more than 15 authors):

Darby S, Hill D, Auvinen A, *et al*. Radon in homes and risk of lung cancer: Collaborative analysis of individual data from 13 European case-control studies. BMJ. 2005; 330:223.

Example 3 (Sample book reference):

Shalev AY. Post-traumatic stress disorder: Diagnosis, history and life course. In: Post-traumatic Stress Disorder, Diagnosis, Management and Treatment (Nutt DJ, Davidson JR, Zohar J, eds.). Martin Dunitz, London, UK, 2000; pp. 1-15.

Example 4 (Sample web page reference):

World Health Organization. The World Health Report 2008 – primary health care: Now more than ever. *https://apps.who.int/iris/handle/10665/43949* (accessed September 23, 2022).

Tables: All tables should be prepared in Microsoft Word or Excel and should be arranged at the end of the manuscript after the References section. Please note that tables should not in image format. All tables should have a concise title and should be numbered consecutively with Arabic numerals. If necessary, additional information should be given below the table.

Figure Legend: The figure legend should be typed on a separate page of the main manuscript and should include a short title and explanation. The legend should be concise but comprehensive and should be understood without referring to the text. Symbols used in figures must be explained. Any individually labeled figure parts or panels (A, B, *etc*.) should be specifically described by part name within the legend.

Figure Preparation: All figures should be clear and cited in numerical order in the text. Figures must fit a one- or two-column format on the journal page: 8.3 cm (3.3 in.) wide for a single column, 17.3 cm (6.8 in.) wide for a double column; maximum height: 24.0 cm (9.5 in.). Please make sure that artwork files are in an acceptable format (TIFF or JPEG) at minimum resolution (600 dpi for illustrations, graphs, and annotated artwork, and 300 dpi for micrographs and photographs). Please provide all figures as separate files. Please note that low-resolution images are one of the leading causes of article resubmission and schedule delays.

Units and Symbols: Units and symbols conforming to the International System of Units (SI) should be used for physicochemical quantities. Solidus notation (*e.g*. mg/kg, mg/mL, mol/mm^2/min) should be used. Please refer to the SI Guide *www.bipm.org/en/si/* for standard units.

Supplemental data: Supplemental data might be useful for supporting and enhancing your scientific research and *Drug Discoveries & Therapeutics* accepts the submission of these materials which will be only published online alongside the electronic version of your article. Supplemental files (figures, tables, and other text materials) should be prepared according to the above guidelines, numbered in Arabic numerals (*e.g*., Figure S1, Figure S2, and Table S1, Table S2) and referred to in the text. All figures and tables should have titles and legends. All figure legends, tables and supplemental text materials should be placed at the end of the paper. Please note all of these supplemental data should be provided at the time of initial submission and note that the editors reserve the right to limit the size

and length of Supplemental Data.

7. Online Submission

Manuscripts should be submitted to *Drug Discoveries & Therapeutics* online at *https://www.ddtjournal.com/login*. Receipt of your manuscripts submitted online will be acknowledged by an e-mail from Editorial Office containing a reference number, which should be used in all future communications. If for any reason you are unable to submit a file online, please contact the Editorial Office by e-mail at *office@ddtjournal.com*

8. Accepted Manuscripts

Page Charge: Page charges will be levied on all manuscripts accepted for publication in *Drug Discoveries & Therapeutics* (Original Articles / Brief Reports / Reviews / Policy Forum / Communications: $140 per page for black white pages, $340 per page for color pages; News / Letters: a total cost of $600). Under exceptional circumstances, the author(s) may apply to the editorial office for a waiver of the publication charges by stating the reason in the Cover Letter when the manuscript online.

Misconduct: *Drug Discoveries & Therapeutics* takes seriously all allegations of potential misconduct and adhere to the ICMJE Guideline (*https://icmje.org/recommendations*) and COPE Guideline (*https://publicationethics.org/files/Code_of_conduct_for_journal_editors.pdf*). In cases of suspected research or publication misconduct, it may be necessary for the Editor or Publisher to contact and share submission details with third parties including authors' institutions and ethics committees. The corrections, retractions, or editorial expressions of concern will be performed in line with above guidelines.

(As of December 2022)

Drug Discoveries & Therapeutics
Editorial and Head Office
Pearl City Koishikawa 603,
2-4-5 Kasuga, Bunkyo-ku,
Tokyo 112-0003, Japan.
E-mail: office@ddtjournal.com